

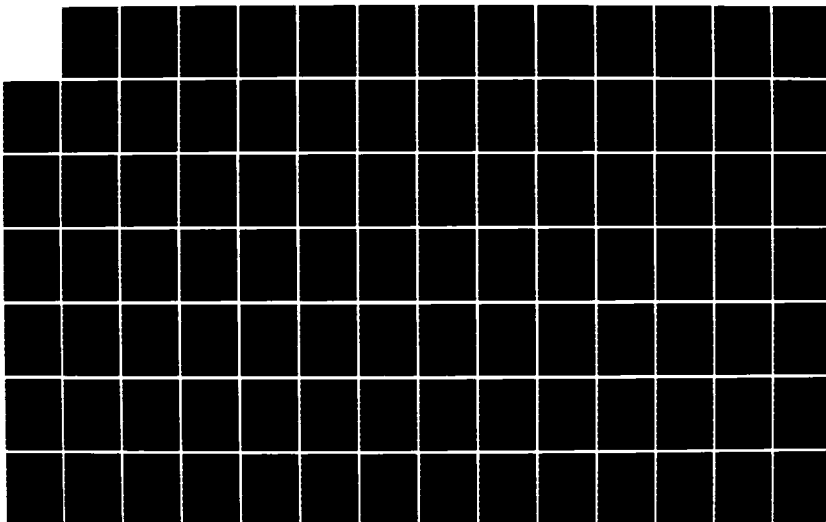
AD-A166 730

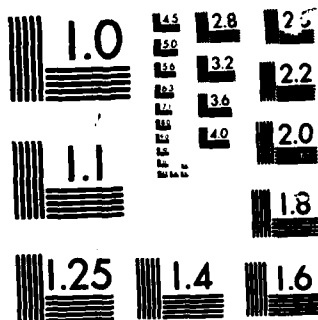
DISTURBANCE VECTOR IN SPACE FROM SURFACE GRAVITY
ANOMALIES USING COMPLEME.. (U) OHIO STATE UNIV COLUMBUS
DEPT OF GEODETIC SCIENCE AND SURVEYI.. J Y CRUZ AUG 85
DSU/DG55-366 AFGL-TR-85-8209 F/G 8/5

1/2

UNCLASSIFIED

NL





MICROCOPY

CHART

AD-A166 730

12

AFGL-TR-85-0209

**DISTURBANCE VECTOR IN SPACE FROM SURFACE GRAVITY ANOMALIES
USING COMPLEMENTARY MODELS**

Jaime Y. Cruz

The Ohio State University
Research Foundation
Columbus, Ohio 43212

August 1985

Scientific Report No. 10

Approved for public release; distribution unlimited

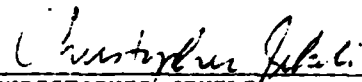
AIR FORCE GEOPHYSICS LABORATORY
AIR FORCE SYSTEMS COMMAND
UNITED STATES AIR FORCE
HANSCOM AFB, MASSACHUSETTS 01731

DTIC FILE COPY

DTIC
ELECTE
APR 17 1986
S D E

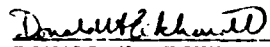
CONTRACTOR REPORTS

This technical report has been reviewed and is approved for publication.


CHRISTOPHER JEKELI
Contract Manager


THOMAS P. ROONEY
Chief, Geodesy & Gravity Branch

FOR THE COMMANDER


DONALD H. ECKHARDT
Director
Earth Sciences Division

This report has been reviewed by the ESD Public Affairs Office (PA) and is releasable to the National Technical Information Service (NTIS).

Qualified requesters may obtain additional copies from the Defense Technical Information Center. All others should apply to the National Technical Information Service.

If your address has changed, or if you wish to be removed from the mailing list, or if the addressee is no longer employed by your organization, please notify AFGL/DAA, Hanscom AFB, MA 01731. This will assist us in maintaining a current mailing list.

unclassified

SECURITY CLASSIFICATION OF THIS PAGE (When Data Entered)

REPORT DOCUMENTATION PAGE		READ INSTRUCTIONS BEFORE COMPLETING FORM
1. REPORT NUMBER AFGL-TR-85-0209	2. GOVT ACCESSION NO. ADA 166 730	3. RECIPIENT'S CATALOG NUMBER
4. TITLE (and Subtitle) DISTURBANCE VECTOR IN SPACE FROM SURFACE GRAVITY ANOMALIES USING COMPLEMENTARY MODELS		5. TYPE OF REPORT & PERIOD COVERED Scientific Report No. 10
		6. PERFORMING ORG. REPORT NUMBER OSU/DGSS No. 366
7. AUTHOR(s) Jaime Y. Cruz		8. CONTRACT OR GRANT NUMBER(s) F19628-82- K-0022
9. PERFORMING ORGANIZATION NAME AND ADDRESS The Ohio State University Research Foundation 1958 Neil Avenue Columbus, Ohio 43210		10. PROGRAM ELEMENT, PROJECT, TASK AREA & WORK UNIT NUMBERS 61102F 2309G1BC
11. CONTROLLING OFFICE NAME AND ADDRESS Air Force Geophysics Laboratory Hanscom AFB, Massachusetts 01730 Monitor/Christopher Jekeli/LWG		12. REPORT DATE August 1985
		13. NUMBER OF PAGES 154
14. MONITORING AGENCY NAME & ADDRESS (if different from Controlling Office)		15. SECURITY CLASS. (of this report) Unclassified
		15a. DECLASSIFICATION DOWNGRADING SCHEDULE
16. DISTRIBUTION STATEMENT (of this Report) Approved for public release; distribution unlimited		
17. DISTRIBUTION STATEMENT (of the abstract entered in Block 20, if different from Report)		
18. SUPPLEMENTARY NOTES		
19. KEY WORDS (Continue on reverse side if necessary and identify by block number) Earth's Gravity Field Topographic Mass Effects Spherical Harmonics Collocation Ellipsoidal Corrections Integral Formulas		
20. ABSTRACT (Continue on reverse side if necessary and identify by block number) The modeling of the external disturbance vector of the earth from surface gravity anomaly data is discussed. The low frequency features of the signal are represented in spherical harmonic series. The recovery of the coefficients of the series from the given gravity anomalies is discussed focusing on the use of analytical continuation and ellipsoidal corrections to account for the earth's topography and ellipticity. The spectrum and data response of the spatial disturbance vector are studied to aid the		

DD FORM 1 JAN 73 1473

EDITION OF 1 NOV 65 IS OBSOLETE

unclassified

SECURITY CLASSIFICATION OF THIS PAGE (When Data Entered)

20.

design of models and experiments. The local models studied to complement the globally valid spherical harmonic model are (a) the residual topographic model (RTM); generated by integrating the gravitational influence of certain shallow topographic masses of assumed constant density; (b) the classical integral model, generated by integrating surface gravity anomalies that are assumed to refer to a mean level surface in the area; (c) three versions of the Dirac approach to collocation; namely, those that imply the inversion of surface gravity anomaly data into gravity anomaly impulses Δg^* , point masses μ^* , and point dipoles $\bar{\mu}^*$ on the Bjerhammar sphere; and finally (d) two versions of the least squares collocation (l.s.c.) approach; namely, those that are based on generating covariance functions from white noise distribution of gravity anomaly Δg^* and of disturbing potential T^* on the Bjerhammar sphere. The integral and collocation models are compared in their ability to recover the high frequency disturbance components implied by the RTM. Results indicate that the RTM itself should be used to model the high frequency signal variations whenever detailed (e.g., 1km x 1km) height data is available, since the integral and collocation models are limited in resolution through their use of gravity data with feasible spacing that can only be expected to be around 10 km x 10 km. The residual signal not already modeled by the RTM and spherical harmonic model can in most cases be accurately modeled by the integral model with mean topography accounted for. For high accuracies in mountainous areas, however, a collocation model should be used to account for the full variations of the topography, not just the mean topography. Matrix conditioning problems with the l.s.c. approach support preference to the Dirac systems for rigorous treatment of the topography at detailed (5'x5') resolutions.

FOREWORD

This report was prepared by Jaime Y. Cruz, Graduate Research Associate, Department of Geodetic Science and Surveying, The Ohio State University under Air Force Contract No. F19268-K-0022, The Ohio State University Research Foundation Project No. 714274. This project is supervised by Professor Richard H. Rapp. The contract covering this research is administered by the Air Force Geophysics Laboratory, Hanscom Air Force Base, Massachusetts, with Dr. Christopher Jekeli, Scientific Program Officer.

This report is also being submitted to the Graduate School of The Ohio State University in partial fulfillment of the requirements for the degree Doctor of Philosophy.

Accession For	
NTIS GRA&I	<input checked="" type="checkbox"/>
DTIC TAB	<input type="checkbox"/>
Unannounced	<input type="checkbox"/>
Justification	
By	
Distribution/	
Availability Codes	
Dist	Avail. and/or Special
A-1	



ACKNOWLEDGEMENTS

I would like to thank Dr. R.H. Rapp for stimulating discussions and providing guidance towards the improvement of this work. Thanks are also due to Drs. I.I. Mueller and U.A. Uotila for their constructive comments as members of the reading committee.

A one-year Presidential Fellowship from The Ohio State University helped support this study, in addition to the support under a project sponsored by the Air Force Geophysics Laboratory (Hanscom AFB). Most of the computer funds were supplied by the Instruction and Research Computer Center of The Ohio State University, through the Department of Geodetic Science and Surveying.

The typing of the manuscript was efficiently done by Ms. Laura Brumfield and Ms. Tracy Runyon.

Amusements were provided through lunch hours with Chugiat Wichiencharoen of Thailand, Mike Baker of the United States, and Lucia Tsaoussi of Greece.

Finally, this work would never have been completed without the comfort and relaxation afforded by the company of my wife Edna, and twin daughters Eden and Erin.

TABLE OF CONTENTS

	Page
FOREWORD.....	iii
ACKNOWLEDGEMENTS.....	iv
LIST OF TABLES.....	vii
LIST OF FIGURES.....	ix
 Chapter	
1. INTRODUCTION.....	1
1.1 This Work vs. Katsambalos (1981).....	1
1.2 Preliminaries.....	2
1.3 Scope of This Study.....	10
2. ON THE RECOVERY OF POTENTIAL COEFFICIENTS FROM SURFACE GRAVITY ANOMALIES.....	16
3. FAMILIARIZATION WITH THE SPATIAL DISTURBANCE VECTOR SIGNAL.....	34
3.1 Formulas for Spherical Harmonic and Integral Representations.....	35
3.2 Spectral Information Content.....	40
3.3 Truncation Theory.....	44
3.3.1 Isotropic Kernels.....	44
3.3.2 Non-Isotropic Kernels.....	49
3.3.3 Truncation Coefficients.....	52
3.3.4 Numerical Investigations.....	53
4. ACCOUNTING FOR THE TOPOGRAPHY IN MODELING THE SPATIAL DISTURBANCE VECTOR, A CONTINUOUS APPROACH.....	61
4.1 Some General Considerations on the Topography Problem.....	61
4.2 Complementary Models.....	69
4.2.1 The Spherical Harmonic Model.....	69
4.2.2 The Residual Integral Model.....	72
4.2.3 The Residual Topographic Model.....	74

4.3	Numerical Investigations.....	76
4.3.1	The Data.....	76
4.3.2	The Test Area.....	77
4.3.3	Description of Tests and Numerical Results...	83
4.3.4	Discussion of Numerical Results.....	85
5.	DISCRETE APPROACHES TO MODELING THE SPATIAL DISTURBANCE VECTOR.....	91
5.1	The Collocation Procedure.....	92
5.2	The Dirac Approach to Collocation.....	95
5.3	The Least Squares Collocation Approach.....	106
5.4	Numerical Investigations.....	113
5.4.1	Tailoring of Covariance Functions.....	113
5.4.2	Real Data Prediction of Gravity Anomalies in Canada.....	117
5.4.3	Comparison of Discrete and Continuous Models in the New Mexico Test Area.....	120
6.	SUMMARY, CONCLUSIONS, RECOMMENDATIONS.....	127
APPENDIX -	Summary of Suggested Computational Procedures for the Computation of the Gravity Disturbance Components in Space from Surface Gravity Anomaly Data.....	132
LIST OF REFERENCES.....		136

LIST OF TABLES

Table	Page
1 Relative Error Caused by the Omission of Terms Proportional to Certain Powers of e , in the Recovery of Potential Coefficients C_{nm}^* from Anomaly Data Δg_E on the Ellipsoid...	31
2 Effect of Potential Coefficient Errors δC_{nm}^* on Computed Gravity Anomalies Δg and Height Anomalies ζ . Units: $\sigma(\Delta g)$ in mgals; $\sigma(\zeta)$ in meters.....	32
3 Anomaly Degree Variances of Various Types of Fields.....	64
4 RMS Error in Various Types of Disturbance Fields Due to a 1.5 km Error in the Vertical Position of the Boundary Surface for the Anomaly Data.....	68
5 Maximal Values (mgals) of the Different Quantities Being Computed in Tests 1 to 9 of Chapter 4 (see text).....	86
6 "Mean \pm Standard Deviation" (mgals) of the Errors of the Direct Integration Method in Representing the Disturbance Components of the Residual Topographic Field. The statistics were computed from the five test points of the given altitude.....	89
7 Values of the Disturbance Components in Space as Evaluated from the Models of Chapter 4, for the Test Point A ($\phi = 33^\circ N$, $\lambda = 254^\circ 5E$). Row V gives the errors of the direct integration method in representing the residual topographic model (see Test 9). Units: mgals.....	90
8 "Number of Iterations/RMS Error (mgal)" Under Various Discrete Approaches, When Predicting 50 Withheld Gravity Anomalies from 87 Known Gravity Anomalies in Manitoba, Canada.....	120
9 Disturbance Components (mgals) Along the Vertical Test lines A, B, C, D, E, Generated by Prism Integration of the Gravitational Influence of Residual Topographic Masses in the 2°x2° New Mexico Test Area.....	122

10	"Number of Iterations/RMS Error (mgal)" Under Various Discrete Approaches, When Modeling the Disturbance Components of the Residual Topographic Field, from 5'x5' Surface Gravity Anomalies in the 2"x2" New Mexico Test Area.....	123
11	RMS and Maximal Differences Between Various Models of Disturbance Vector Components (mgals).....	126

LIST OF FIGURES

Figure		Page
1	Construction of the Gravity Anomaly.....	4
2	Mapping Under the Spherical Approximation.....	7
3	Gravity Anomalies on Different Boundary Surfaces.....	17
4	Radial or Horizontal Gravity Disturbance Information (RMS) Beyond a Given Harmonic Degree N_{min} , for Various Altitudes H Above the Earth.....	43
5	Altitudes for 1%, 3%, and 10% Relative Omission Error in Radial or Horizontal Gravity Disturbance, for a Given Maximum Degree N_{max} of Gravity Field Representation....	43
6	Splitting of the Original Kernel K for the Com- bination of Terrestrial Gravity Anomaly and Spherical Harmonic Coefficient Information, in Isotropic Gravimetric Integration.....	47
7	Radial Disturbance Truncation Error at Altitude $H=100$ km as a Function of Cap Radius, When Using a Reference Field of Degree $N_{ref}=20, 36, 180, 360$ Under an Unmodified Molodensky Truncation Method. (<u>solid line</u> : Commission plus Omission Error; <u>circles</u> : Omission Error Only).....	55
8	Radial Disturbance Truncation Error at Altitude $H=100$ km as a Function of Cap Radius, When Using a Reference Field of Degree $N_{ref}=20, 36, 180,$ 360 Considering Commission plus Omission Error. (<u>solid line</u> : Unmodified Molodensky; <u>circles</u> : Improved Molodensky Truncation Method, $\bar{n}=10$).....	55
9	Radial Disturbance Truncation Error at Altitude $H=5$ km as a Function of Cap Radius, When Using a Reference Field of Degree $N_{ref}=20, 36, 180, 360$ Under an Unmodified Molodensky Truncation Method. (<u>solid line</u> : Commission plus Omission Error; <u>circles</u> : Omission Error Only).....	56

10	Radial Disturbance Truncation Error at Altitude H=5 km as a Function of Cap Radius, When Using a Reference Field of Degree $N_{ref}=20, 36, 180,$ 360 Considering Commission plus Omission Error. (<u>solid line</u> : Unmodified Molodensky; <u>circles</u> : Improved Molodensky Truncation Method, $\bar{n}=10$).....	56
11	Horizontal Disturbance Truncation Error at Altitude H=100 km as a Function of Cap Radius, When Using a Reference Field of Degree $N_{ref}=20, 36, 180, 360$ Under an Unmodified Molodensky Truncation Method. (<u>solid line</u> : Commission plus Omission Error; <u>circles</u> : Omission Error Only).....	57
12	Horizontal Disturbance Truncation Error at Altitude H=100 km as a Function of Cap Radius, When Using a Reference Field of Degree $N_{ref}=20, 36, 180, 360$ Considering Commission plus Omission Error (<u>solid</u> <u>line</u> : Unmodified Molodensky, <u>circles</u> : Improved Molodensky Truncation Method, $\bar{n}=10$).....	57
13	Horizontal Disturbance Truncation Error at Altitude H=5 km as a Function of Cap Radius, When Using a Reference Field of Degree $N_{ref}=20, 36, 180, 360$ Under an Unmodified Molodensky Truncation Method. (<u>solid</u> <u>line</u> : Commission plus Omission Error; <u>circles</u> : Omission Error Only).....	58
14	Horizontal Disturbance Truncation Error at Altitude H=5 km as a Function of Cap Radius, When Using a Reference Field of Degree $N_{ref}=20, 36, 180, 360$ Considering Commission plus Omission Error (<u>solid</u> <u>line</u> : Unmodified Molodensky; <u>circles</u> : Improved Molodensky Truncation Method, $\bar{n}=10$).....	58
15	Radial or Horizontal Gravity Disturbance Information (RMS) Beyond a Given Harmonic Degree N_{min} , for Various Altitudes H Above the Earth, for the Residual- Topography Reduced Field with Airy-Heiskanen Com- pensation Depth D=30 km.....	65
16	Altitudes for 1%, 3%, and 10% Relative Omission Error in Radial or Horizontal Gravity Disturbance, for a Given Maximum Degree N_{max} of Field Represen- tation, for the Residual-Topography Reduced Field with Airy-Heiskanen Compensation Depth D=30 km.....	65

17	Percentage Error of Various Disturbance Fields at a Given Altitude, Due to a 1.5 km Error in the Vertical Position of the Boundary Surface for the Anomaly Data..	68
18	Notations for Gravity Disturbance Vector Modeling.....	71
19	Topography in a Portion of the New Mexico Test Site. Contour Interval = 50 meters.....	77
20	Faye Anomalies in a Portion of the New Mexico Test Site. Contour Interval = 5 mgals.....	77
21	Refined Bouguer Anomalies in a Portion of the New Mexico Test Site. Contour Interval = 5 mgals.....	78
22	Residual Refined Bouguer Anomalies in a Portion of the New Mexico Test Site. Contour Interval = 5 mgals..	78
23	180x180 Spherical Harmonic Expansion of the Topography and Trajectory Foot Points in the New Mexico Test Site. Contour Interval = 50 meters.....	80
24	Rapp-180 Spherical Harmonic Expansion of the Radial (δ_r), North-South (δ_θ), and East-West (δ_λ) Disturbance Components at Altitudes 0 and 30 km in the Vicinity of the Test Trajectories in New Mexico. Contour Interval = 5 mgals.....	81
25	Test Points and Inner Zone Data Configuration, New Mexico.....	82
26	Gravity Anomaly Auto-Covariance Functions on the Mean Earth Sphere ($R = 6371$ km), Generated from White Noise Distribution of Gravity Anomaly (top diagram) and Disturbing Potential (bottom diagram) on an Internal Sphere of Depth $D = 10, 20, 30, 50, 100, 500$ km. Diagrams reveal that for the White Noise Gravity Anomaly System there is correlation length $\zeta \approx 1.5 D$, and for the White Noise Disturbing Potential System $\zeta \approx 0.75 D$	115
27	Gravity Anomaly Auto-Covariance Function on the Mean Earth Sphere ($R = 6371$ km), Tailored from the Tscherning and Rapp (1974) Covariance Model by Using Different Depths D to the Internal Sphere ($D = 1, 2, 3, 5, 10, 15$ km) and Subtracting Lower Harmonics $3 \leq n \leq N$ (left to right; $N = 20, 36, 180$). Very short correlation lengths on the order of 15 km can only be obtained by subtracting the lower 180 harmonics.....	116

- 28 Point Location of Surface Gravity Anomalies, Manitoba, Canada (plotted from Sjöberg, 1978, Tables 8.1 and 8.2). Circles: observation points; crosses: withheld prediction points..... 118
- 29 Two Gravity Anomaly Solutions (C.I. = 5 mgals) for the Area Marked off in Figure 28. Predicted Using the Dirac Approach with Gravity Anomaly Impulses on the Internal Sphere of Radius = (6371 km - D). Left: D = 30 km; Right: D = 75 km; No. of iterations = 5..... 118

1. INTRODUCTION

1.1 This Work vs. Katsambalos (1981)

This work is concerned with the computation of the gravity disturbance vector external to the earth, from given gravity anomaly data referred to the earth's surface. The central problem is how to rigorously account for the irregular shape of the topographic surface to which the data refer. This work is a continuation of the work of Katsambalos (1981) entitled "Simulation Studies on the Computation of the Gravity Vector in Space from Surface Data Considering the Topography of the Earth".

There are a number of differences between the present work and that of Katsambalos. One difference is the emphasis placed in the present study upon the use of suitable models for the separate modeling of different frequency ranges of the total disturbance vector signal. To this end, greater attention than that in Katsambalos' Section 9.3 is now given to the use of the spherical harmonic representation to model the low frequency components of the signal. And, as an entirely new addition to the work of Katsambalos, a study is now made of modeling the very high frequency components of the signal as the integrated gravitational effects of certain shallow topographic masses of assumed constant density. The representation by topographic mass effects, in which the input consists of detailed terrain elevation data, is advocated in the works of Tscherning and Forsberg (see Tscherning (1979), Forsberg and Tscherning (1981), Tscherning and Forsberg (1983), Forsberg (1984)). The residual signal field, left after subtracting from the total field the fields already represented by spherical harmonics and topographic mass effects, is a relatively smooth and low energy field.

As suitable models for representing the residual field, a study is made here of the classical integral model, the so-called Dirac approach, and the least squares collocation approach, which are models studied also in Katsambalos (ibid). In contrast to Katsambalos, the present study relies upon the use of the classical integral model, but with mean topography accounted for, as one of viable complementary models that can be operationally used. For the Dirac and least squares collocation approaches the present study gives an expanded presentation over that of Katsambalos, in order to be able to numerically experiment on different possible models that actually fall under the heading of being Dirac or least squares collocation approaches. Specifically, point mass modeling and point dipole modeling are experimented on under the heading of being Dirac approaches, in addition to experimenting on the

usual modeling by gravity anomaly impulses on an internal sphere (Katsambalos, *ibid*, Chapter 6). Under the least squares collocation approach, experiments are performed using empirical covariance functions that are based on white noise gravity anomaly and white noise disturbing potential distributions on an internal sphere. Finally, the present study has taken into account the questions raised by Bjerhammar and Sjöberg (1982, private communications) and by Tscherning (1983a) about Katsambalos' conclusions on the Dirac and least squares collocation approaches.

For numerical experimentations the present study has now used real, as opposed to simulated, gravity and terrain elevation data. This allows for the verification and evaluation of various theoretical models as applied to the actual variations present in the earth's gravity field. A detailed study of the spectral characteristics of the spatial disturbance vector signal, as well as its response to gravity anomaly data of varying resolution and distance away from the computation point, is given (Chapter 3) to help in the design of models and numerical experiments.

It should be mentioned that the Green's approach studied also in Katsambalos is not at all used in the present study. The reason is that the said approach requires as data gravity disturbances and disturbing potentials on the earth's surface, the elevations of the surface points, and the North-South and East-West components of the surface inclinations. These data are very difficult or impossible to obtain with sufficient accuracy and density in an operational environment.

1.2 Preliminaries

We use the following conventional notations of gravimetric geodesy:

- \vec{g} gravity vector of the earth, referred to simply as gravity vector
- $\vec{\gamma}$ gravity vector of the reference ellipsoid, referred to as normal gravity vector
- g magnitude of \vec{g} , referred to as gravity
- γ magnitude of $\vec{\gamma}$, referred to as normal gravity
- W potential of \vec{g} (i.e., $\vec{g} = \text{grad } W$), referred to as gravity potential
- U potential of $\vec{\gamma}$ (i.e., $\vec{\gamma} = \text{grad } U$), referred to as normal gravity potential.

In the above we are working in a body-fixed coordinate system (i.e., one rotating with the earth or ellipsoid), and the gravity vector is the resultant of the body's gravitational force and the centrifugal force of the system's rotation.

Fundamental to most gravimetric analyses is the disturbing potential T , defined as

$$T = W - U. \quad (1.1)$$

The force associated with T is the gravity disturbance vector $\vec{\delta}$, i.e.,

$$\vec{\delta} = \text{grad } T. \quad (1.2)$$

Based on the above definitions, $\vec{\delta}$ can also be written in the familiar form:

$$\vec{\delta} = \vec{g} - \vec{\gamma}. \quad (1.3)$$

Equation (1.3) forms a basis for modeling the gravity vector \vec{g} , as the sum of $\vec{\gamma}$ and $\vec{\delta}$. The sum is dominated by the normal gravity vector $\vec{\gamma}$, which is rigorously computable (see, e.g., Heiskanen and Moritz, 1967, sec. 6-2). For the spatial gravity disturbance vector $\vec{\delta}$, no closed computational formulas exist, but its accurate modeling from observational data on the earth's surface is precisely the subject of the present study.

Basically, the modeling of $\vec{\delta}$ proceeds through its relation (1.2) to the fundamental function T . In turn the function T can be linked to quantities obtainable from observations, most commonly the gravity anomaly. Indeed, in this report we use the gravity anomaly as fundamental data for our modeling procedures. In the following we detail the precise meaning of the quantity referred to as gravity anomaly, and discuss the relationship between gravity anomaly and disturbing potential T .

We have the following conventional definition of gravity anomaly at a point P (Heiskanen and Moritz, 1967, pp. 83, 91; Moritz, 1980, p. 353; Jekeli, 1981, pp. 39, 120; Moritz, 1983, pp. 4-7):

$$\Delta g_P = g_P - \gamma_Q. \quad (1.4)$$

That is, the gravity anomaly at P is the difference: gravity at P minus normal gravity at some point Q . Point Q is called the normal point of P , and is established such that (a) the normal gravity potential U at Q is equal to the actual gravity potential W at P (see Figure 1):

$$U(Q) = W(P), \quad (1.5)$$

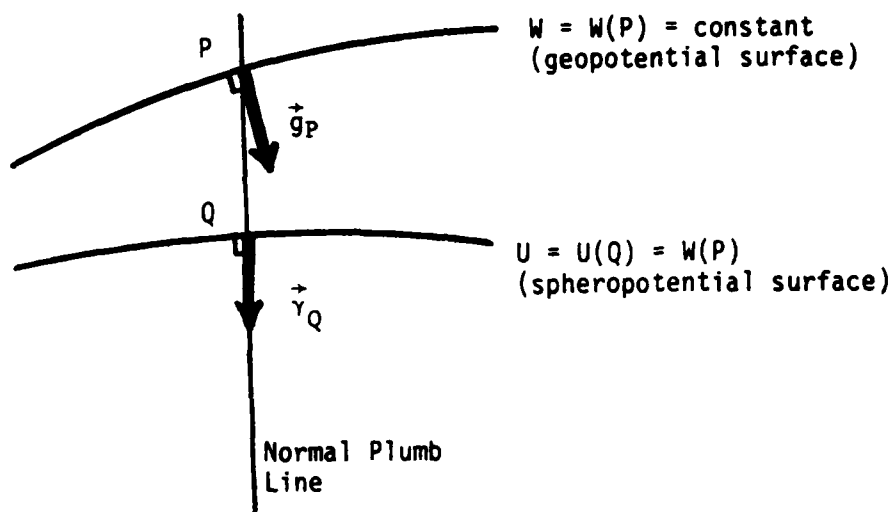


Figure 1. Construction of the Gravity Anomaly.

and that (b) P and Q lie on the same plumb line of the normal gravity field. The gravity anomaly (1.4) is distinct from the gravity anomaly vector, defined as (Heiskanen and Moritz, 1967, p. 83):

$$\Delta \vec{g}_P = \vec{g}_P - \vec{\gamma}_Q. \quad (1.6)$$

Jekeli (1981, Chapter 4) shows that the definition (1.4) leads to the following rigorous relation between the gravity anomaly and the disturbing potential at a point:

$$\Delta g_P = - \frac{\partial T_P}{\partial h_P} + \frac{1}{\gamma_P} \frac{\partial \gamma_P}{\partial h_P} T_P + \varepsilon_P + O(e^4), \quad (1.7)$$

with

$$\varepsilon_P = \frac{\partial W_P}{\partial h_P} - \frac{\partial W_P}{\partial H_P}, \quad (1.8)$$

and where

$\frac{\partial}{\partial H}$ derivative along the plumb line of the actual gravity field

$\frac{\partial}{\partial h}$ derivative along the plumb line of the normal gravity field; this is not distinguished from the derivative along the straight ellipsoidal normal (see *ibid.*, p.119)

$O(e^4)$ indicates that the omitted terms are on the order of $e^4 \Delta g < 0.01$ mgal (e^2 = square of eccentricity ≈ 0.0067 ; and Δg has a maximal value of 300 mgal).

The term ε_p of (1.8) is dependent on the deflections of the vertical (*ibid.*, eqs. (4.8), (4.22)), and has a magnitude of less than 0.34 mgal. Retaining only the first two terms and dropping the subscripts in (1.7), we obtain:

$$\Delta g = - \frac{\partial T}{\partial h} + \frac{1}{\gamma} \frac{\partial \gamma}{\partial h} T. \quad (1.9)$$

Equation (1.9) is exactly the same as the boundary condition that results from conventional linearizations of Molodensky's boundary value problem (see e.g., Molodenskii et al., 1962, chap. V, or Heiskanen and Moritz, 1967, sec. 8-5). Moritz (1980, p.336) writes that such linearizations are "practically sufficiently accurate but not completely rigorous". In the rigorous linearization of Krarup (1973) (see Moritz, *ibid.*, pp. 337-349) the resulting boundary condition is of the form (1.9) also, but with Δg interpreted as the component of the gravity anomaly vector (see (1.6)) in the downward direction of the isozenithal and with the derivatives taken along the direction of the isozenithal. For practical modeling problems, which is our interest in the present report, it is convenient to use (1.9) in our original meaning that Δg is the gravity anomaly (1.4) and that derivatives are taken along the ellipsoidal normal. Moritz (*ibid.*, pp. 352-353) has termed (1.9) as the "practical boundary condition".

Under the so-called spherical approximation (Heiskanen and Moritz, 1967, pp. 87-88), the normal derivative is approximated by the radial derivative,

$$\frac{\partial}{\partial h} \approx \frac{\partial}{\partial r}, \quad (1.10)$$

and the normal gravity is approximated by the attraction of a homogeneous sphere,

$$\gamma \approx \frac{kM}{r^2} \quad (1.11)$$

with kM being the geocentric gravitational constant. Under (1.10) and (1.11), (1.9) transforms to the usual spherical approximation:

$$\Delta g = - \frac{\partial T}{\partial r} - \frac{2}{r} T. \quad (1.12)$$

From Jekeli (ibid., pp. 122-123) a more rigorous transformation of (1.9) neglecting only terms of $O(e^4)$ can be written as follows:

$$\begin{aligned} \Delta g = & - \frac{\partial T}{\partial r} - \frac{2}{r} T - e^2 \sin \bar{\phi} \cos \bar{\phi} \frac{\partial T}{r \partial \bar{\phi}} + \\ & + \left[6J_2 \frac{a^2}{r^3} P_2(\sin \bar{\phi}) - 3 \frac{\omega^2 r^2}{kM} (1 - \sin^2 \bar{\phi}) \right] T. \end{aligned} \quad (1.13)$$

To review standard notations, we have:

$r, \bar{\phi}, \lambda$ geocentric radius, geocentric latitude, and longitude of the point to which the Δg and T refer

e eccentricity of the reference ellipsoid

J_2 second degree zonal harmonic of the normal gravity field

P_2 second degree Legendre polynomial

a semi-major axis of reference ellipsoid

kM geocentric gravitational constant

ω rotational speed of the earth.

Equation (1.13) is of the form of (1.12), but with two terms on the order of e^2 added to correct for the effect of spherical approximation in (1.12). To see that the last term of (1.13) is $O(e^2)$, refer to Equations (2.14) and (2.15) of Chapter 2. The first correction term of (1.13) corrects the first term of (1.12), and the second correction term corrects the second term of (1.12). If terms on the order of the earth's flattening f ($f \approx e^2/2 \approx 0.003$) are neglected, then (1.13) reduces to (1.12).

Indeed, the formal meaning of spherical approximation is the neglect of terms on the order of f in equations such as (1.13) relating quantities of the anomalous gravity field. The anomalous

gravity field is the one associated with the disturbing potential T . A useful geometric meaning of spherical approximation is given in Moritz (1980, pp. 351-352). This meaning is in terms of a spatial mapping of points, as shown in Figure 2.

It is shown that a point P with geocentric coordinates $(r, \bar{\phi}, \lambda)$ is mapped onto a point P' with geocentric coordinates $(R + h, \phi, \lambda)$, where R is a mean earth radius (usually, $R = 6371$ km), h is the height of point P above the reference ellipsoid, and ϕ is the geodetic latitude of P . The spherical approximation consists in using P' instead of P in all calculations. Formally, this means using $(R + h, \phi)$ as geocentric (radius, latitude) in all calculations.

Finally, below we outline the procedure by which the gravity anomaly as defined in (1.4) can be obtained from observational data on the earth's surface. More details can be found in Rapp (1984, pp. 3-7). The procedures result in gravity anomalies that refer to the earth's surface, and these anomalies are the fundamental data for our modeling procedures in this report. We have the following steps:

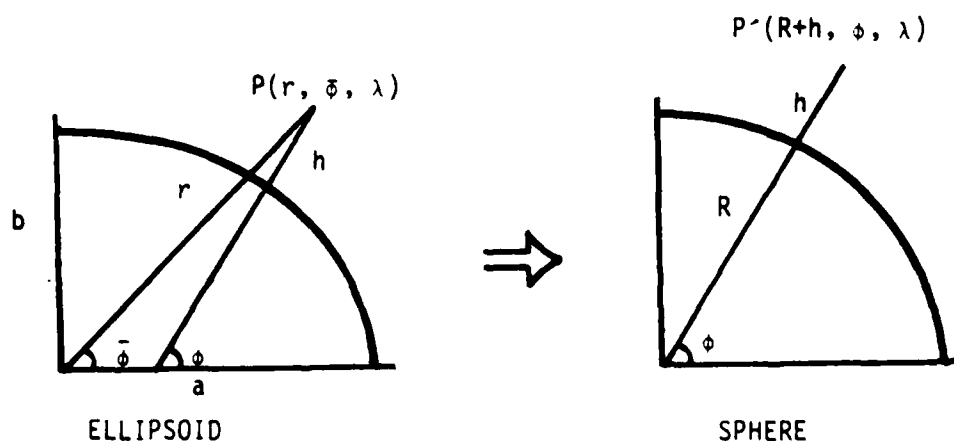


Figure 2. Mapping Under the Spherical Approximation

- a) gravity g_p is measured on the earth's surface
- b) by leveling procedures the potential difference denoted by C_{pi} is obtained, where

$$C_{pi} = W_p - W_{oi} \quad (1.14)$$

with

W_p gravity potential at P

W_{oi} gravity potential on the i th equipotential surface of the earth's gravity field being used as reference surface of leveling. The reference surface of leveling is also referred to as "height datum" or "vertical datum". The index i is used to account for the realistic case of several different height datums being used in different parts of the world, i.e., there is no unique world vertical datum at present.

- c) A "normal height" H_i^* (Heiskanen and Moritz, 1967, sec. 4-5) can be obtained from:

$$H_i^* = \frac{C_{pi}}{\gamma} \quad (1.15)$$

where γ is an average value of normal gravity along the plumb line.

- d) A normal gravity is computed:

$$\gamma_i = \gamma(H_i^*, \phi_p, \lambda_p), \quad (1.16)$$

i.e., as the normal gravity at geodetic coordinates $(H_i^*, \phi_p, \lambda_p)$. In practice, it is satisfactory here to use instead of H_i^* the orthometric height H_i (Cruz and Laskowski, 1984, eq. (3.1.4)).

- e) A gravity anomaly is computed:

$$\Delta g_i = g_p - \gamma_i. \quad (1.17)$$

- f) The Δg_i of (1.17) should then be corrected to yield the gravity anomaly Δg defined by (1.4). We first define (Rapp, 1984, eqs. (13), (22)):

$$\Delta W = W_0 - U_0 \quad (1.18)$$

$$\Delta W_{0i} = W_0 - W_{0i}, \quad (1.19)$$

where

W_0 gravity potential on an assumed world vertical datum (e.g., the geoid)

U_0 normal gravity potential on the surface of the equipotential reference ellipsoid.

Then, the Δg of (1.4) can be obtained from the Δg_i of (1.17) as follows (see Rapp, *ibid.*, eq. (29)):

$$\Delta g = \Delta g_i + \frac{2}{r} \Delta W_{0i} - \frac{2}{r} \Delta W. \quad (1.20)$$

- g) Theoretical developments in gravimetric geodesy have been considerably simplified by assuming the disturbing potential T to be a harmonic function outside the earth's attracting masses. To satisfy this assumption the mass of the atmosphere must be computationally removed from the problem. As it is, for example, the force of "gravity" measured in step (a) includes the attraction of the atmosphere at the point P . The removal of the atmosphere from the main modeling problem, and its subsequent restoration in the final result, can be done in a simple way because of the smallness of atmospheric effects. The theory is discussed in Moritz (1980, pp. 422-425). As a practical procedure for removing atmospheric effects from gravity anomaly data, the mass of the atmosphere is first added to the mass of the earth to form the defined mass of the reference ellipsoid. This affects the value of γ_i in (1.17). Then an "atmospheric correction" δg_A is added to the computed gravity anomaly Δg_i of (1.17) to get the corrected anomaly Δg_i^* :

$$\Delta g_i^* = \Delta g_i + \delta g_A. \quad (1.21)$$

Values of δg_A (<1 mgal) are tabulated as a function of height h in IAG (1970, pp. 72-73). The Δg_i^* instead of Δg_i is the value to use in (1.20) to yield the Δg as defined by (1.4), under the assumption that there is no atmosphere.

- h) Another simplifying procedure in gravimetric computations is the removal of the zero and first degree spherical harmonic terms of the disturbing potential T from the main modeling problem. These terms can be modeled using a separate set of procedures (see, e.g.,

Heiskanen and Moritz, 1967, pp. 98-99, 107). The first degree terms do not specifically affect the gravity anomaly Δg , which is related to T through (1.12). The effect of the zero degree term can be removed from gravity anomaly data Δg_i , to get the corrected value Δg_i^1 , as follows (see Rapp, 1984, p.8):

$$\Delta g_i^1 = \Delta g_i + \frac{\Delta kM}{r^2}, \quad (1.22)$$

where $\Delta kM = kM - kM_E$; kM_E is the gravitational constant of the reference ellipsoid.

- i) Summarizing, the gravity anomaly that satisfies (1.4) under the simplification of steps (g) and (h) is:

$$\Delta g = \Delta g_i + \delta g_A + \frac{2}{r} \Delta W_{0i} - \frac{2}{r} \Delta W + \frac{\Delta kM}{r^2}, \quad (1.23)$$

where the Δg_i is from (1.17).

1.3 Scope of This Study

Gravity anomalies that refer to the earth's surface will be the fundamental data for our modeling procedures in this report. The topography itself is defined through the ellipsoidal heights of surface points. Such heights are, for the purposes of analyzing the anomalous gravity field, not distinguished from available orthometric heights or some approximate heights from topographic maps or digital terrain models (Moritz, 1980, p. 357).

First, we account for the fact that spherical harmonic series representation has turned out to be a very efficient representation of the anomalous gravity field up to some limited resolution (see, e.g., Tscherning, 1983b). Therefore, in Chapter 2 we discuss the re-parameterization of the long-wavelength part of the anomalous gravity field from the given surface gravity anomalies to a set of spherical harmonic coefficients of the earth's disturbing potential. Currently envisioned maximum degree of spherical harmonic expansions is around $n = 360$, corresponding roughly to a $30' \times 30'$ resolution. Theoretical and practical problems associated with the determination of the coefficients in such high degree expansions, using a combination of coefficients derived from satellite motion analysis and of coefficients implied by terrestrial gravity anomaly information, are recently reviewed and discussed in Rapp (1984). Our specific concern in Chapter 2 is the computation of spherical harmonic coefficients from surface gravity anomaly data, in a manner that takes into account the problems of ellipticity and topography of the earth. These problems are also

discussed in Rapp (ibid.), with references to the treatment of ellipticity by Pellinen (1982). Our contribution via Chapter 2 is in providing a geometric interpretation to the so-called ellipsoidal correction terms derived in Pellinen (ibid.), by using elementary Taylor series considerations in re-deriving those terms. Using this geometric interpretation in combination with the treatment of topography in Rapp (1984) we form recommendations on the computation of harmonic coefficients from surface gravity anomaly data. These recommendations have some differences with those of Rapp (ibid.).

The spherical harmonic representation is feasible only up to some limited resolution, currently on the order corresponding to a maximum harmonic degree of about $n = 360$. Problems that increase in importance with unlimited increase in the degree of spherical harmonic representation include (a) the effects of series divergence below the smallest sphere bounding the earth (see, e.g., Jekeli, 1981; Colombo, 1982); (b) the computer storage and time requirements for handling a very large number of coefficients (see Tscherning et al., 1983); and (c) the determination of the coefficients of the series, causing problems on computer requirements, numerical quadratures and the implementation of a relation between coefficients and gravity anomaly data that accounts for the earth's ellipticity and topography (see Rapp, 1984). Therefore, to complete the modeling of the gravity field up to very detailed resolutions, the globally valid spherical harmonic representation must be complemented by locally valid solutions.

Before embarking on a detailed study of various locally valid models, in Chapter 3 we first present a familiarization study of our signal of interest, namely, the gravity disturbance vector in space. The information in Chapter 3 will help in the design of solutions and numerical experiments. Spherical earth formulas for spherical harmonic and integral representations of the disturbance vector are first reviewed in Section 3.1. The neglect of the earth ellipticity and topography should not affect the conclusions of the chapter, and at the same time allows for the use of spectral analysis. In Section 3.2, spectral analysis yields the power of the signal within a given frequency range, as a function of altitude in space. Knowledge of such power distributions is useful for determining the model resolutions required for representing all significant signal energies at a given altitude. In Section 3.3 the so-called truncation theory yields the sensitivity of the signal at a given altitude, to gravity anomaly data of certain resolution and distance away from the computation point. Such information is useful for minimizing the required data cap size for a given resolution of gravity anomaly data. In Section 3.3 we also examine the use of different truncation theories, namely, the unmodified Molodensky truncation, Meissl truncation, Wong/Gore truncation, and Improved Molodensky truncation as applied to disturbance vector computations at altitude.

In Chapter 4 we begin to look at the modeling of the entire frequency range of the disturbance vector signal, from low to high

frequencies. In Section 4.1 some general considerations are first given to help understand the effect of the non-spherical shape of the boundary surface (i.e., the topography to which the given gravity anomaly data refer) on the modeling of the external disturbance vector field. Then in Section 4.2 a composite model is presented that in principle models the total disturbing potential T in space as the sum of three components:

$$T = T^s + T^0 + T^t, \quad (1.24)$$

where

T^s long wavelength component, generated from the spherical harmonic representation;

T^t short wavelength component, generated as the potential of certain shallow topographic masses of assumed constant density;

T^0 medium wavelength residual component, equal to whatever is the difference ($T - T^s - T^t$). The T^0 is modeled in Section 4.2.2 using the classical direct integration of gravity anomaly data, with mean topography accounted for.

The gravity anomalies Δg^0 that are integrated to yield T^0 are expressed through (1.12):

$$\Delta g^0 = - \frac{\partial T^0}{\partial r} - \frac{2}{r} T^0, \quad (1.25)$$

which by definition of T^0 becomes:

$$\Delta g^0 = \left[- \frac{\partial T}{\partial r} - \frac{2}{r} T \right] - \left[- \frac{\partial T^s}{\partial r} - \frac{2}{r} T^s \right] - \left[- \frac{\partial T^t}{\partial r} - \frac{2}{r} T^t \right], \quad (1.26)$$

or

$$\Delta g^0 = \Delta g - \Delta g^s - \Delta g^t, \quad (1.27)$$

i.e., the Δg^0 is the residual anomaly left after subtracting from the original anomaly Δg the anomalies Δg^s implied by T^s and Δg^t implied by T^t . Note that Δg^0 continues to refer to the earth's surface.

The components of the disturbance vector corresponding to T^s , T^0 , and T^t are:

$$(\delta^s, \delta^0, \delta^t) = \text{grad}(T^s, T^0, T^t), \quad (1.28)$$

and the total disturbance vector is then modeled as:

$$\delta = \delta^s + \delta^0 + \delta^t. \quad (1.29)$$

In Section 4.3 numerical experiments are conducted on the complete modeling of δ using (1.29). In all experiments real gravity anomaly and elevation data are used over a $7^\circ \times 9^\circ$ mountainous test area in New Mexico. Of special interest are the experiments that give a feeling for how well the δ^0 can absorb the resulting unmodeled part caused by the omission of either δ^s or δ^t in (1.29). The ability of δ^0 to absorb δ^s is mainly related to the size of the anomaly data cap used in δ^0 . The ability of δ^0 to absorb δ^t is related to the modeling error introduced by accounting only for a mean topography, and not for the full variations of the topography, in computing δ^0 from the surface data Δg^0 .

The solution expressed by (1.24) may be called a continuous approach, since the underlying theories assume a continuous coverage of the earth's surface by gravity anomaly data. Under this continuous approach the integration of anomaly data for the computation of the residual potential T^0 must strictly be performed along the earth's surface where the data refer. Molodensky and later Brovar have written the solution in terms of a series of integrals (see Moritz, 1980, secs. 43 and 44, with reference to Molodenskii, et al., 1962 and Brovar, 1964). However, there is an equivalent solution which is convenient for conceptualizations and discussions, because it is full of physical meaning. Details of this solution are given in Heiskanen and Moritz (1967, sec. 8-10 and pp. 324-325, with reference to Bjerhammar, 1964) and in Moritz (1980, secs. 45, 46 and pp. 419-420). The solution consists of (a) analytical continuation of surface anomaly data to a level surface, followed by (b) classical integration along the level surface as approximated by a sphere (see Figure 2).

In practice, the computation of analytically continued anomalies poses rather severe data density and accuracy requirements especially in areas of rough gravity field (see, e.g., Noe, 1980). Therefore, the motivation of the form (1.24) is to make the field T^0 as smooth as possible, by "moving" the high frequency components of T away from T^0 into T^t . With T^0 smooth, the difference between the surface anomalies Δg^0 of (1.27) and the corresponding analytically continued anomalies can be so small as to be negligible. This way we avoid the specific computation of analytically continued anomalies by simply equating these anomalies to the surface anomalies. Numerical investigations related to

these ideas are also included in Chapter 4.

A more rigorous way to avoid the above analytical continuation computations of the continuous approach would be to perform collocation in space (see Moritz, 1983, p. 31). The theory is reviewed and numerical investigations performed in Chapter 5 of this study. Two approaches to collocation are studied here, namely, the so-called Dirac approach and the least squares collocation approach. Collocation is a discrete approach, i.e., the theory assumes the data to be given only at a finite number of discrete points on the earth's surface. The collocation solution yields an approximation to the disturbing potential, that (a) is harmonic down to an internal sphere (spherical approximation) completely embedded within the earth and (b) satisfies the data at the given points. For feasible economy and convergence of solution, it is still desirable to use the complementary models T^s and T^t as much as possible, as in (1.24). In this case we have the model:

$$T = T^s + T^c + T^t, \quad (1.30)$$

where T^c denotes the residual component

$$T^c = T - T^s - T^t, \quad (1.31)$$

as modeled by collocation procedures from the gravity anomaly data (see (1.27)):

$$\Delta g^c = \Delta g^0 = \Delta g - \Delta g^s - \Delta g^t. \quad (1.32)$$

Corresponding to (1.29) we now have:

$$\delta = \delta^s + \delta^c + \delta^t \quad (1.33)$$

with

$$\delta^c = \text{grad } T^c. \quad (1.34)$$

As before, of special interest in the numerical studies in Chapter 5 would be to see how well δ^c can absorb the resulting unmodeled part caused by not using δ^t in (1.33). The discrete model δ^c would expectedly absorb δ^t better than would the continuous model δ^0 of (1.29), because of the more rigorous way that the topography is taken into account in the collocation procedures. This point is numerically

studied in Section 5.4.3.

Finally, a summary along with conclusions and recommendations are given in Chapter 6.

2. ON THE RECOVERY OF POTENTIAL COEFFICIENTS FROM SURFACE GRAVITY ANOMALIES

Various theoretical and operational aspects of solving the problem have been recently reviewed by Rapp (1984), discussing also the combination of the resulting coefficients with those derived from satellite motion analysis. In this chapter we focus on one aspect of the problem, namely, the development of a mathematical relation between potential coefficients and surface gravity anomaly data that accounts for the topography and ellipticity of the earth. A feasible solution is to first analytically continue the surface values to values that refer to a sphere, and then use these values on a sphere for directly determining potential coefficients using the orthogonality relationships of spherical harmonics. The question lies on how, and to which sphere, the analytical continuation should be done, and it is to this discussion that we propose to contribute in this chapter.

The disturbing potential T can be represented in spherical harmonics, usually in the following form which is convenient in connection with satellite dynamics (see Rapp, 1982b, (5)):

$$T(r, \bar{\phi}, \lambda) = \frac{kM}{a} \sum_{n=2}^{\infty} \sum_{m=-n}^n \left(\frac{a}{r}\right)^{n+1} \bar{C}_{nm}^* \bar{Y}_{nm}(\bar{\phi}, \lambda), \quad (2.1)$$

where

\bar{C}_{nm}^* potential coefficients. The overbar denotes full normalization, and the asterisk denotes the subtraction of the potential coefficients of the reference ellipsoid;

$$\bar{Y}_{nm}(\bar{\phi}, \lambda) = \bar{P}_{n|m|}(\cos \bar{\phi}) \begin{cases} \cos m\lambda, & m \geq 0 \\ \sin |m|\lambda, & m < 0 \end{cases} \quad (2.2)$$

$\bar{P}_{n|m|}(\cos \bar{\phi})$ fully normalized Legendre functions of degree n and order $|m|$.

Now taking (2.1) in conjunction with either (1.12) or (1.13), one can conceive the recovery of the coefficients \bar{C}_{nm}^* from given gravity anomaly data. For our purposes we will use the more accurate (1.13), especially

since it turns out that its more complicated form does not add any serious difficulties to the techniques of recovery that we will discuss.

First we ask, to which sphere should the surface gravity anomalies be analytically continued? The answer is ultimately the equatorial sphere of radius $r=a$, since the coefficients \bar{C}_{nm}^* as defined through (2.1) actually refer to this sphere. This is the reason why, for example, although Rapp (1984, pp. 17-18) initially upward continued the surface anomalies to the sphere of radius $r_b \approx a + 6$ km bounding the earth, the factor $(r_b/a)^{n+2}$ had to be eventually present (see *ibid.*, (53)) in order to downward continue the bounding sphere anomalies back to the equatorial sphere where the values are directly needed for the determination of \bar{C}_{nm}^* . Since the sphere $r = a$ partly penetrates the earth's masses, it can be questioned whether the required analytical continuation exists for the true disturbing potential T . However, here we avoid this problem by taking the view that we are working within the context of solving the Bjerhammar problem. That is, we are using the harmonic function T expressed by (2.1) to approximate the true T , and such function (2.1) is indeed convergent on the sphere $r = a$ and can be adjusted to agree with observational data through the free parameters \bar{C}_{nm}^* . The instability that arises from the downward continuation of surface data to the embedded part of the sphere $r = a$ is remedied by the fact that we are developing (2.1) only up to some limited resolution, expressed by truncating the series at some maximum

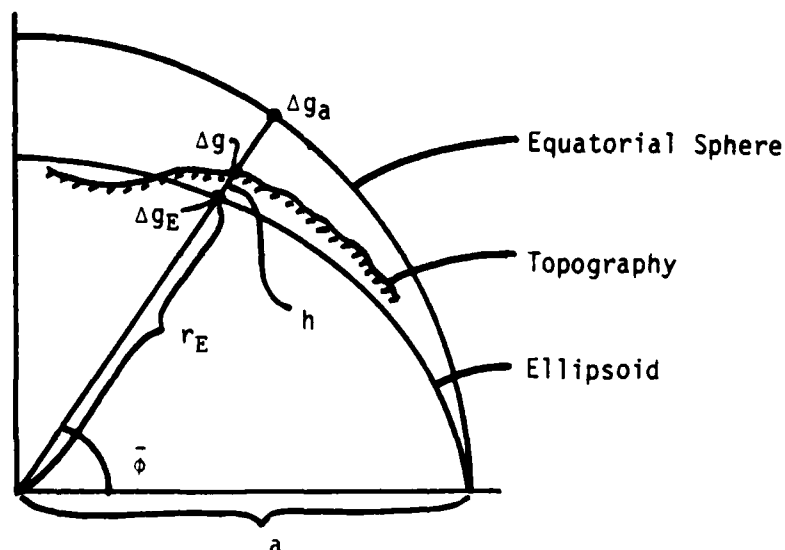


Figure 3. Gravity Anomalies on Different Boundary Surfaces.

harmonic degree N_{\max} (see Jekeli, 1981, pp. 10-11)

The next question is how to implement the analytical continuation from the topographic surface to the sphere $r = a$. This can be done by first reducing the data from the earth's surface to the ellipsoid or the geoid as follows (see Rapp, *ibid.*, p. 15):

$$\Delta g_E = \Delta g - \frac{\partial \Delta g}{\partial r} h + \frac{1}{2!} \frac{\partial^2 \Delta g}{\partial r^2} h^2 - \dots \quad (2.3)$$

where Δg refers to the earth's surface, Δg_E refers to the ellipsoid, and h can be considered the orthometric height of the surface point. As a next step that we will detail later, the Δg_E will be continued to Δg_a referred to the equatorial sphere (see Figure 3).

Operationally the gradients in (2.3) can be obtained from an existing high degree spherical harmonic expansion, in application of the ideas in Rapp (*ibid.*, p. 20). The correction terms in (2.3) are then evaluated numerically and applied to the first term Δg to obtain Δg_E . Since in this operational solution (2.3) is not being implemented rigorously, it is appropriate that its application be limited to the continuation of Δg to Δg_E over the distance h , and that it is not used to continue Δg_E to Δg_a over the distance $(a - r_E)$. As can be seen in Rapp (*ibid.*, Table 1), the magnitudes of the correction terms to transform Δg to Δg_E are on the average an order of magnitude smaller than the terms to transform Δg_E to Δg_a .

For the continuation of Δg_E to Δg_a we implicitly use also a Taylor series expansion, analogous to (2.3), but this time we find that the Taylor series terms can be evaluated in an analytical as opposed to a numerical fashion. This is possible because the deviation between the surfaces of the ellipsoid and equatorial sphere is such a simple function of latitude that the Taylor terms themselves can be expanded in spherical harmonics. Therefore, we find that in a single derivation we can express the unknown potential coefficients in terms of Δg_E , without any need to continue Δg_E to Δg_a is a separate step. The starting point of the derivations is (1.13) applied on the ellipsoid:

$$\begin{aligned} \Delta g_E = & - \frac{\partial T_E}{\partial r_E} - \frac{2}{r_E} T_E - e^2 \sin^2 \phi \cos^2 \phi \frac{\partial T_E}{\partial r_E} + \\ & + \left[6J_2 \frac{a^2}{r_E^3} P_2(\sin \phi) - 3 \frac{\omega^2 r_E^2}{kM} (1 - \sin^2 \phi) \right] T_E, \end{aligned} \quad (2.4)$$

with T_E obtained by applying (2.1) on the ellipsoid:

$$T_E = \frac{kM}{a} \sum_{n=2}^{\infty} \sum_{m=-n}^n \left(\frac{a}{r_E} \right)^{n+1} \bar{C}_{nm}^* \bar{Y}_{nm}(\bar{\phi}, \lambda). \quad (2.5)$$

Before proceeding to the detailed derivation of \bar{C}_{nm}^* from Δg_E using (2.4) and (2.5), we should note that (2.5) implies the use of the series (2.1) below its sphere of guaranteed convergence, i.e., the sphere of radius $r = a$. However, numerical investigations by Jekeli (1981) using a realistic gravity field model would indicate that the use of (2.5) is justified at least up to maximum degrees N_{\max} of practical interest, e.g., N_{\max} around 300.

Let us now discuss the recovery of potential coefficients \bar{C}_{nm}^* occurring in (2.1), from an inversion of (2.4) with (2.5) given Δg_E . In our derivations we will arrive at so-called ellipsoidal correction expressions. A check of our derivations is provided by the agreement of certain expressions with those of Pellinen (1982) who also deals with ellipsoidal corrections. The newness of our results over those of Pellinen (ibid.) consists in deriving new equations (e.g., (2.33)-(2.36) giving ellipsoidal corrections when geocentric latitudes, not geodetic latitudes, are used as coordinates) and in using a different derivational approach. Our derivations use elementary Taylor series considerations and naturally lead to insightful physical interpretations of the various formulas. The general idea of the solution will be to first somehow transform (2.4) into the form:

$$\Delta g_E = \sum_{n=2}^{\infty} \sum_{m=-n}^n D_{nm\bar{\phi}} Y_{nm}(\bar{\phi}, \lambda) \quad (2.6)$$

where

$D_{nm\bar{\phi}}$ conventional spherical harmonic coefficients; these are constants independent of $(\bar{\phi}, \lambda)$; the subscript $\bar{\phi}$ is used to denote the use of geocentric latitude in the expansion.

$Y_{nm}(\bar{\phi}, \lambda)$ conventional spherical harmonics; the use of conventional as opposed to fully-normalized harmonics is for convenience in the derivations.

It will turn out after the transformation of (2.4) to the form (2.6) that the $D_{nm\bar{\phi}}$ are expressed as some function of the conventional potential coefficients C_{nm} (unnormalized counterpart of \bar{C}_{nm}^*), symbolically:

$$D_{nm\bar{\phi}} = f_1(C_{nm}), \quad (2.7)$$

An inversion of (2.7) yields, symbolically:

$$C_{nm} = f_1^{-1}(D_{nm}\bar{\varphi}) . \quad (2.8)$$

Meanwhile, the $D_{nm}\bar{\varphi}$ can also be directly obtained by an inversion of (2.6) given the Δg_E (see Heiskanen and Moritz, 1967, 1-70):

$$D_{n0}\bar{\phi} = \frac{2n+1}{4\pi} \int_{\sigma} \Delta g_E(\bar{\varphi}, \lambda) P_n(\sin \bar{\varphi}) d\sigma ;$$

$$D_{nm}\bar{\phi} = \frac{2n+1}{2\pi} \frac{(n-k)!}{(n+k)!} \int_{\sigma} \Delta g_E(\bar{\phi}, \lambda) Y_{nm}(\bar{\phi}, \lambda) d\sigma \quad (2.9)$$

($m \neq 0$; $k = |m|$).

Therefore, the combination of (2.8) and (2.9) yields the desired solution for the recovery of potential coefficients C_{nm} from Δg_E ; the full-normalization of C_{nm} yields C_{nm}^* (see (2.19) below) which is the final desired quantity. The just outlined solution involves several steps, which we will now describe.

First, let us collect the following relations where terms proportional to e^4 have been dropped (e is the earth's first eccentricity, $e^2 \approx 0.0067$):

$$r_E = a \left(1 - \frac{e^2}{2} \sin^2 \phi \right) + O(e^4) \quad (2.10)$$

$$\left(\frac{a}{r_E} \right)^{n+2} \approx 1 + \frac{n+2}{2} e^2 \sin^2 \phi \quad (2.11)$$

$$\left(\frac{a}{r_E} \right)^{n+1} \approx 1 + \frac{n+1}{2} e^2 \sin^2 \phi \quad (2.12)$$

$$P_2(\sin \phi) = \frac{3}{2} \sin^2 \phi - \frac{1}{2} \quad (\text{exact}) \quad (2.13)$$

$$J_2 \approx \frac{e^2}{6} \quad (\text{Heiskanen and Moritz, 1967, (2-118)}) \quad (2.14)$$

$$\frac{\omega^2 r_E^2}{kM} \approx \frac{e^2}{2a} \quad (\text{see ibid., (2-107), (2-127)}) \quad (2.15)$$

It is important to note that in order to maintain a certain accuracy level, the values of n and ϕ in equations of type (2.11) and (2.12) must be limited. For example, the next term in (2.11) is:

$$\frac{(n+2)(n+1)}{2!} \frac{e^2 \sin^4 \phi}{4} \quad (2.16)$$

and, if this term is not to exceed e^2 (say) then $n \leq 180$ and $\phi \leq 26^\circ$ (for example) - if n increases then ϕ must correspondingly decrease, and conversely, in order to still keep the term below e^2 . Therefore, analyses based on approximations such as (2.11) and (2.12) maintain a stated accuracy level up to a certain limited harmonic degree only.

Second, in the following developments it will be more in line with literature to use conventional rather than fully-normalized spherical harmonics. Instead of (2.5) we will therefore use:

$$T_E = \frac{kM}{a} \sum_{n=2}^{\infty} \sum_{m=-n}^n \left(\frac{a}{r_E} \right)^{n+1} C_{nm} Y_{nm}(\vartheta, \lambda), \quad (2.17)$$

where

C_{nm} conventional spherical harmonic potential coefficients;
coefficients are again referenced to a defined reference ellipsoid as in (2.1), but this time we do not denote this fact by an asterisk, for convenience in notation

Y_{nm} conventional spherical harmonics.

From Heiskanen and Moritz (1967, 1-73 and 1-78) we have these relations between conventional and fully normalized harmonics and their coefficients ($k = |m|$):

$$Y_{n0} = \frac{1}{\sqrt{2n+1}} \bar{Y}_{n0}$$

$$Y_{nm} = \sqrt{\frac{1}{2(2n+1)} \frac{(n+k)!}{(n-k)!}} \bar{Y}_{nm} \quad (m \neq 0) \quad (2.18)$$

$$C_{n0} = \sqrt{2n+1} \bar{C}_{n0}$$

$$C_{nm} = \sqrt{2(2n+1) \frac{(n-k)!}{(n+k)!}} \bar{C}_{nm} \quad (m \neq 0). \quad (2.19)$$

Third, let us re-write the various terms of (2.4). Using (2.17) and (2.11) the first two terms of (2.4) become:

$$\begin{aligned} -\frac{\partial T_E}{\partial r_E} - \frac{2}{r_E} T_E &= \frac{kM}{a^2} \sum_{n=2}^{\infty} \sum_{m=-n}^n (n-1) C_{nm} Y_{nm}(\vartheta, \lambda) + \\ &+ \frac{e^2 kM}{2a^2} \sum_{n=2}^{\infty} \sum_{m=-n}^n (n+2)(n-1) C_{nm} \sin^2 \vartheta Y_{nm}(\vartheta, \lambda). \end{aligned} \quad (2.20)$$

Note that for the purpose of (2.20) we used ϑ instead of ϕ in the (small) e^2 -term of (2.11). To re-write the third term of (2.4) we substitute (2.17), use (2.10) and (2.12), and neglect terms involving e^4 to get:

$$-e^2 \sin \vartheta \cos \vartheta \frac{\partial T_E}{r_E \partial \vartheta} = -\frac{e^2 kM}{a^2} \sum_{n=2}^{\infty} \sum_{m=-n}^n C_{nm} \sin \vartheta \cos \vartheta \frac{\partial Y_{nm}}{\partial \vartheta}(\vartheta, \lambda). \quad (2.21)$$

To re-write the last group of terms in (2.4), we first use (2.14), (2.10), (2.13), and (2.15) to simplify the quantity in brackets in (2.4); then we use (2.12) and (2.17); in all manipulations we drop terms involving e^4 ; we get:

$$\left[6J_2 \frac{a^2}{r_E^3} P_2(\sin \vartheta) - \frac{3\omega^2 r_E^2}{kM} (1 - \sin^2 \vartheta) \right] T_E = \frac{e^2}{a} (3 \sin^2 \vartheta - 2) T_E \quad (2.22)$$

$$\begin{aligned} &= \frac{3e^2 kM}{a^2} \sum_{n=2}^{\infty} \sum_{m=-n}^n C_{nm} \sin^2 \vartheta Y_{nm}(\vartheta, \lambda) - \\ &- \frac{2e^2 kM}{a^2} \sum_{n=2}^{\infty} \sum_{m=-n}^n C_{nm} Y_{nm}(\vartheta, \lambda). \end{aligned} \quad (2.23)$$

Fourth, let us write three relations that have always been found useful in ellipsoidal correction theory. The first of these relations is (see Moritz, 1980, 39-46):

$$\sin \vartheta \cos \vartheta \frac{\partial Y_{nm}(\vartheta, \lambda)}{\partial \vartheta} = a_{nm} Y_{n+2,m} + b_{nm} Y_{nm} + c_{nm} Y_{n-2,m}, \quad (2.24)$$

where (letting $k = |m|$)

$$\begin{aligned} a_{nm} &= \frac{-n(n-k+1)(n-k+2)}{(2n+1)(2n+3)} ; \\ b_{nm} &= \frac{n^2-3k^2+n}{(2n+3)(2n-1)} ; \\ c_{nm} &= \frac{(n+1)(n+k)(n+k-1)}{(2n+1)(2n-1)} . \end{aligned} \quad (2.25)$$

The second relation is (see *ibid.*, 39-76):

$$\sin^2\varphi Y_{nm}(\varphi, \lambda) = \alpha_{nm} Y_{n+2,m} + \beta_{nm} Y_{nm} + \gamma_{nm} Y_{n-2,m} \quad (2.26)$$

where (again letting $k = |m|$)

$$\begin{aligned} \alpha_{nm} &= \frac{(n-k+1)(n-k+2)}{(2n+1)(2n+3)} ; \\ \beta_{nm} &= \frac{(2n^2-2k^2+2n-1)}{(2n+3)(2n-1)} ; \\ \gamma_{nm} &= \frac{(n+k)(n+k-1)}{(2n+1)(2n-1)} . \end{aligned} \quad (2.27)$$

Note that the left hand sides of (2.24) and (2.26) occur in (2.20), (2.21), and (2.23), and this is why (2.24) and (2.26) are useful to us. Finally, the third useful relation is a simplifying relation, which says that a summation index can be shifted; for example (see *ibid.*, 39-48):

$$\sum_{n=2}^{\infty} = c_{nm} C_{nm} Y_{n-2,m} = \sum_{n=0}^{\infty} c_{n+2,m} C_{n+2,m} Y_{nm} . \quad (2.28)$$

It is to be noted that the use of relations such as (2.28) introduces zero and first degree (i.e., $n=0$ and $n=1$) harmonic terms in the formulas. However, as customary in gravimetric analyses, we will suppress these terms for convenience by always starting all summations from $n=2$. The consideration of these $n=0, 1$ terms can be treated as a separate problem, such as what was done in Lelgemann (1970), with numerical evaluations in Rapp (1981a), for geoid undulation computations.

Fifth, we substitute (2.20), (2.21), and (2.23) into (2.4), then use the relations (2.24) and (2.26). Summation indices are then shifted as in (2.28) in order to have only $Y_{nm}(\bar{\varphi}, \lambda)$, and not $Y_{n+2,m}(\bar{\varphi}, \lambda)$ or $Y_{n-2,m}(\bar{\varphi}, \lambda)$, occurring in the expression. All coefficients of $Y_{nm}(\bar{\varphi}, \lambda)$, which by now are all constants independent of position $(\bar{\varphi}, \lambda)$ are then collected to yield a coefficient which must then be exactly equal to the $D_{nm\bar{\varphi}}$ of (2.6). Observing further that, from (2.25) and (2.27):

$$a_{nm} = -n \alpha_{nm} \quad (2.29)$$

$$2b_{nm} = 3\beta_{nm} - 1 \quad (2.30)$$

$$c_{nm} = (n+1) \gamma_{nm} , \quad (2.31)$$

We finally get the simplified expression:

$$D_{nm\bar{\varphi}} = \frac{kM}{a^2} (n-1)C_{nm} + \frac{e^2 kM}{2a^2} \left\{ \frac{(n^2-n+2)}{2} \alpha_{n-2,m} C_{n-2,m} + \right. \\ \left. + \left[(n^2+n+1)\beta_{nm}-3 \right] C_{nm} + (n^2+3n+4) \gamma_{n+2,m} C_{n+2,m} \right\} . \quad (2.32)$$

which is in the form (2.7).

The last equation agrees with Pellinen (1982, eq. 14), after putting $m=e^2/2$ (cf. Moritz, 1980, 39-12). As in Pellinen (1982), underlining a term will mean that the term will be omitted for $n < 4$ (note in (2.32) that if $n=3$ for example, the underlined term will involve $C_{1,m}$ which is to be suppressed since we are suppressing all harmonics with $n < 2$).

Given the values Δg_E on the ellipsoid, the form (2.6) can actually be inverted to yield the constants $D_{nm\bar{\varphi}}$ directly. In fact, the inverted expression is (2.9). Therefore, we can assume that the $D_{nm\bar{\varphi}}$ on the left-side of (2.32) is known, and hence we are now in a position of being able to recover the potential coefficients C_{nm} occurring in (2.17), simply by inverting (2.32). To do the inversion, in the first place we set $e^2=0$ in (2.32) to get the spherical approximation solution:

$$C_{nm\bar{\varphi}}^{\circ} = \frac{a^2}{kM(n-1)} D_{nm\bar{\varphi}} , \quad (2.33)$$

where the superscript " \circ " denotes spherical approximation and the subscript " $\bar{\varphi}$ " denotes the use of geocentric latitude. Knowing the $C_{nm\bar{\varphi}}^{\circ}$,

these values are used in the e^2 terms of (2.32), and the equation then inverted to yield the C_{nm} . In addition using (2.27), the solution can be finally written in the form:

$$C_{nm} = C_{nm}^{\circ} + \delta C_{nm}^{\circ} \quad (2.34)$$

where

$$\delta C_{nm}^{\circ} = e^2 (p_{nm} C_{n-2, m}^{\circ} + q_{nm} C_{nm}^{\circ} + r_{nm} C_{n+2, m}^{\circ}), \quad (2.35)$$

and with $k = |m|$:

$$\begin{aligned} p_{nm} &= \frac{-(n^2 - n + 2)(n - k - 1)(n - k)}{2(n - 1)(2n - 3)(2n - 1)} \\ q_{nm} &= \frac{-2n^4 + 2n^2 k^2 - 4n^3 + 2nk^2 + 9n^2 + 2k^2 + 11n - 8}{2(n - 1)(2n + 3)(2n - 1)} \\ r_{nm} &= \frac{-(n^2 + 3n + 4)(n + k + 2)(n + k + 1)}{2(n - 1)(2n + 5)(2n + 3)} \end{aligned} \quad (2.36)$$

The above equations agree with the ones recently given by Rapp (1984).

In some cases we may be handling the Δg_E -data using geodetic latitudes ϕ instead of geocentric latitudes $\bar{\phi}$. In such cases we have, instead of (2.6), the expansion:

$$\Delta g_E = \sum_{n=2}^{\infty} \sum_{m=-n}^n D_{nm} Y_{nm}(\phi, \lambda). \quad (2.37)$$

We now want to know how the solution consisting of (2.33)-(2.36) will change. First, let us relate $D_{nm\phi}$ and $D_{nm\bar{\phi}}$ by transforming (2.6) to the form (2.37). Omitting terms involving e^4 , we have from Rapp (1981a, p. 2) that:

$$Y_{nm}(\bar{\phi}, \lambda) = Y_{nm}(\phi, \lambda) + \frac{\partial Y_{nm}}{\partial \bar{\phi}} (\bar{\phi} - \phi); \quad (2.38)$$

$$(\bar{\phi} - \phi) \approx -e^2 \sin \bar{\phi} \cos \bar{\phi}. \quad (2.39)$$

We substitute (2.38) and (2.39) into (2.6), then use the relation (2.24). Analogous to the derivation of (2.32), summation indices are then shifted in order to have only Y_{nm} , and not $Y_{n-2, m}$ or $Y_{n+2, m}$, occurring in the

expression. All coefficients of $Y_{nm}(\phi, \lambda)$, which by now are all constants independent of (ϕ, λ) , are then collected to yield a coefficient which must be exactly equal to the coefficient $D_{nm\phi}$ of (2.37). We get:

$$D_{nm\phi} = D_{nm\bar{\phi}} - e^2(a_{n-2,m} D_{n-2,m} + b_{nm} D_{nm} + c_{n+2,m} D_{n+2,m}) \quad (2.40)$$

which is the desired relation between $D_{nm\phi}$ and $D_{nm\bar{\phi}}$. Substituting (2.32) into (2.40), using the approximation (see (2.33))

$$D_{nm} \approx \frac{kM}{a^2} (n-1) C_{nm} \quad (2.41)$$

in the (small) terms involving e^2 , and simplifying we get:

$$\begin{aligned} D_{nm\phi} = & \frac{kM}{a^2} (n-1) C_{nm} + \frac{e^2 kM}{2a^2} \left\{ (3n^2 - 11n + 14) \alpha_{n-2,m} C_{n-2,m} + \right. \\ & + \left[(n^2 + n + 1) \beta_{nm} - 2(n-1) b_{nm} - 3 \right] C_{nm} \\ & \left. - (n^2 + 5n + 2) \gamma_{n+2,m} C_{n+2,m} \right\}. \end{aligned} \quad (2.42)$$

Equation (2.42) can now be inverted, in exactly the same way as (2.32) was inverted, to give the following solution based on geodetic latitudes:

$$C_{nm\phi} = \frac{a^2}{kM(n-1)} D_{nm\phi} \quad (2.43)$$

$$C_{nm} = C_{nm\phi} + \delta C_{nm\phi} \quad (2.44)$$

where

$$\delta C_{nm\phi} = e^2(p_{nm\phi} C_{n-2,m\phi} + q_{nm\phi} C_{nm\phi} + r_{nm\phi} C_{n+2,m\phi}),$$

and with $k = |m|$:

$$\begin{aligned} p_{nm\phi} &= \frac{-(3n^2 - 11n + 14)(n-k-1)(n-k)}{2(n-1)(2n-3)(2n-1)} \\ q_{nm\phi} &= \frac{-2n^4 + 2n^2 k^2 - 2n^3 - 4nk^2 + 9n^2 + 8k^2 + 9n - 8}{2(n-1)(2n+3)(2n-1)} \\ r_{nm\phi} &= \frac{(n^2 + 5n + 2)(n+k+2)(n+k+1)}{2(n-1)(2n+5)(2n+3)}. \end{aligned} \quad (2.45)$$

The above equations agree with Pellinen (1982, (16)-(18)).

In summary, we are given the values of gravity anomalies Δg_E on the surface of the ellipsoid. The Δg_E are the analytically continued version of the actually available Δg on the earth's surface. The anomalies on the ellipsoid can be formally expanded into a series (2.6) or (2.37) of spherical harmonics, with coefficients $D_{nm\phi}$ or $D_{nm\varphi}$ obtained through (2.9). The coefficients $D_{nm\phi}$ or $D_{nm\varphi}$ can then be used in (2.43)-(2.45) or (2.33)-(2.36), respectively, to generate the conventional potential coefficients C_{nm} (see (2.17)). Finally, the C_{nm} can be fully normalized by (2.19) to yield the \bar{C}_{nm}^* occurring in (2.1), completing the recovery of potential coefficients.

In our derivations we have always omitted terms involving the fourth and higher powers of the earth's first eccentricity e . This does not mean, however, that the relative error introduced by omission of terms is only $O(e^4)$ every time. Specifically, in (2.11) and (2.12) (see comments under (2.15)) the relative error depends also on the harmonic degree n and on the latitude ϕ , in addition to depending on the omitted powers of e . In the case of (2.12), the omission of terms was not critical, and in fact, only the first term of (2.12) was eventually used; the reason is that the use of (2.12) was to write (2.21) and (2.23), which were equations that already involved only small terms of $O(e^2)$. In the case of (2.11), however, the omission of terms was critical; the reason is that (2.11) was used to write (2.20), which was an equation for the (principal) first two terms of (2.4). In fact, the dominating source of inaccuracy in our whole derivations was the omission of terms in (2.11), directly causing significant relative error to (2.20) (see error estimates later this section).

For higher accuracies we need to consider the next omitted term in (2.11), namely, the term (2.16). This can be done as follows. First, there will be the following additional term to the right-side of (2.20):

$$dg_E^1 = \frac{e^4 k M}{8a^2} \sum_{n=2}^{\infty} \sum_{m=-n}^n (n+2)(n+1)(n-1) C_{nm} \sin^4 \varphi Y_{nm}(\varphi, \lambda). \quad (2.46)$$

By recursive application of (2.26) we have:

$$\begin{aligned} \sin^4 \varphi Y_{nm}(\varphi, \lambda) = & K_{nm} Y_{n+4,m} + L_{nm} Y_{n+2,m} + \\ & M_{nm} Y_{nm} + N_{nm} Y_{n-2,m} + P_{nm} Y_{n-4,m} \end{aligned} \quad (2.47)$$

where

$$\begin{aligned}
K_{nm} &= \alpha_{nm} \alpha_{n+2,m} \\
L_{nm} &= \alpha_{nm}(\beta_{nm} + \beta_{n+2,m}) \\
M_{nm} &= \alpha_{nm} \gamma_{n+2,m} + \beta_{nm}^2 + \alpha_{n-2,m} \gamma_{nm} \\
N_{nm} &= \gamma_{nm}(\beta_{n-2,m} + \beta_{nm}) \\
P_{nm} &= \gamma_{n-2,m} \gamma_{nm} .
\end{aligned} \tag{2.48}$$

Equation (2.47) with (2.48) is also given in Pellinen (1982, (9)). Analogous to the construction of $D_{nm\bar{\nu}}$ in (2.32), we substitute (2.47) into (2.46). Summation indices are then shifted as in (2.28) in order to have only Y_{nm} , and not $(Y_{n+4,m}, Y_{n+2,m}, Y_{n-2,m}, Y_{n-4,m})$ occurring in the expression. All coefficients of $Y_{nm}(\bar{\nu}, \lambda)$ are then collected to yield a coefficient $D_{nm\bar{\nu}}$:

$$D_{nm\bar{\nu}} = \frac{e^4 kM}{8a^2} S_{nm\bar{\nu}} \tag{2.49}$$

where

$$\begin{aligned}
S_{nm\bar{\nu}} &= (n-2)(n-3)(n-5) K_{n-4,m} C_{n-4,m} + \\
&+ n(n-1)(n-3) L_{n-2,m} C_{n-2,m} + \\
&+ (n+2)(n+1)(n-1) M_{nm} C_{nm} + \\
&+ (n+4)(n+3)(n+1) N_{n+2,m} C_{n+2,m} + \\
&+ (n+6)(n+5)(n+3) P_{n+4,m} C_{n+4,m} .
\end{aligned} \tag{2.51}$$

A more complete version of (2.32) can now be written as follows:

$$D_{nm\bar{\nu}} = \frac{kM}{a^2} (n-1)C_{nm} + \frac{e^2 kM}{2a^2} R_{nm\bar{\nu}} + \frac{e^4 kM}{8a^2} S_{nm\bar{\nu}} \tag{2.52}$$

where $R_{nm\bar{\nu}}$ denotes the quantity in braces in (2.32). Equation (2.52) can then be inverted to yield the unknown C_{nm} . The inversion can be done by first writing (2.52) in the form:

$$C_{nm} = \frac{a^2}{kM(n-1)} D_{nm\bar{\nu}} - \frac{e^2}{2(n-1)} R_{nm\bar{\nu}} - \frac{e^4}{8(n-1)} S_{nm\bar{\nu}} . \tag{2.53}$$

From (2.53) we have the "zero order" solution:

$$C_{nm}^{\circ} = \frac{a^2}{kM(n-1)} D_{nm\varphi} . \quad (2.54)$$

Equation (2.54) is the same as the spherical approximation solution (2.33), and corresponds to the case when only the first term in (2.11) (therefore, only the first term in (2.20)) is used. Using (2.54) in (2.53) we obtain the "first-order" solution:

$$C_{nm}^1 = C_{nm}^{\circ} - \frac{e^2}{2(n-1)} R_{nm\varphi}^{\circ} . \quad (2.55)$$

Equation (2.55) is the same as the solution (2.34), and corresponds to the case when the first and second terms of (2.11) (therefore, also the first and second terms in (2.20)), plus the correction terms of $O(e^2)$ given by (2.21) and (2.23), are accounted for in the solution. Finally, using (2.55) into (2.53) yields the "second-order" solution:

$$C_{nm}^{(2)} = C_{nm}^{\circ} - \frac{e^2}{2(n-1)} R_{nm\varphi}^1 - \frac{e^4}{8(n-1)} S_{nm\varphi}^1 , \quad (2.56)$$

where the superscript "1" means that $C_{n-4,m}^1, C_{n-2,m}^1, C_{nm}^1, C_{n+2,m}^1, C_{n+4,m}^1$ from (2.55) are used to obtain $R_{nm\varphi}^1$ and $S_{nm\varphi}^1$. The solution (2.56) corresponds to the case when the terms of (2.11) and (2.16) (therefore, also the terms of (2.20) and (2.46)) are accounted for in the solution along with the terms of (2.21) and (2.23).

A physical interpretation can be given to the zero-, first-, and second-order solution for the recovery of potential coefficients from Δg_E -data. This is seen from first noting that we can write the Taylor expansion:

$$\begin{aligned} dg_E = dg_a + \frac{\partial dg}{\partial r} \Big|_{r=a} (r_E - a) + \frac{1}{2!} \frac{\partial^2 dg}{\partial r^2} \Big|_{r=a} (r_E - a)^2 + \\ + \frac{1}{3!} \frac{\partial^3 dg}{\partial r^3} \Big|_{r=a} (r_E - a)^3 + \dots \end{aligned} \quad (2.57)$$

where we define:

$$dg = -\frac{\partial T}{\partial r} - \frac{2}{r} T = \frac{kM}{a^2} \sum_{n=2}^{\infty} \sum_{m=-n}^n \left(\frac{a}{r}\right)^{n+2} (n-1) C_{nm} Y_{nm}(\varphi, \lambda) ; \quad (2.58)$$

and

$$(r_E - a) = -\frac{ae^2}{2} \sin^2 \phi + O(e^4); \quad (2.59)$$

$$dg_E = dg(r_E, \varphi, \lambda); \quad (dg \text{ on the ellipsoid}) \quad (2.60)$$

$$dg_a = dg(a, \varphi, \lambda) \quad (dg \text{ on the equatorial sphere}) \quad (2.61)$$

Equation (2.20) with the additional term (2.46), which is a starting point of our derivation, is in the general form of the Taylor expansion (2.57) truncated after the third term. The zero-order solution in effect uses only the first term in (2.57), thereby setting $dg_a = dg_E$; this means that in this solution a given boundary value Δg_E at position (r_E, φ, λ) is formally considered to be on the equatorial sphere at position (a, φ, λ) . The first-order solution on the other hand, uses the first two terms of (2.57), thereby using the first radial derivative of the dg -field to distinguish between dg_a and dg_E . Finally, the second-order solution uses the first three terms of (2.57), thereby using the first and second radial derivatives of the dg -field to distinguish between dg_a and dg_E .

To examine numerically the effect of omission of terms, we write (2.11) more completely as:

$$\begin{aligned} \left(\frac{a}{r_E}\right)^{n+2} = & 1 + (n+2) \frac{e^2}{2} \sin^2 \phi + \frac{(n+2)(n+1)}{2!} \frac{e^4}{4} \sin^4 \phi + \\ & + \frac{(n+2)(n+1)(n)}{3!} \frac{e^6}{8} \sin^6 \phi + \dots \end{aligned} \quad (2.62)$$

With $e^2/2 \approx 0.003 \approx f$ (the earth's flattening), the maximal orders of magnitude of the terms in (2.62) are obtained at the poles with $\sin \phi = 1$:

$$O(e^2\text{-term}) = nf = 3 \times 10^{-3} n$$

$$O(e^4\text{-term}) = \frac{n^2 f^2}{2!} = 5 \times 10^{-6} n^2 \quad (2.63)$$

$$O(e^6\text{-term}) = \frac{n^3 f^3}{3!} = 5 \times 10^{-9} n^3 .$$

The omission of terms estimated in (2.63) directly causes a relative error in our derivations. Since this source of error is dominating, we can

also interpret (2.63) as giving maximal estimates of the total relative error itself, caused by the omission of certain powers of e in the recovery of potential coefficients \bar{C}_{nm}^* from Δg_E -data. Such estimates, which agree with those of Pellinen (1982), are evaluated in Table 1 for various values of n and various powers of omitted e -terms.

Table 1 says that for $n=200$, for example, the omission of e^2 and higher powers (i.e., the use of only the first term in (2.34), (2.44), or (2.53)) causes a relative computational error of 60% in $\bar{C}_{200,m}^*$; the percentage error decreases to 20% and to 4% when terms proportional to e^2 and e^4 , respectively, are considered in the formulas.

Table 1. Relative Error Caused by the Omission of Terms Proportional to Certain Powers of e , in the Recovery of Potential Coefficients \bar{C}_{nm}^* from Anomaly Data Δg_E on the Ellipsoid.

Minimum Power of e in Omitted Terms	Relative Error ε_R $\left[\frac{0(\delta \bar{C}_{nm}^*)}{0(\bar{C}_{nm}^*)} \right]$	Value of Relative Error for			
		$n=30$	$n=100$	$n=200$	$n=300$
e^2	$3 \times 10^{-3} n$	0.09	0.03	0.60	0.90
e^4	$5 \times 10^{-6} n^2$	0.0045	0.05	0.20	0.45
e^6	$5 \times 10^{-9} n^3$	0.0001	0.005	0.04	0.13

The relative errors ε_R given in Table 1 affect the gravimetric quantities computed from the \bar{C}_{nm}^* . We can look at short and long wavelength effects separately by looking at effects on computed gravity anomalies Δg and height anomalies. The global RMS effects when using an expansion to degree and order N_{max} can be expressed as the square root of (in a sphere of radius $r=a$):

$$\sigma^2(\Delta g) = \left(\frac{kM}{a^2} \right)^2 \sum_{n=2}^{N_{max}} (n-1)^2 (2n+1) [0(\delta \bar{C}_{nm}^*)]^2 ; \quad (2.64)$$

$$\sigma^2(\zeta) = a^2 \sum_{n=2}^{N_{max}} (2n+1) [0(\delta \bar{C}_{nm}^*)]^2 ; \quad (2.65)$$

where

$$0(\delta \bar{C}_{nm}^*) = \varepsilon_R \cdot 0(\bar{C}_{nm}^*) ; \quad (2.66)$$

$$\varepsilon_R \text{ is the relative error from Table 1 or (2.63) .} \quad (2.67)$$

From Kaula's rule of thumb, we have the following order of magnitude of potential coefficients:

$$0(\bar{C}_{nm}^*) = \frac{10^{-5}}{n^2} . \quad (2.68)$$

Let us further use values from the Geodetic Reference System 1980:

$$kM = 3986005 \times 10^8 \text{ m}^3 \text{ s}^{-2} \quad (2.69)$$

$$a = 6378137 \text{ m} . \quad (2.70)$$

Using (2.64)-(2.70), values of $\sigma(\Delta g)$ and $\sigma(\zeta)$ were computed and shown in Table 2, for various maximum degrees of expansion N_{max} . For $N_{max}=200$, for example, the effect of omitting the (e^2 , e^4 , e^6) and higher powers would be to cause an error of about (5.9, 1.4, 0.2) mgals in gravity anomalies and an error of about (0.62, 0.06, 0.01) meter in height anomalies, on a sphere of radius $r=a$.

Table 2. Effect of Potential Coefficient Errors $\delta \bar{C}_{nm}^*$ on Computed Gravity Anomalies Δg and Height Anomalies ζ .
Units: $\sigma(\Delta g)$ in milligals; $\sigma(\zeta)$ in meters.

Minimum Power of e in Omitted Terms	Relative Error ε_R of Potential Coefficients (from Table 1)	Value of $\begin{Bmatrix} \sigma(\Delta g) \\ \sigma(\zeta) \end{Bmatrix}$ from $\begin{Bmatrix} (2.64) \\ (2.65) \end{Bmatrix}$			
		$N_{max}=30$	$N_{max}=100$	$N_{max}=200$	$N_{max}=300$
e^2	$3 \times 10^{-3} n$	0.85 mgals 0.49 m	2.91 0.57	5.85 0.62	8.79 0.64
e^4	$5 \times 10^{-6} n^2$	0.03 0.01	0.35 0.03	1.39 0.06	3.12 0.10
e^6	$5 \times 10^{-9} n^3$	0.00 0.00	0.03 0.00	0.22 0.01	0.77 0.02

It is not surprising that relatively large errors are associated with the zero-order solution (see the first row of values in Tables 1 and 2): the reason is that the true gravity anomaly $\Delta g_a(a, \varphi, \lambda)$ on the equatorial sphere and $\Delta g_E(r_E, \varphi, \lambda)$ on the ellipsoid can easily differ significantly, so that equating $\Delta g_a = \Delta g_E$ (strictly, equating $dg_a = dg_E$), as the zero-order solution does, incurs large errors. The consideration of the e^2 -terms, as in the first-order solution, means the consideration of the first radial derivative of the gravity anomaly field to relate Δg_a and Δg_E , resulting in much smaller errors (see second row of values in Tables 1 and 2) than those of the zero-order solution. Finally, a consideration of e^4 terms, as in the second-order solution, means the additional consideration of the second radial derivative of the field to relate Δg_a and Δg_E , resulting in even smaller computational errors (third row of Tables 1 and 2). As seen from Tables 1 and 2, the higher the harmonic degrees (n) of interest, the higher the order of radial derivatives of the gravitational field that need to be considered in the ellipsoidal correction theory.

Summarizing, the determination of potential coefficients requires the surface gravity anomalies to be analytically continued to some sphere. Rather than continuing to a bounding sphere as in Rapp (1984), we recommend continuing to the equatorial sphere where the standard form of spherical harmonic representation (2.1) refers. For operational implementation we recommend carrying out the analytical continuation in two steps. The first step would be to continue the surface data to the ellipsoid. This can be done (ibid.) by numerically computing the correction terms of the Taylor series using surface heights and vertical gradients from an existing spherical harmonic expansion. The second step would be to analytically continue from the ellipsoid to the equatorial sphere. This step can be carried out also by Taylor series, but with the Taylor terms applied analytically through the ellipsoidal corrections of Pellinen (1982). At maximum degrees of expansions around $n = 300$, up to second order Taylor terms need to be applied, and this can be done through (2.56). Tables 1 and 2 indicate the number of Taylor terms required for given maximum degrees of expansion and desired accuracy of continuation from ellipsoid to equatorial sphere. The effects of the Taylor terms for the continuation from the topography to the ellipsoid are on the average an order of magnitude less than the values in Tables 1 and 2 (see Rapp, ibid., Table 1).

3. FAMILIARIZATION WITH THE SPATIAL DISTURBANCE VECTOR SIGNAL

Given potential coefficients \bar{C}_{nm}^* , the anomalous potential $T(r, \varphi, \lambda)$ is expressed in spherical harmonics by (2.1). Then with (2.1) as fundamental equation, other gravimetric quantities of interest can be derived in spherical harmonics using (2.1) and its first and second order derivatives. As an example, Rapp (1982) gives a collection of such derivations for common gravimetric quantities, specifically the height anomaly, gravity anomaly, three components of the gravity disturbance vector, and two components of the deflection of the vertical. On the other hand, given the gravity anomalies Δg_E on the ellipsoid, the anomalous potential $T(r, \varphi, \lambda)$ is expressed in an integral formula by (3.14) below. Now using (3.14) and its first and second order derivatives, integral formulas for other gravimetric quantities can also be derived. Examples of such derivations are found in Heiskanen and Moritz (1967, Sec. 6-4) for the components of both the gravity disturbance vector and the deflection of the vertical.

Both parameterizations from \bar{C}_{nm}^* and Δg_E have their respective theoretical and practical problems. The theoretical problem with the \bar{C}_{nm}^* parameterization is the divergence of downward continued spherical harmonic series. The total (i.e., infinite) spherical harmonic series (2.1) representing the anomalous potential is not guaranteed to converge, and in fact will probably diverge, when evaluated below the smallest sphere, called the minimum sphere, bounding the earth. The errors arising from this total series divergence generally grow with the depth of penetration into the minimum sphere and the power (expressed by degree variances) of the high frequency variations in the anomalous field. For depths of penetration down to the earth's surface and for the degree variance decay of the earth's anomalous potential, Jekeli (1981) shows completely negligible errors coming from total-series divergence when using a spherical harmonic representation of the earth's anomalous field to maximum degree $N_{max}=300$.

Of great concern also would be the practical problems associated with the \bar{C}_{nm}^* - parameterization. The slow decay of the \bar{C}_{nm}^* with n necessitates the handling of a very large number of coefficients in order to represent all significant variations in the anomalous field. For example, a 5'x5' resolution which may be needed in certain computations near the earth's surface would require approximately $N_{max}=2000$ or a total of $(2001)^2 \approx 4$ million coefficients. The use of such high degree spherical harmonic representation will require a prohibitive amount of computer storage and time. Also, such high degree representation will require some sort of re-parameterization from the available Δg to the \bar{C}_{nm}^* , and such re-parameterization will involve difficult practical

problems related to computer requirements, quadratures, and implementation of a relation between \bar{C}_{nm}^* and Δg that accounts for the ellipticity and topography of the earth (Rapp, 1984). Finally, there is the problem of updating a spherical harmonic representation to incorporate updated gravity anomaly data. Such updates are inconvenient as they everytime require a new solution for the entire \bar{C}_{nm}^* set of parameters. Today, taking altogether the theoretical and practical problems of the \bar{C}_{nm}^* -parameterization it would appear that a feasible upper limit to use would be around $N_{max}=360$.

At higher frequencies (harmonic degrees greater than $n=360$ or spatial resolution greater than $30' \times 30'$) the direct parameterization from Δg_E via an integral formula based on (3.14) below would be appropriate. Since the high frequency variations are attributable to Δg_E -data close to the computation point, the integral formula can be truncated to within a data cap of limited radius around the computation point. This minimizes the practical problem of integral formula representations, that of having to integrate data over a large cap.

Since the spherical harmonic and integral representations complement each other's deficiencies, the ideal would be to combine the two representations. Such combination is performed under the heading of "truncation theory" as originated by Molodensky (see Molodensky, et al., 1962), or more recently, under the heading of "least squares spectral combination theory" (Moritz, 1975; Sjöberg, 1981; Wenzel, 1982). We will discuss the combination by truncation theory in this chapter, with special emphasis on the computation of the gravity disturbance vector components at altitude.

3.1 Formulas for Spherical Harmonic and Integral Representations

From (2.1) we can express the anomalous potential as:

$$T = \frac{kM}{a} \sum_{n=2}^{\infty} \sum_{m=-n}^n \left(\frac{a}{r}\right)^{n+1} \bar{C}_{nm}^* \bar{Y}_{nm}(\varphi, \lambda) . \quad (3.1)$$

Using (3.1) in the usual definitions of the radial and horizontal gravity disturbance vector components and the definition of the gravity anomaly in spherical approximation, we can collect the following equations:

$$\delta_r = \frac{-\partial T}{\partial r} = \frac{kM}{a^2} \sum_{n=2}^{\infty} \sum_{m=-n}^n (n+1) \left(\frac{a}{r}\right)^{n+2} \bar{C}_{nm}^* \bar{Y}_{nm}(\varphi, \lambda) \quad (3.2)$$

$$\delta\varphi = \frac{1}{r} \frac{\partial T}{\partial \varphi} = \frac{kM}{a^2} \sum_{n=2}^{\infty} \sum_{m=-n}^n \left(\frac{a}{r}\right)^{n+2} \bar{C}_{nm}^* \frac{\partial \bar{Y}_{nm}(\varphi, \lambda)}{\partial \varphi} \quad (3.3)$$

$$\delta\lambda = \frac{1}{r \cos \varphi} \frac{\partial T}{\partial \lambda} = \frac{kM}{a^2 \cos \varphi} \sum_{n=2}^{\infty} \sum_{m=-n}^n \left(\frac{a}{r}\right)^{n+2} \bar{C}_{nm}^* \frac{\partial \bar{Y}_{nm}(\varphi, \lambda)}{\partial \lambda} \quad (3.4)$$

$$\Delta g_r = \frac{-\partial T}{\partial r} - \frac{2}{r} T = \frac{kM}{a^2} \sum_{n=2}^{\infty} \sum_{m=-n}^n (n-1) \left(\frac{a}{r}\right)^{n+2} \bar{C}_{nm}^* \bar{Y}_{nm}(\varphi, \lambda) \quad (3.5)$$

The above formulas are suited under the spherical harmonic representation of the anomalous field, that is, under a parameterization from the \bar{C}_{nm}^* coefficients. Under the so-called integral representation we need expressions of gravimetric quantities in terms of "terrestrial" gravity anomalies. A set of spectral forms for such expressions can be written by inspection of (3.2)-(3.5) as follows:

$$T = \sum_{n=2}^{\infty} \left(\frac{r_E}{n-1}\right) \left(\frac{r_E}{r}\right)^{n+1} \Delta g_n \quad (3.6)$$

$$\delta_r = \sum_{n=2}^{\infty} \left(\frac{n+1}{n-1}\right) \left(\frac{r_E}{r}\right)^{n+2} \Delta g_n \quad (3.7)$$

$$\begin{pmatrix} \delta\varphi \\ \delta\lambda \end{pmatrix} = \sum_{n=2}^{\infty} \left(\frac{1}{n-1}\right) \left(\frac{r_E}{r}\right)^{n+2} \begin{pmatrix} \frac{\partial}{\partial \varphi} \Delta g_n \\ \frac{1}{\cos \varphi} \frac{\partial}{\partial \lambda} \Delta g_n \end{pmatrix}, \quad (3.8)$$

where

r_E ... geocentric radius to the point on the reference ellipsoid with the same coordinates (φ, λ) as the computation point

$$\Delta g_n = \frac{kM}{a^2} \sum_{m=-n}^n (n-1) \left(\frac{a}{r_E}\right)^{n+2} \bar{C}_{nm}^* \bar{Y}_{nm}(\varphi, \lambda) \quad (3.9)$$

... n th surface harmonic of the gravity anomalies on the geocentric sphere of radius r_E , under a (φ, λ) -mapping of these anomalies onto a unit sphere.

A second set of spectral forms can be written analogous to (3.6)-(3.9) in anticipation of the use, under the integral representation, of the mapping of points and functions discussed in Section 1.2 (see Figure 2); we have:

$$T = \sum_{n=2}^{\infty} \left(\frac{R}{n-1} \right) \left(\frac{R}{r_1} \right)^{n+1} \Delta g_{En} \quad (3.10)$$

$$\delta_r = \sum_{n=2}^{\infty} \left(\frac{n+1}{n-1} \right) \left(\frac{R}{r_1} \right)^{n+2} \Delta g_{En} \quad (3.11)$$

$$\begin{pmatrix} \delta_{\varphi} \\ \delta_{\lambda} \end{pmatrix} = \sum_{n=2}^{\infty} \left(\frac{1}{n-1} \right) \left(\frac{R}{r_1} \right)^{n+2} \begin{pmatrix} \frac{\partial}{\partial \varphi} \Delta g_{En} \\ \frac{1}{\cos \varphi} \frac{\partial}{\partial \lambda} \Delta g_{En} \end{pmatrix}, \quad (3.12)$$

where now:

$$r_1 = R + h \quad (3.13)$$

R ... mean earth radius (6371 km)

h ... height of the computation point above the ellipsoid or the geoid

Δg_{En} ... n th surface harmonic of the gravity anomalies on the ellipsoid or geoid, under a (ϕ, λ) -mapping of these anomalies onto a unit sphere. I.e., geodetic latitudes ϕ are to be used in the defining equation (3.42) below.

Our practical use for the type of equations (3.10)-(3.12), as well as for their versions where truncation coefficients have been introduced (details next sections), will only be for degree variance propagations. This is in view of the fact that degree variances are usually quoted for the Δg_{En} of (3.10)-(3.12) and not for the Δg_n of (3.6)-(3.8). For actual computation of contributions from potential coefficients, however, we will use the type of equations (3.6)-(3.8) along with their versions where truncation coefficients have been introduced.

For use under the integral formula representation, we need the space domain equivalents of (3.10)-(3.12). These space domain equivalents will express the gravimetric quantities in terms of Δg_E . The space domain expressions for (3.6)-(3.8) follow immediately from those of (3.10)-(3.12) by just changing R to r_E , r_1 to r , ϕ to ϕ , and Δg_E to Δg in the formulas; however, such expressions will be essentially of no practical value since we do not have the required detailed Δg on a geocentric sphere of radius r_E . We have the following space domain equivalents of (3.10)-(3.12) from Heiskanen and Moritz (1967, Section 6-4):

$$T(r, \varphi, \lambda) = \frac{R}{4\pi} \int_{\sigma} S(r_1, \psi) \Delta g_E d\sigma \quad (3.14)$$

$$\delta_r(r, \varphi, \lambda) = \frac{-R}{4\pi} \int_{\sigma} \frac{\partial S(r_1, \psi)}{\partial r_1} \Delta g_E d\sigma \quad (3.15)$$

$$\begin{bmatrix} \delta\varphi \\ \delta\lambda \end{bmatrix} (r, \varphi, \lambda) = \frac{-R}{4\pi r_1} \int_{\sigma} \frac{\partial S(r_1, \psi)}{\partial \psi} \Delta g_E \begin{bmatrix} \cos \alpha \\ \sin \alpha \end{bmatrix} d\sigma, \quad (3.16)$$

where, assuming:

(ϕ, λ) : geodetic coordinates of the computation point P

(ϕ', λ') : geodetic coordinates of the moving integration point P' ,

we have:

$$d\sigma = \cos\phi' d\phi' d\lambda' \\ \text{(integration element)}$$

$$\cos\psi = \sin\phi\sin\phi' + \cos\phi\cos\phi'\cos(\lambda'-\lambda) \\ \text{(angular distance between } P \text{ and } P') \quad (3.17)$$

$$\tan \alpha = \frac{\cos \phi' \sin(\lambda'-\lambda)}{\cos \phi \sin \phi' - \sin \phi \cos \phi' \cos(\lambda'-\lambda)} \\ \text{(azimuth from } P \text{ to } P').$$

The integral kernels in (3.14)-(3.16) can be obtained in the space domain using (ibid., p. 235); see also Paul, 1983, (1); Shepperd, 1982, p. 102):

$$S(r_1, \psi) = t - 5t^2y + \frac{2t}{D} - 3tD - 3t^2y E \quad (3.18)$$

$$\frac{-R}{r_1} \frac{\partial S(r_1, \psi)}{\partial r_1} = \frac{t^2(1-t^2)}{D^3} - t^2 - 3t^3y + 2t S(r_1, \psi) \quad (3.19)$$

$$\frac{-t}{\psi} \frac{\partial S(r_1, \psi)}{\partial \psi} = -t^3 \sin \psi \left[\frac{2}{D^3} + \frac{6}{D} - 8 - 3 \left(\frac{1-ty-D}{D \sin^2 \psi} \right) - 3 E \right], \quad (3.20)$$

in which

$$t = \frac{R}{r_1}; \quad r_1 = R+h \quad (3.21)$$

$$y = \cos \psi \quad (3.22)$$

$$D = (1 - 2ty + t^2)^{1/2} \quad (3.23)$$

$$E = \ln \left(\frac{1 - ty + D}{2} \right). \quad (3.24)$$

The integral kernel for (3.14) and (3.15) are isotropic (independent of α), whereas that for (3.16) is non-isotropic (dependent on α). Equation (3.18) expresses the familiar space-extended Stokes function, while (3.20) expresses the space-extended Vening-Meinesz function.

It is of interest to write the spectral forms of the kernels (3.18)-(3.20). Comparing (3.10) and (3.11) to (3.14) and (3.15), respectively, applying the principles of eigenvalues and eigenfunctions of isotropic integral operators (see, e.g., Jekeli, 1980, p. 6; Sunkel, 1981a, pp. 18-19), we must have that:

$$R S(r_1, \psi) = \sum_{n=2}^{\infty} (2n+1) \left(\frac{R}{n-1} \right) \left(\frac{R}{r_1} \right)^{n+1} P_n(y) \quad (3.25)$$

$$\frac{-R}{r_1} \frac{\partial S(r_1, \psi)}{\partial r_1} = \sum_{n=2}^{\infty} (2n+1) \left(\frac{n+1}{n-1} \right) \left(\frac{R}{r_1} \right)^{n+2} P_n(y) \quad (3.26)$$

A simple check is provided by the fact that if we take the negative of the derivative of (3.25) with respect to r_1 we arrive at (3.26) as it should be. The spectral form of the function (3.20) which forms part of the kernel for the horizontal disturbance components (3.16) can be obtained by differentiating (3.25) directly, and verifying from the definitions in Heiskanen and Moritz (1967, p. 22) that:

$$\frac{\partial}{\partial \psi} P_n(y) = -P_{n1}(y) , \quad (3.27)$$

where the $P_{n1}(y)$ are the associated Legendre functions of the first order ($m=1$). We arrive at:

$$-\frac{t}{\partial \psi} S(r_1, \psi) = \sum_{n=2}^{\infty} (2n+1) \left(\frac{1}{n-1} \right) \left(\frac{R}{r_1} \right)^{n+2} P_{n1}(y) . \quad (3.28)$$

Equation (3.28) has a similar structure to (3.25) and (3.26), except that in (3.28) the $P_{n1}(y)$ and not the $P_n(y)$ is used - this is a consequence of the non-isotropy of the integral kernel in (3.16).

3.2 Spectral Information Content

This section is a study of the spectral information content of the radial and horizontal gravity disturbance vector components at various altitudes. The global RMS (root mean square) value of the radial disturbance in (3.11) can be expressed analogously to Heiskanen and Moritz (1967, pp. 260-261) as the square root of:

$$\sigma^2(\delta_r) = \sum_{n=2}^{\infty} \left(\frac{n+1}{n-1} \right)^2 \left(\frac{R}{r_1} \right)^{2n+4} C_n . \quad (3.29)$$

where the C_n are the degree variances of the gravity anomalies Δg_E . Of interest also is the RMS information beyond a given harmonic degree N , expressed from (3.29) as the square root of:

$$\sigma_N^2(\delta_r) = \sum_{n=N+1}^{\infty} \left(\frac{n+1}{n-1} \right)^2 \left(\frac{R}{r_1} \right)^{2n+4} C_n . \quad (3.30)$$

The relative omission error incurred by truncating the signal representation to a maximum degree N can be expressed in percentage as:

$$\varepsilon_N(\delta_r) = \frac{\sigma_N(\delta_r)}{\sigma(\delta_r)} \times 100\% , \quad (3.31)$$

where $\sigma_N(\delta_r)$ and $\sigma(\delta_r)$ are the square roots of the quantities $\sigma_N^2(\delta_r)$ and $\sigma^2(\delta_r)$, respectively. Quantities analogous to (3.29)-(3.31) can be written for the total horizontal disturbance δ_H , defined as:

$$\delta_H^2 = \delta_\varphi^2 + \delta_\lambda^2 , \quad (3.32)$$

where δ_φ and δ_λ are given by (3.12). Applying *ibid.*, p. 262, the global RMS value of the horizontal disturbance in (3.32) can be expressed as the square root of:

$$\sigma^2(\delta_H) = \sum_{n=2}^{\infty} \frac{n(n+1)}{(n-1)^2} \left(\frac{R}{r_1} \right)^{2n+4} C_n , \quad (3.33)$$

then we have analogous to (3.30) and (3.31):

$$\sigma_N^2(\delta_H) = \sum_{n=N+1}^{\infty} \frac{n(n+1)}{(n-1)^2} \left(\frac{R}{r_1} \right)^{2n+4} C_n , \quad (3.34)$$

$$\varepsilon_N(\delta_H) = \frac{\sigma_N(\delta_H)}{\sigma(\delta_H)} \times 100\% , \quad (3.35)$$

We numerically evaluated the above expressions for various altitudes h above the ellipsoid, using $R=6371$ km, $r_1=R+h$, and the so-called two-component degree variance model (Rapp, 1979; unit: mgal^2):

$$C_n = 3.405 \frac{(n-1)}{(n+1)} (0.998006)^{n+2} + \frac{140.03 (n-1)}{(n-2)(n+2)} (0.914232)^{n+2} , \quad n \geq 3 \quad (3.36)$$

$$C_2 = 7.5 \text{ mgal}^2 .$$

The summations were carried out to $n=5400$, corresponding to a space domain solution resolution of $2'$ half-wavelength ($180^\circ/5400=2'$).

A presentation of the results is shown in Figures 4 and 5. Since practically identical graphs were obtained for the radial as for the horizontal component, only graphs for the radial component are shown. The only notable difference between radial and horizontal results was that $\sigma(\delta_r)$ always exceeded $\sigma(\delta_H)$ by about 1.5 mgals for all altitudes tested. Figure 4 actually shows the quantity $\sigma_N(\delta_r)$ from (3.30), or basically also the quantity $\sigma_N(\delta_H)$ from (3.34). The parameters used were altitudes $h=5, 10, 20, 30, 50, 100, 200, 500$ km, and various harmonic degrees N_{min} defining the lower limit of the summation in (3.30). For example, Figure 4 says that the use of a radial or horizontal disturbance representation to harmonic degree $n=360$ leaves about (16.2, 10.2, 4.5) mgals to be resolved at (5, 10, 20) km altitude. For altitudes of 100 km and higher, however, such representation to $n=360$ is seen to be essentially complete in representing all the information content of the field. A representation to $n=360$ may be interpreted as being a spherical harmonic representation with potential coefficients C_{nm}^* complete to degree and order 360, or it may be interpreted as an integral formula representation using "terrestrial" gravity anomaly data with a space domain half-wavelength resolution of $0.5' (\approx 55$ km on the surface of the earth).

Figure 5 presents another view of the situation by plotting from the quantity $\varepsilon_N(\delta_r)$ of (3.31), or with basically the same numerical values also from $\varepsilon_N(\delta_H)$ of (3.35). To construct Figure 5 a given altitude was first taken, then values of N_{max} that define the upper limit of signal field representations were searched using (3.31), such that the relative omission error $\varepsilon_{N_{max}}$ took values of 1%, 3% and 10%. The procedure was repeated for altitudes ranging from 5 km to 500 km. For example, Figure 5 says that for an altitude of 30 km we need a representation to at least $n=(720, 540, 360)$ in order to keep the relative omission error down to (1%, 3%, 10%). Such values of n correspond to a space domain resolution of ($15', 20', 30'$) half-wavelength, corresponding to about (30, 40, 55) km on the surface of the earth. Using Figure 5 in another way, one concludes that a representation to $n=360$ incurs less than 1% relative omission error for altitudes above 70 km, incurs 3% error at 45 km, and incurs greater than 10% error for altitudes below 30 km.

A final remark should be made. As we have seen the radial and horizontal disturbance signals both require about the same resolution of representation to satisfy certain accuracy levels. For example, again from Figure 5 we see that at an altitude of 5 km and desired accuracy level of 1%, we need a representation to about $n=2500$. This corresponds to a need in an integral representation for $5' \times 5'$ gravity anomalies ($180^\circ/2500 \approx 5'$) on the surface of the earth. This is true, but it is also true that the $5' \times 5'$ values need be given only within a very limited data cap around the computation point and not all over the earth. This is because of the decay of the integral kernel with distance from the computation point. Farther and farther away from the computation point, less and less resolution of data is required. In this aspect, as

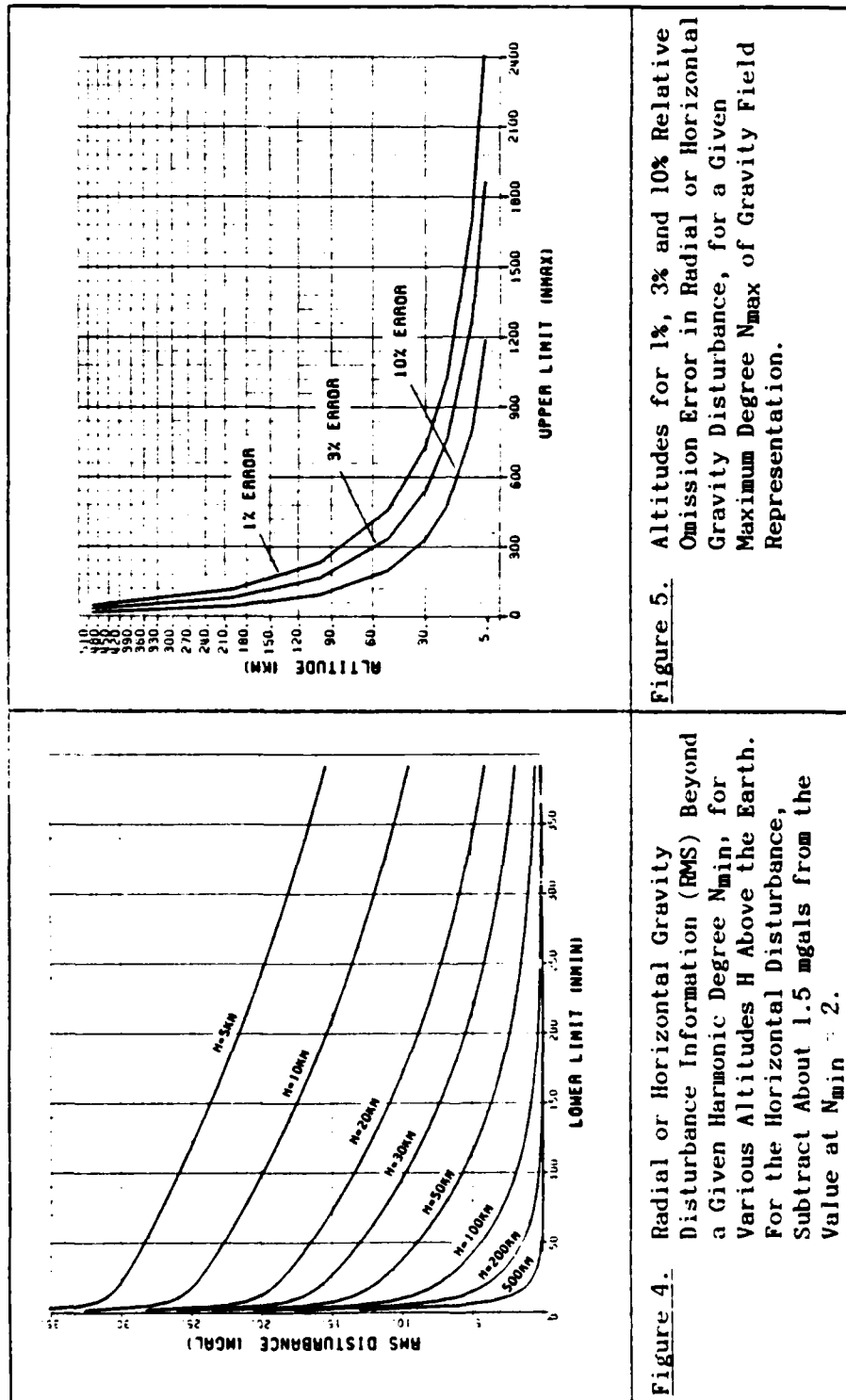


Figure 4. Radial or Horizontal Gravity Disturbance Information (RMS) Beyond a Given Harmonic Degree N_{\min} , for Various Altitudes H Above the Earth. For the Horizontal Disturbance, Subtract About 1.5 mgals from the Value at $N_{\min} = 2$.

Figure 5. Altitudes for 1%, 3% and 10% Relative Omission Error in Radial or Horizontal Gravity Disturbance, for a Given Maximum Degree N_{\max} of Gravity Field Representation.

we will detail in the next section, we have the difference that the horizontal disturbance component requires significantly larger data caps than the radial component. Therefore, aside from the spectral study that we have done above, we also need a space domain study of the actual response of the disturbance signal components in space to terrestrial gravity anomaly data of certain resolution and distance from the computation point. The spectral study shows the required maximum resolutions, but the space domain study will show the required cap sizes or the actual spatial location and resolution of the required Δg -data.

3.3 Truncation Theory

3.3.1 Isotropic Kernels

Let us write a general isotropic integral operation on the gravity anomalies Δg_E , producing a gravimetric quantity f , as follows:

$$f = \frac{1}{4\pi} \int_{\sigma} K(\psi) \Delta g_E d\sigma . \quad (3.37)$$

In this section $K(\psi)$ is the isotropic integral operator kernel, that depends on the angular distance ψ but not on the azimuth α from the computation point to the moving integration point. The coordinates to use in (3.37) are the geodetic coordinates (ϕ, λ) , e.g., to compute the ψ as in (3.17). This is a consequence of the mapping being used to convert from an ellipsoid to a spherical boundary surface when handling Δg_E -data (Figure 2). The foregoing discussions can easily be made to apply to the handling of boundary values Δg that refer to a geocentric sphere of radius r_E (those defined under (3.9)), by just changing R to r_E , r_1 to r , ϕ to $\bar{\phi}$, and Δg_E to Δg in the formulas. Examples of the form (3.37) are the expressions (3.14) for T and (3.15) for δ_r . We can express (3.37) in spectral form as follows:

$$f = \frac{1}{2} \sum_{n=2}^{\infty} k_n \Delta g_{En} , \quad (3.38)$$

consistent with the expansions:

$$K = \sum_{n=2}^{\infty} \frac{2n+1}{2} k_n P_n(y) ; y = \cos \psi \quad (3.39)$$

$$k_n = \int_{-1}^1 K(\psi) P_n(y) dy \quad (3.40)$$

$$\Delta g_E = \sum_{n=2}^{\infty} \Delta g_{En} \quad (3.41)$$

$$\Delta g_{En} = \frac{2n+1}{4\pi} \int_{\sigma} \Delta g_E P_n(y) d\sigma. \quad (3.42)$$

The central idea in truncation theory is that there are two estimates that we denote by Δg_E^T and Δg_E^s available for Δg_E , these estimates having their respective errors ε^T and ε^s :

$$\Delta \hat{g}_E^T = \Delta g_E + \varepsilon^T \quad (3.43)$$

$$\Delta \hat{g}_E^s = \Delta g_E + \varepsilon^s. \quad (3.44)$$

In these equations the superscript "T" denotes the estimate from terrestrial data and the superscript "s" denotes the estimate implied by an available finite set of spherical harmonic coefficients, these two types of estimates being the ones most often considered. The role of truncation theory is then to combine the information from the above estimates for the purpose of computing the unknown quantity f . It is generally regarded that $\Delta \hat{g}_E^T$ will be used as carrier of high frequency information, while $\Delta \hat{g}_E^s$ will be used as carrier of low frequency information about the gravity field. Considering that high frequency information is associated with data close to the computation point while low frequency information is associated with data farther away, then the combination of $\Delta \hat{g}_E^T$ and $\Delta \hat{g}_E^s$ to produce an estimate \hat{f} is effected through the following split of (3.37), as illustrated in Figure 6:

$$f = \hat{f} + \Delta f \quad (3.45)$$

$$\hat{f} = \frac{1}{4\pi} \int_{\sigma} (K-K^s) \Delta \hat{g}_E^T + \frac{1}{2} \sum_{n=2}^q k_n^s \Delta \hat{g}_{En}^s \quad (3.46)$$

$$\Delta f = f - \hat{f} = \frac{-1}{4\pi} \int_{\sigma} (K-K^s) \varepsilon^T d\sigma - \frac{1}{2} \sum_{n=2}^q k_n^s \varepsilon_n^s + \frac{1}{2} \sum_{n=q+1}^{\infty} k_n^s \Delta g_{En}, \quad (3.47)$$

where we have the kernel for the spherical harmonic contribution (see Figure 6):

$$K^s = \begin{cases} K^c, & 0 < \psi \leq \psi_0 \\ K, & \psi_0 < \psi \leq \pi \end{cases} \quad (3.48)$$

ψ_0 ... truncation cap radius

with the alternative "modification" functions (Molodensky et al., 1962; Meissl, 1971; Wong and Gore, 1969; Jekeli, 1980):

$$K^c = \begin{cases} K_1^c = 0 & [\text{Unmodified Molodensky Truncation}] \\ K_2^c = K(\psi_0) & [\text{Meissl Truncation}] \\ K_3^c = \sum_{n=2}^{\bar{n}} \frac{2n+1}{2} k_n P_n(y) & [\text{Wong/Gore Truncation}] \\ K_4^c = \sum_{n=2}^{\bar{n}} \frac{2n+1}{2} S_n P_n(y), \text{ with } S_n \text{ such that} \\ \int_{\psi_0}^{\pi} (K - K_4^c)^2 \sin \psi \, d\psi \rightarrow \min. & [\text{Improved Molodensky Truncation}] \end{cases} \quad (3.49)$$

In (3.46) and (3.47) the k_n^s are the coefficients in the Legendre expansion of K^s , expressed as an integral of K^s in (3.40); the ϵ_n^s are the surface harmonics of the error ϵ^s , expressed as an integral of ϵ^s as in (3.42); and q is the highest degree of spherical harmonic representation. As mentioned under (3.13) of the last section we do not use Δg_{En} in the actual computation of the spherical harmonic coefficient contribution to f (i.e., in the second term of (3.46)); rather, we use Δg_n as given by (3.9) which for estimates \hat{C}_{nm}^* of potential coefficients C_{nm}^* becomes:

$$\Delta \hat{g}_{En}^s \rightarrow \Delta \hat{g}_n = \frac{kM}{a^2} \sum_{m=-n}^n (n-1) \left(\frac{a}{r_E} \right)^{n+2} \hat{C}_{nm}^* \bar{Y}_{nm}(\varphi, \lambda) \quad (3.50)$$

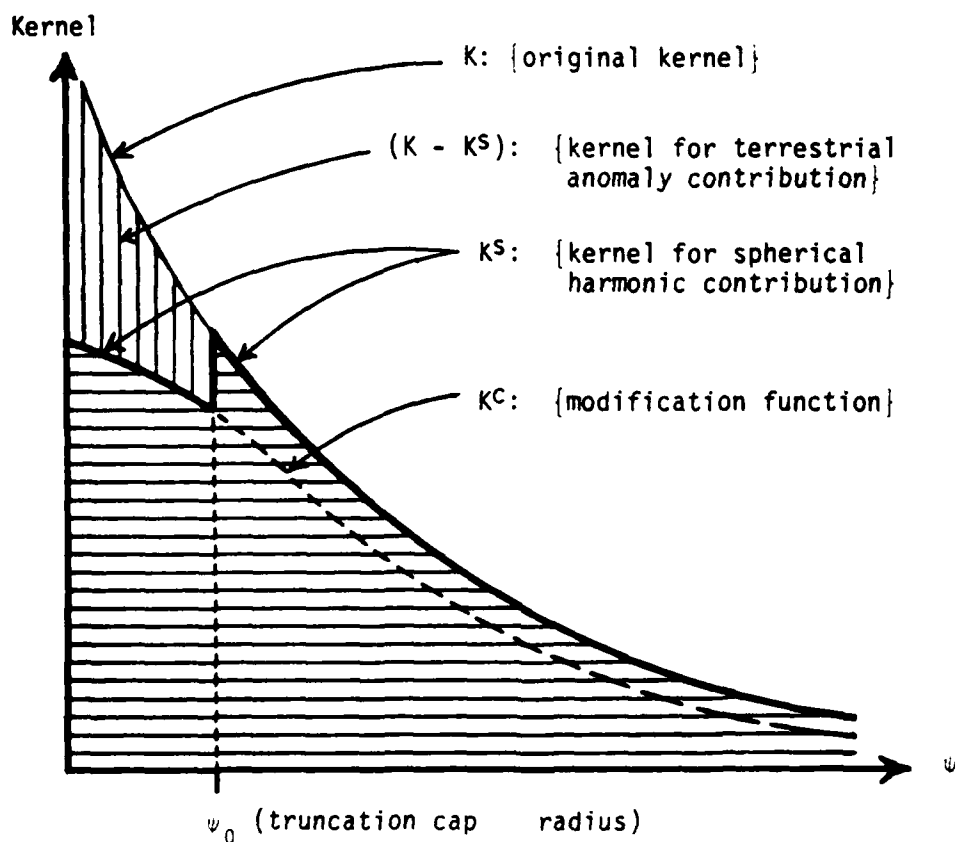


Figure 6. Splitting of the Original Kernel K for the Combination of Terrestrial Gravity Anomaly and Spherical Harmonic Coefficient Information, in Isotropic Gravimetric Integration.

The replacement (3.50) has also been used in Rapp (1981a, second term of (34)).

The kernel split illustrated in Figure 6 conforms to the idea that detailed (i.e., high frequency) terrestrial information need be used only out to some limited radius ψ_0 around the computation point, and therefore the kernel $(K-K^s)$ for the terrestrial contribution is set to zero outside ψ_0 . From the space domain point of view the role of the modification function K^c is then to effect a certain degree of continuity to the transition from the non-zero values of $(K-K^s)$ for $\psi < \psi_0$ to its zero values for $\psi > \psi_0$. Or, equivalently, the modification function provides a certain degree of continuity to each of the component kernels $(K-K^s)$ and K^s of the total kernel K . In this respect the unmodified Molodensky truncation ($K^c=0$) does not provide good continuity, as in fact in this case the kernels $(K-K^s)$ and K^s become sharply discontinuous at $\psi = \psi_0$. Such sharp discontinuities of the kernels in the space domain, both in function values and derivatives, are to be avoided because in the frequency domain they directly cause unwanted oscillations in the Legendre coefficients $(k_n - k_n^s)$ and k_n^s . These oscillations had been variously called "ringing", "ripples", or "Gibbs phenomenon" in Fourier series analysis. If we have these oscillations then we are not getting a "clean" separation between high and low frequency information: $(K-K^s)$ may have significant energy leaks into the low frequencies, and K^s may have significant leaks into the high frequencies. In terms of our expression (3.47) for the total error Δf , the low frequency leaks of $(K-K^s)$ will enlarge the terrestrial data propagation error (first term in (3.47)) by allowing more low frequency energies of ϵ^T to pass, and the high frequency leaks of k_n^s will enlarge the spherical harmonic coefficient omission error (third term in (3.47)) and to some extent the spherical harmonic coefficient commission error (second term in (3.47)) by allowing more high frequency Δg_{En} and ϵ_n^s to pass.

Several authors have numerically confirmed the significance of carefully choosing the modification function in the kernel split of the type shown in Figure 6. We mention only two authors, who present several comparisons covering all the famous modification functions listed in (3.49). Jekeli (1980) presents comparisons for the case of the Stokes kernel and Jekeli (1982) deals with the Stokes, Vening-Meinesz, and Poisson kernels. Chen (1982) presents comparisons for the Vening-Meinesz kernel. The treatment of truncation theory for the (non-isotropic) Vening-Meinesz kernel is only slightly different from an isotropic case, and we will explain this below. Also below we will present our own numerical comparisons, for the case of gravity disturbance vector computations at altitude. In these computations the basic kernel is the space-extended Stokes kernel, which is differentiated to yield the radial disturbance kernel and to form the horizontal disturbance kernel (which is also essentially the space-extended Vening-Meinesz kernel).

The decision on which modification function is the best is usually based on least RMS value of the total error (commission plus omission) of the spherical harmonic coefficient contribution to f . Specifically, denoting this error by Δf^s , we have from (3.47):

$$\Delta f^s = -\frac{1}{2} \sum_{n=2}^q k_n^s z_n^s + \frac{1}{2} \sum_{n=q+1}^{\infty} k_n^s \Delta g_{En} \quad (3.51)$$

with the goal to have the least value for the global RMS, expressed as the square root of:

$$\sigma^2(\Delta f^s) = \frac{1}{4} \sum_{n=2}^q (k_n^s)^2 \delta C_n + \frac{1}{4} \sum_{n=q+1}^{\infty} (k_n^s)^2 C_n \quad (3.52)$$

Here the δC_n are the anomaly error degree variances implied by the spherical harmonic coefficient errors and the C_n are the anomaly degree variances themselves, e.g., as modeled in (3.36). Equation (3.52) applies to any isotropic kernel. The expression for the non-isotropic Vening-Meinesz kernel will be given below. To summarize the numerical comparisons (see Jekeli, 1980, 1982; and Chen, 1982 for details) the improved Molodensky truncation method consistently gives better results (i.e., smaller $\sigma(\Delta f^s)$) than any of the other truncation methods listed in (3.49). For truncation cap radii and accuracy levels of interest, the Meissl truncation method gives better results than the unmodified method in the case of the Stokes kernel, but yields poorer results for more local kernels (those with less remote zone effects) such as the Poisson and Vening-Meinesz kernel. The Wong/Gore method is only of interest but has not been specifically designed to avoid the kernel continuity problem discussed above, and in fact this method gives significantly poorer results than the other methods (including the unmodified method) in typical cases.

3.3.2 Non-Isotropic Kernels

Let us now turn to a non-isotropic integral operation on the gravity anomalies Δg_E . Specifically, we will discuss the integral (3.16) for the computation of the North-South and East-West components of the gravity disturbance vector in space. We can write (3.16) in the form:

$$\begin{pmatrix} \delta\psi \\ \delta\lambda \end{pmatrix} = \frac{1}{4\pi} \int_{\sigma} V(\psi) \Delta g_E \begin{pmatrix} \cos \alpha \\ \sin \alpha \end{pmatrix} d\sigma, \quad (3.53)$$

where $V(\psi)$ is the space-extended Vening-Meinesz function as given in (3.20). The spectral form of (3.53) can be written as (see (3.12)):

$$\begin{pmatrix} \delta\psi \\ \delta\lambda \end{pmatrix} = \frac{1}{2} \sum_{n=2}^{\infty} v_n \begin{pmatrix} \frac{\partial}{\partial\psi} \Delta g_{En} \\ \frac{1}{\cos\psi} \frac{\partial}{\partial\lambda} \Delta g_{En} \end{pmatrix}, \quad (3.54)$$

where now we are using an expansion in terms of the associated Legendre functions of the first order (see (3.28)):

$$V = \sum_{n=2}^{\infty} \frac{2n+1}{2} v_n P_{n1}(y) \quad (3.55)$$

with the coefficients (see, e.g., Chen, 1982):

$$v_n = \frac{1}{n(n+1)} \int_{-1}^1 V(\psi) P_{n1}(y) dy. \quad (3.56)$$

Analogous to the split (3.45)-(3.47) for an isotropic integral operation, we now have the following split of (3.53) for the computation of estimates $\hat{\delta}\psi$ and $\hat{\delta}\lambda$ from a combination of terrestrial gravity anomaly and spherical harmonic coefficient information:

$$\begin{pmatrix} \delta\psi \\ \delta\lambda \end{pmatrix} = \begin{pmatrix} \hat{\delta}\psi \\ \hat{\delta}\lambda \end{pmatrix} + \begin{pmatrix} \Delta\delta\psi \\ \Delta\delta\lambda \end{pmatrix} \quad (3.57)$$

$$\begin{pmatrix} \hat{\delta}\psi \\ \hat{\delta}\lambda \end{pmatrix} = \frac{1}{4\pi} \iint_{\sigma} (V - V^s) \Delta \hat{g}_{En}^I \begin{pmatrix} \cos \alpha \\ \sin \alpha \end{pmatrix} d\sigma + \\ + \frac{1}{2} \sum_{n=2}^q v_n^s \begin{pmatrix} \frac{\partial}{\partial\psi} \Delta \hat{g}_{En}^s \\ \frac{\partial}{\cos\psi} \frac{\partial}{\partial\lambda} \Delta \hat{g}_{En}^s \end{pmatrix}, \quad (3.58)$$

$$\begin{pmatrix} \Delta\delta_{\varphi} \\ \Delta\delta_{\lambda} \end{pmatrix} = \frac{-1}{4\pi} \int_{\sigma} (V-V^s) \varepsilon^T \begin{pmatrix} \cos \alpha \\ \sin \alpha \end{pmatrix} d\sigma - \\ - \frac{1}{2} \sum_{n=2}^q v_n^s \begin{pmatrix} \frac{\partial}{\partial \varphi} z_n^s \\ \frac{\partial}{\cos \varphi \partial \lambda} z_n^s \end{pmatrix} + \frac{1}{2} \sum_{n=q+1}^{\infty} v_n^s \begin{pmatrix} \frac{\partial}{\partial \varphi} \Delta g_{En} \\ \frac{\partial}{\cos \varphi \partial \lambda} \Delta g_{En} \end{pmatrix} \quad (3.59)$$

The splitting of the original function V into the function $(V-V^s)$ for the terrestrial anomaly contribution and the function V^s for the spherical harmonic contribution is completely analogous to the splitting of K into $(K-K^s)$ and K^s (see Figure 6). A modification function, which can now be denoted as V^c , is also used. The difference is that now all expansions are in terms of $P_{n1}(y)$ rather than $P_n(y)$, e.g., in such equation as (3.49). The replacement indicated in (3.50) is also used. The total error (commission plus omission) of spherical harmonic coefficient contribution is given as the sum of the second and third terms in (3.59):

$$\begin{pmatrix} \Delta\delta_{\varphi}^s \\ \Delta\delta_{\lambda}^s \end{pmatrix} = -\frac{1}{2} \sum_{n=2}^q v_n^s \begin{pmatrix} \frac{\partial}{\partial \varphi} z_n^s \\ \frac{\partial}{\cos \varphi \partial \lambda} z_n^s \end{pmatrix} + \frac{1}{2} \sum_{n=q+1}^{\infty} v_n^s \begin{pmatrix} \frac{\partial}{\partial \varphi} \Delta g_{En} \\ \frac{\partial}{\cos \varphi \partial \lambda} \Delta g_{En} \end{pmatrix} \quad (3.60)$$

The total horizontal error $\Delta\delta_H^s$ from (3.60) is obtained from:

$$(\Delta\delta_H^s)^2 = (\Delta\delta_{\varphi}^s)^2 + (\Delta\delta_{\lambda}^s)^2 \quad (3.61)$$

The goal of the choice of modification function in this non-isotropic case is to have the least global RMS value for $\Delta\delta_H^s$, this RMS value being expressed as the square root of (cf. Heiskanen and Moritz, 1967, pp. 261-262):

$$\sigma^2(\Delta\delta_H^s) = \frac{1}{4} \sum_{n=2}^q n(n+1)(v_n^s)^2 \delta C_n + \\ + \frac{1}{4} \sum_{n=q+1}^{\infty} n(n+1)(v_n^s)^2 C_n \quad (3.62)$$

3.3.3 Truncation Coefficients

Now let us discuss how to obtain the so-called truncation coefficients k_n^s and v_n^s needed in (3.46) and (3.58) for actual estimations and in (3.42) and (3.62) for error analyses. We will discuss the coefficients for the computation of the disturbance vector components, for which the unsplit kernels are (3.19) for the radial and (3.20) for the horizontal components. The starting point of discussion is the recursive computation of the unmodified truncation coefficients (i.e., those corresponding to the use of $K^c=K, c=0$; see (3.49)) for the space-extended Stokes function given in (3.18). Two significantly different sets of recursive formulas exist, one by Shepperd (1979) and the other by Paul (1983). Although Paul's recursives are claimed to be more stable than Shepperd's (see Paul, 1983, Table 3) our own computations showed practically the same numerical values of individual truncation coefficients from the two solutions. We did our tests (not shown here) using the program given in Shepperd (ibid.) and a program supplied to us by Paul, with all computations implemented in double precision. We used various altitudes and compared truncation coefficients from degree 2 up to some reasonable maximum degree of required field representation for the altitude in question (see Figure 5). Since there was no significant difference between using Paul's or Shepperd's solution, we simply decided to use Shepperd's solution for all subsequent applications.

From the unmodified truncation coefficients for the space-extended Stokes function, Shepperd (ibid.) makes extensions to compute the unmodified truncation coefficients for the functions (3.19) and (3.20) of radial and horizontal disturbance computation, and gives recursive formulas and programs for these computations. Shepperd's programs were converted to double precision computations for our applications.

Now given the unmodified truncation coefficients for the functions (3.19) and (3.20) of radial and horizontal disturbance computation, it is relatively easy to convert these coefficients using a few additional recursive relations to obtain the truncation coefficients under the Meissl, Wong/Gore, and improved Molodensky truncation methods. For this purpose we used formulas from Jekeli (1980), which were given for the Stokes function but are actually applicable to any isotropic kernel such as the radial disturbance kernel (3.19). For the non-isotropic case of horizontal disturbance computation we used formulas from Chen (1982) for the conversion from the unmodified truncation coefficients from Shepperd's program to modified truncation coefficients under the various truncation methods. This completes the discussion of how to obtain the truncation coefficients for radial and horizontal disturbance computations.

3.3.4 Numerical Investigations

For error analyses using (3.52) and (3.62) we needed the anomaly degree variances C_n , for which we used the two-component model (3.36). We also needed the anomaly error degree variances δC_n , implied by the errors in the spherical harmonic coefficient set to degree q . Since we wanted to test several reference field degrees ($q=20, 36, 180, 360$) we decided to use a model for δC_n , testing two models A and B derived from a white noise process:

Model A:

$$\begin{aligned} \delta C_n^A &= \sigma_o^2 (2n+1), \quad n = 2, 3, \dots, q \\ &\text{with } \sigma_o^2 \text{ such that } \delta C_q^A = 0.5 C_q. \end{aligned} \quad (3.63)$$

Model B:

$$\begin{aligned} \delta C_n^B &= 0, \quad n = 2, 3, \dots, 10 \\ \delta C_n^B &= \sigma_o^2 (2n+1), \quad n = 11, 12, \dots, q \\ &\text{with } \sigma_o^2 \text{ such that } \delta C_q^B = 0.3 C_q. \end{aligned} \quad (3.64)$$

To visualize the above noise processes we note that a white noise process approximates an uncorrelated error process in blocks of certain size. Specifically, if we have uncorrelated errors, with variance $m^2(\Delta g)$, in Δg in blocks of size $\theta \times \theta$ (radians) then we can write (Jekeli and Rapp, 1980, (10)):

$$\sigma_o^2(m^2(\Delta g_{nm})) = \frac{\theta^2}{4\pi} m^2(\Delta g). \quad (3.65)$$

From (3.63) and (3.64) we can also express σ_o^2 as:

$$\sigma_o^2 = \frac{x \cdot C_q}{2q+1}, \quad (3.66)$$

where x denotes a constant factor ($x = 0.5$ in (3.63), and $x = 0.3$ in (3.64)). A harmonic degree q corresponds to block size θ of:

$$\theta = \frac{\pi}{q} \text{ (radians)}. \quad (3.67)$$

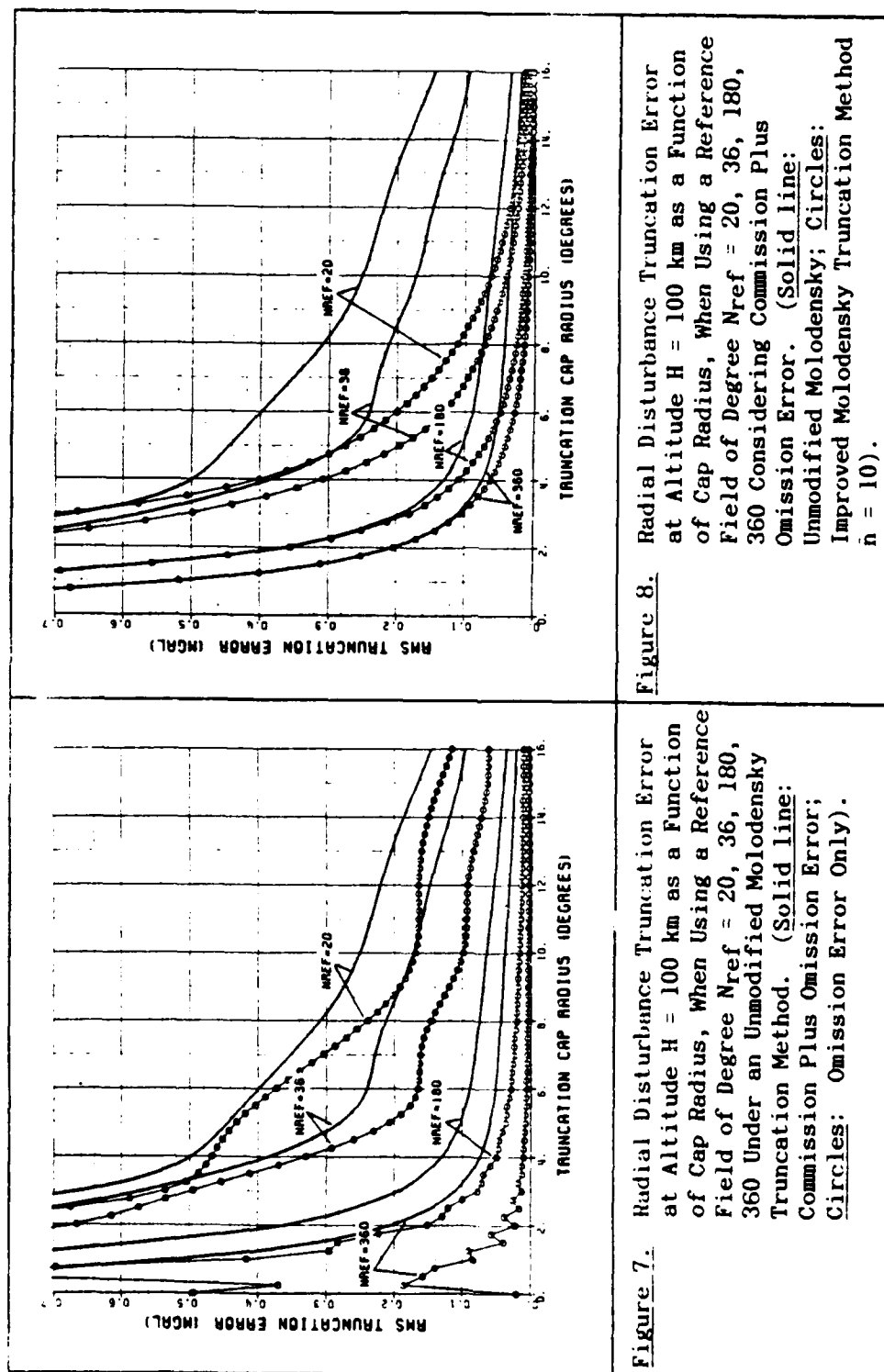
Combining (3.65) - (3.67) we get:

$$m^2(\Delta g) = \frac{4 \cdot x \cdot C_q}{2q+1} \frac{(q)^2}{\pi} . \quad (3.68)$$

Using (3.68) and the two-component model (3.36) for C_q we can now visualize the noise process in (3.63) ($x=0.5$) as being uncorrelated errors of $m(\Delta g)=(5, 6, 12, 14)$ mgals in blocks of size $\theta=(9, 5, 1, 0.5)$ degrees when using a reference field to degree $q=(20, 36, 180, 360)$. For (3.64) ($x=0.3$) the visualization is that of uncorrelated errors of $m(\Delta g)=(3, 3.5, 7, 8)$ mgals in blocks of size $\theta=(9, 5, 1, 0.5)$ degrees when using a reference field to degree $q=(20, 36, 180, 360)$. In (3.64) there is an additional removal of long-wavelength errors corresponding to harmonic degrees 2 to 10. We believe that (3.64) is a more realistic portrayal of available data, with (3.63) being on the pessimistic side.

Since only the improved Molodensky truncation method (with $\bar{n}=10$, see (3.49)) yielded consistently better error analysis results than the unmodified truncation method, we do not present results for the Meissl and Wong/Gore truncation methods listed in (3.49). Our results for the improved Molodensky and unmodified Molodensky truncation methods are given as Figures 7 to 14. The figures show the RMS truncation error (in mgals) from (3.52) and (3.62) versus the truncation cap radius ψ_0 (in degrees). Several reference field degrees q , denoted as n_{ref} in the figures with $n_{ref}=20, 36, 180, 360$, were tested using a "high" altitude of 100 km and a "low" altitude of 5 km. Specifically, the Figures 7, 8, 9, 10 give results for the radial disturbance case, while the Figures 11, 12, 13, 14 show results for the horizontal case. The odd numbered Figures 7, 9, 11, 13 contrast the case of having commission plus omission errors (solid line) against the case of having omission errors only, i.e., the case of perfect reference field (circled line), under the unmodified Molodensky truncation. The even numbered Figures 8, 10, 12, 14 contrast the case of using the unmodified Molodensky truncation (solid line) against the case of using the improved Molodensky truncation (circled line). The upper limit \bar{n} of the summation for K^c in the improved Molodensky truncation (see (3.49)) was taken as $\bar{n}=10$, which is a typical value that can be chosen (see Jekeli, 1982). A value of $\bar{n}=20$ produced slightly larger truncation errors for a given cap size. Also, the graphs reflect the use of only model B for δC_n (see (3.64)). The effect of using model A for δC_n (see (3.63)) was mainly the introduction of an additional long wavelength error, generally making the graphs higher by about 0.5 mgal for small cap sizes ($\psi_0 < 3^\circ$) decreasing very slowly to 0.2 mgal for large cap sizes (ψ_0 up to 40° were tested). The magnitudes of RMS truncation errors should be judged against the magnitudes of the RMS signals themselves, which at altitude 100 km is about 20 mgals and at altitude 5 km is about 36 mgals for both the radial and total horizontal disturbances (see Figure 4).

Looking at Figure 7 (solid lines) we see that if we everytime tolerate a 1% truncation error (≈ 0.2 mgal) at 100 km altitude, then we can use $n_{ref}=20$ (equivalent to the use of mean anomalies in block sizes of roughly $10^\circ \times 10^\circ$) outside a cap of radius $\psi=13^\circ$ from the computation



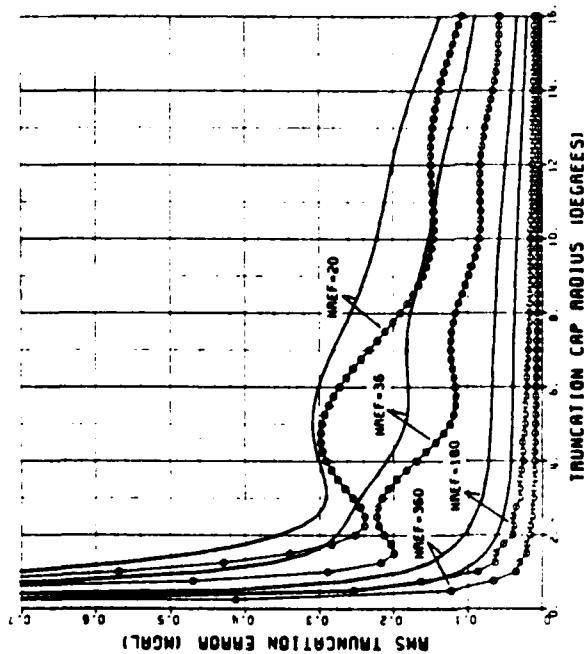


Figure 9. Radial Disturbance Truncation Error at Altitude $H = 5$ km as a Function of Cap Radius, When Using a Reference Field of Degree $N_{ref} = 20, 36, 180, 360$ Under an Unmodified Molodensky Truncation Method. (Solid line: Commission Plus Omission Error; Circles: Omission Error Only).

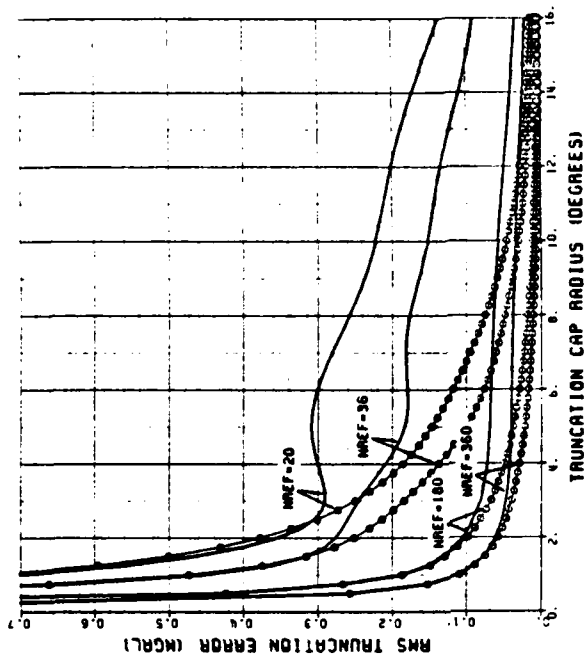
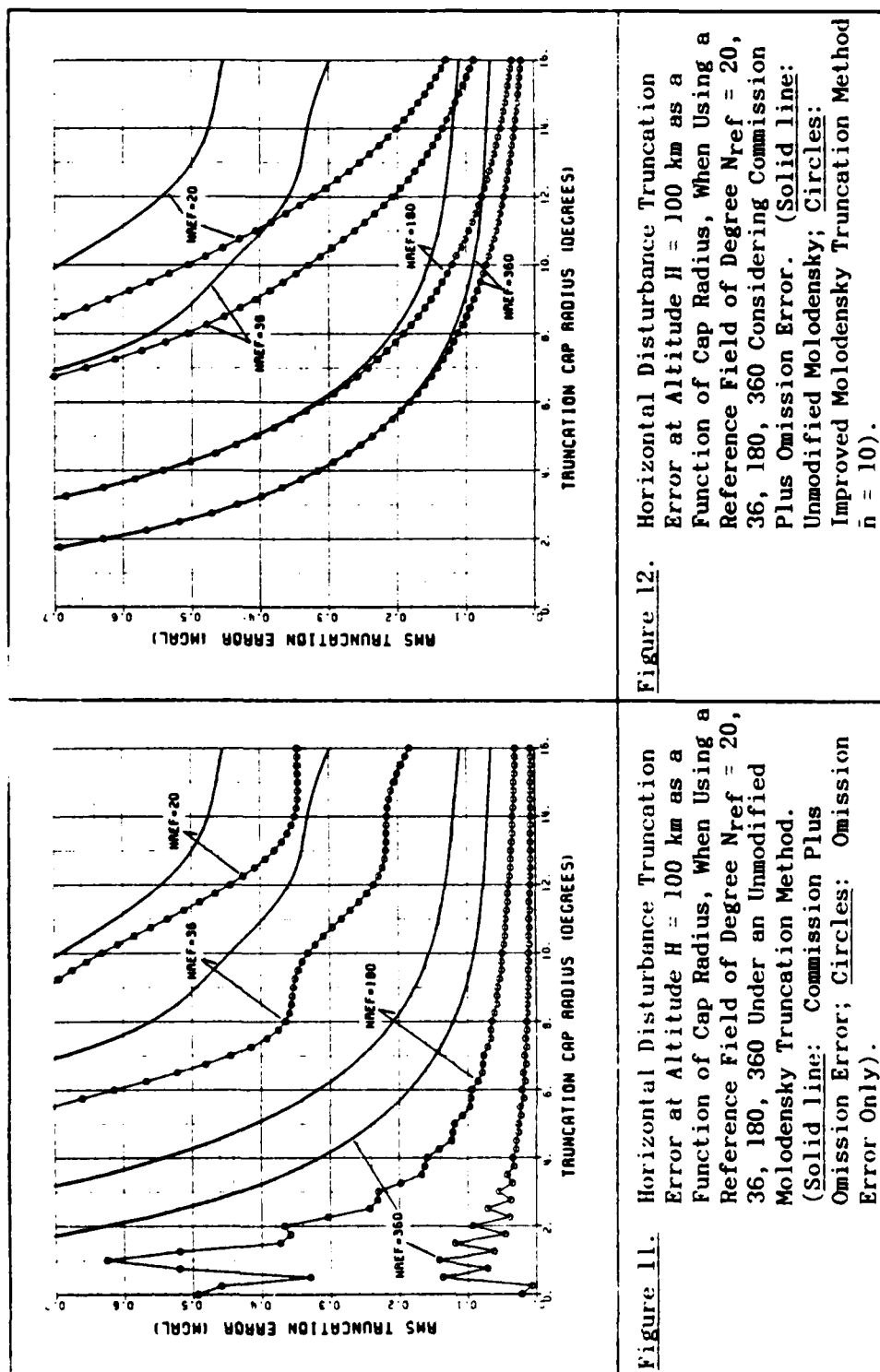


Figure 10. Radial Disturbance Truncation Error at Altitude $H = 5$ km as a Function of Cap Radius, When Using a Reference Field of Degree $N_{ref} = 20, 36, 180, 360$ Considering Commission Plus Omission Error. (Solid line: Unmodified Molodensky; Circles: Improved Molodensky Truncation Method $\bar{n} = 10$).



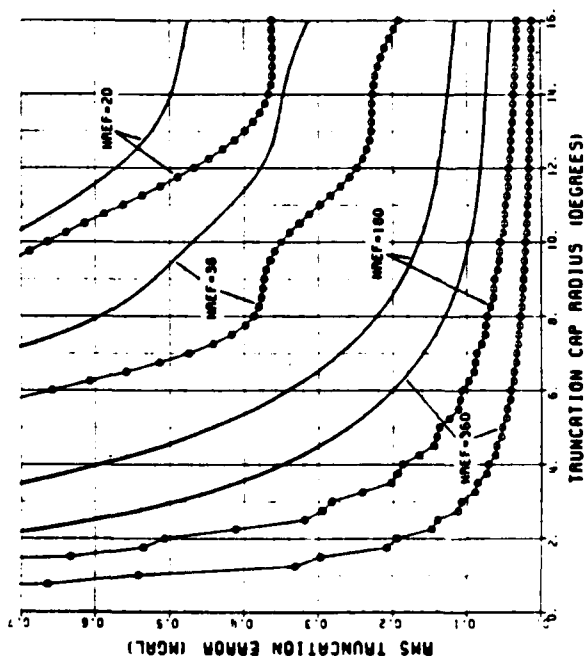


Figure 13. Horizontal Disturbance Truncation Error at Altitude $H = 5$ km as a Function of Cap Radius, When Using a Reference Field of Degree $N_{ref} = 20, 36, 180, 360$ Under an Unmodified Molodensky Truncation Method. (Solid line: Commission Plus Omission Error; Circles: Omission Error Only).

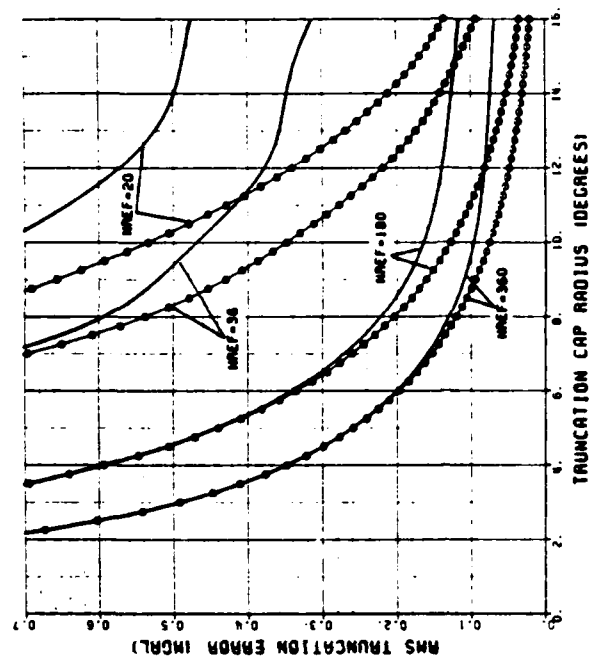


Figure 14. Horizontal Disturbance Truncation Error at Altitude $H = 15$ km as a Function of Cap Radius, When Using a Reference Field of Degree $N_{ref} = 20, 36, 180, 360$ Considering Commission Plus Omission Error. (Solid line: Unmodified Molodensky; Circles: Improved Molodensky Truncation Method $\bar{n} = 10$).

point. Inside this cap Figure 7 shows that the use of $n_{ref}=20$ will make the truncation error exceed 0.2 mgal, and in order to avoid this we can shift to the use of $n_{ref}=36$ ($\approx 5^\circ \times 5^\circ$ Δg -data) which gives less than 0.2 mgal error down to $\psi=9^\circ$. For $\psi < 9^\circ$ we can shift to $n_{ref}=180$ ($\approx 1^\circ \times 1^\circ$ Δg -data) and this will control the error to below 0.2 mgal down to $\psi=3^\circ$. For $\psi=2^\circ$ to 3° Figure 7 shows that $n_{ref}=360$ ($\approx 0.5^\circ \times 0.5^\circ$ Δg -data) can be used to keep the truncation error below 0.2 mgal. For $\psi < 2^\circ$, we can extrapolate from Figure 7 that in order to keep the error below 0.2 mgal we can use higher and higher order reference field (denser and denser Δg -data). Alternatively, for $\psi < 2^\circ$ we can use a more accurate reference field to degree 360 (more accurate $0.5^\circ \times 0.5^\circ$ Δg -data), because in fact Figure 7 shows that an errorless reference field to degree 360 is sufficient to define the radial disturbance at altitude 100 km with a 1% relative omission error (this result is consistent with Figure 5 of the last section). As mentioned at the end of the last section and now illustrated by Figure 7, there is no need to maintain a single data density all over the earth. Instead, Δg -data of less and less resolution as indicated above can be used farther and farther away from the computation point. Therefore, graphs from truncation theory such as those we show here directly reveal information about the response of gravimetric quantities to terrestrial gravity anomaly data of certain resolution and distance from the computation point.

Comparing Figure 11 with Figure 7, one can see that the horizontal disturbance requires significantly larger data caps (more than 2 times larger than the radial case) in order to keep truncation errors below, e.g., a 0.2 mgal level. Therefore, the horizontal disturbance is much more sensitive to remote zone data than the radial disturbance. This is true also at the low altitude of 5 km, where Figure 13 (5 km) shows only slightly different curves from Figure 11 (100 km) in the horizontal case, while Figure 9 (5 km) shows even smaller cap requirements than Figure 7 (100 km) in the radial case.

To summarize: using a reasonably typical case, assume we have detailed gravity anomaly data (e.g., $5^\circ \times 5^\circ$) in a cap of radius 3° around the computation point. In quoting truncation theory errors, only the errors contributed from outside the inner cap are considered, with the error coming from inside the cap being propagated separately using the first terms in (3.47) or (3.59), if desired. Now in order to account for remote zone effects ($\psi > 3^\circ$) assume that we use a reference field to degree $n_{ref}=180$, e.g., the Rapp (1981) field. Assume further that the 180-field implies the errors δC_n^B given by (3.64) (not an unreasonable assumption for the Rapp-180 field). Then the RMS truncation error under the unmodified Molodensky truncation theory has a relative value of under 1% at altitudes 100 km and 5 km for the radial disturbance case, and can reach 4% at 100 km and 2% at 5 km for the horizontal disturbance case. With the additional presence of long wavelength ($n \leq 10$) errors in the 180-field and implying the errors δC_n^A given by (3.63), then the relative truncation errors became 2% at altitude 100 km but still 1% at 5 km in the radial case, and may reach 6% for altitudes 100 km and 5 km in the horizontal case.

Looking at the Figures 8, 10, 12, 14 contrasting the unmodified versus the improved Molodensky truncation methods, one can see that the improved method gives better results for relatively large cap sizes only. From the practical point of view, anticipating the use of $n_{ref}=180$, then we can say that for cap sizes and accuracy levels of interest the improved Molodensky method offers no significant gain over the unmodified case in both radial and horizontal disturbance computations.

4. ACCOUNTING FOR THE TOPOGRAPHY IN MODELING THE SPATIAL DISTURBANCE VECTOR, A CONTINUOUS APPROACH

In Chapter 1 we introduced the gravity anomaly Δg , related to the disturbing potential T through (1.9):

$$\Delta g = - \frac{\partial T}{\partial h} + \frac{1}{\gamma} \frac{\partial \gamma}{\partial h} T \quad (4.1)$$

or, in spherical approximation, through (1.12):

$$\Delta g = - \frac{\partial T}{\partial r} - \frac{2}{r} T. \quad (4.2)$$

If the given gravity anomalies refer to an equipotential surface, then the modeling of the anomalous gravity field by classical integral formulas (Heiskanen and Moritz, 1967, sec. 6-4) would be correct to the order of the earth's flattening (ibid., pp. 240-241). This is usually considered a sufficient accuracy. In reality, however the gravity anomaly data refer to the earth's topography, which may significantly deviate from being an equipotential surface. Therefore, there is a problem of accounting for the topography in the modeling procedures.

In this chapter we will be concerned with the above topography problem. We will present a composite model that accounts for the topography to a good degree of approximation, and which at the same time is convenient for practical applications. In essence, the composite model consists of the spherical harmonic model to represent the long wavelength part of the field, the residual topographic model to represent the short wavelength part of the field, and the classical integral model to represent the remaining (medium wavelength) part of the field. In the next chapter we will additionally examine the least squares collocation and Bjerhammar's Dirac type models, which are two other models that can be introduced to account for the topography in modeling the external gravity field.

4.1 Some General Considerations on the Topography Problem

Some general characteristics of the topography problem can be concluded by considering the simple crustal density model used also by Moritz (1968), Lambeck (1979), Jekeli (1981), and Rapp (1982a). From

Jekeli (ibid., (2.130)) we have that the spherical harmonic coefficients h_{nm} of the equivalent rock topography generate the spherical harmonic coefficients g_{nm}^h of what we will call "topographic gravity anomalies", as follows:

$$g_{nm}^h = 4\pi R G \rho \left(\frac{n-1}{R} \right) \frac{h_{nm}}{2n+1} \quad (4.3)$$

where R is a mean earth radius (6371 km), G is the constant of gravitation, and ρ is a constant crustal density (2.67 g/cm³). Equation (4.3) assumes that the topographic masses have been condensed onto the mean earth sphere of radius R , and the g_{nm}^h refer to this same sphere. Under an Airy-Heiskanen isostatic compensation model, compensating masses at depth D generate spherical harmonic coefficients g_{nm}^c of what we will call "isostatic gravity anomalies", referred to the mean earth sphere of radius R . Assuming that the compensating masses have been condensed onto a geocentric sphere of radius $(R-D)$, then the g_{nm}^c are simply the negative attenuated version of g_{nm}^h , as follows:

$$g_{nm}^c = - \left(\frac{R-D}{R} \right)^n g_{nm}^h . \quad (4.4)$$

The coefficients of the total gravity anomaly referred to the mean earth sphere can be expressed as:

$$g_{nm} = g_{nm}^h + g_{nm}^c . \quad (4.5)$$

Combining (4.3)-(4.5) we also have:

$$g_{nm} = \left[1 - \left(\frac{R-D}{R} \right)^n \right] g_{nm}^h . \quad (4.6)$$

Given the anomaly degree variances C_n as in (3.36), then using (4.6) we can propagate C_n to the degree variances C_n^h of topographic gravity anomalies, as follows:

$$C_n^h = \frac{C_n}{\left[1 - \left(\frac{R-D}{R} \right)^n \right]^2} \quad (4.7)$$

Equation (4.7) expresses the degree variances of the gravity anomaly field generated by topographic masses, i.e., the field implied by the spherical harmonic coefficients g_{nm}^h of (4.3). The presence of the isostatic depth D in the equation is caused by the following: we first of all used D to define the g_{nm}^c -field as in (4.4), then with the condition (4.5) that the sum of the g_{nm}^h - and g_{nm}^c -fields is equal to the observed

field g_{nm} , the dependence of the g_{nm}^h -field on the depth D follows.

Now using (4.4) and (4.7), we have the degree variances C_n^c of the gravity anomalies generated by isostatic compensating masses:

$$C_n^c = \frac{\left(\frac{R-D}{R}\right)^{2n}}{\left[1 - \left(\frac{R-D}{R}\right)^n\right]^2} C_n \quad (4.8)$$

Using the degree variances C_n , C_n^h , C_n^c and assuming that we can computationally isolate the gravitational effect of topographic masses at harmonic degrees $n \leq N$, then we can define various types of fields with their corresponding gravity anomaly degree variances, as shown in Table 3.

As shown in Table 3 the "total field" is the total observed field, with associated anomaly degree variances C_n as modeled for example by (3.36) for $n=2$ to ∞ . The "residual topographic field" is generated by the gravitational influence of topographic masses beyond a given harmonic degree N . Specifically, the anomaly degree variances for this field are assumed to be zero for $n=2$ to N , and equal to the C_n^h of (4.7) for $n > N$. Analogously, the "residual isostatic field" is generated by the gravitational influence of isostatic compensating masses beyond degree N , resulting in anomaly degree variances of zero for $n=2$ to N and the C_n^c of (4.8) for $n > N$. The "residual-topography reduced field" is found by subtracting the residual topographic field from the total field, leaving a field with anomaly degree variances of C_n for $n=2$ to N (as in the total field) and C_n^c for $n > N$ (as in the residual isostatic field). Of interest also is the "N-field" (for example, called the 180-field for $N=180$) which is the part of the total field that is implied by harmonic degrees less than or equal to N , giving degree variances of C_n for $n=2$ to N and zero for $n > N$. Note that the N-field theoretically results by subtracting from the total field the gravitational influence of both the residual topographic masses and their compensation.

For first numerical considerations, let us illustrate that the residual-topography reduced field is much smoother (i.e., with much less power in the high frequencies) than the original "total field." To do this for the disturbance vector field at altitude the construction of Figures 4 and 5 of the previous chapter was repeated, this time using degree variances C_n for $n=2$ to 180 and C_n^c for $n=181$ to 5400, instead of using C_n entirely for $n=2$ to 5400 as was done in Figures 4 and 5. For C_n the two-component model (3.36) was again used, and for C_n^c the standard depth of compensation $D=30$ km was assumed in (4.8). For smoother looking graphs around $n=180$, a linear transition was arbitrarily provided between C_{180} and C_{200}^c thereby avoiding a sharp discontinuity that originally occurred between C_{180} and C_{181}^c . Again, graphs obtained for the radial and horizontal disturbance components

Table 3. Anomaly Degree Variances of Various Types of Fields.

Field Designation	Degree Variances on a Sphere of Radius $R = 6371$ km	
	$n = 2$ to N	$n > N$
Total Field	C_n	C_n
Residual Topographic Field	0	C_n^h
Residual Isostatic Field	0	C_n^e
Residual-Topography Reduced Field	C_n	C_n^e
N-field (e.g., 180-field for $N=180$)	C_n	0

were practically identical so that only graphs for the radial component are shown. The final graphs are shown as Figures 15 and 16, corresponding to Figures 4 and 5, respectively.

For example, Figure 15 says that for the residual-topography reduced field the use of a radial or horizontal disturbance representation to harmonic degree $n=360$ leaves only about (1.8, 1.3, 0.7) mgals to be resolved at (5, 10, 20) km altitude, whereas for the total field (Figure 4) these values are correspondingly (16.2, 10.2, 4.5) mgals. On the other hand, Figure 16 shows for example that for the residual topography-reduced field, at an altitude of 30 km, we need a representation to only $n=(390, 290, 195)$ in order to keep the relative omission error down to (1%, 3%, 10%), whereas the corresponding numbers for the total field (Figure 5) are $n=(720, 540, 360)$. Even at the lowest altitude shown (5 km) the reduced field needs a representation to only $n=620$ whereas the total field needs up to $n=2500$ for 1% relative omission error. Thus, using a simple crustal model we see in a general way a considerable smoothing of the field by removal of high-frequency topographic effects; real data computations later this chapter will further illustrate this smoothing. An alternative would be to remove both the effects of high frequency topographic masses and their compensation; however, we did not choose this approach because of some practical reasons stated in Section 4.2.3.

A second numerical investigation of interest would be to answer the question: how sensitive are the various fields of Table 3 to errors in

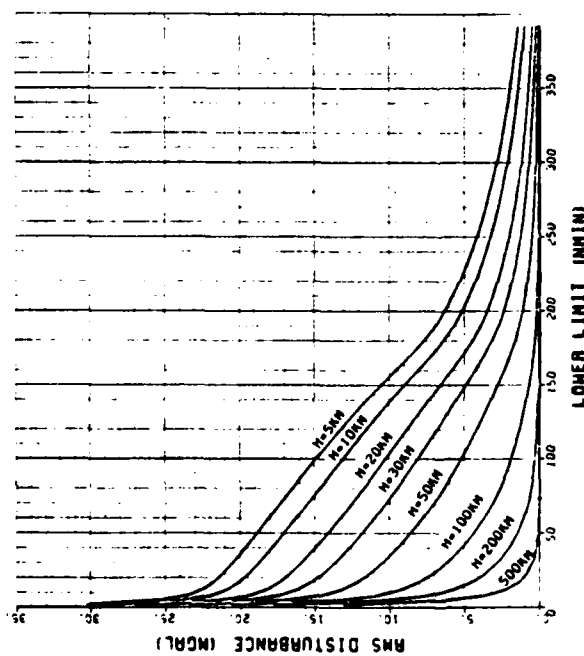


Figure 15. Radial or Horizontal Gravity Disturbance Information (RMS) Beyond a Given Harmonic Degree N_{\min} , for Various Altitudes H Above the Earth, for the Residual-Topography Reduced Field with Airy-Heiskanen Compensation Depth $D = 30$ km.

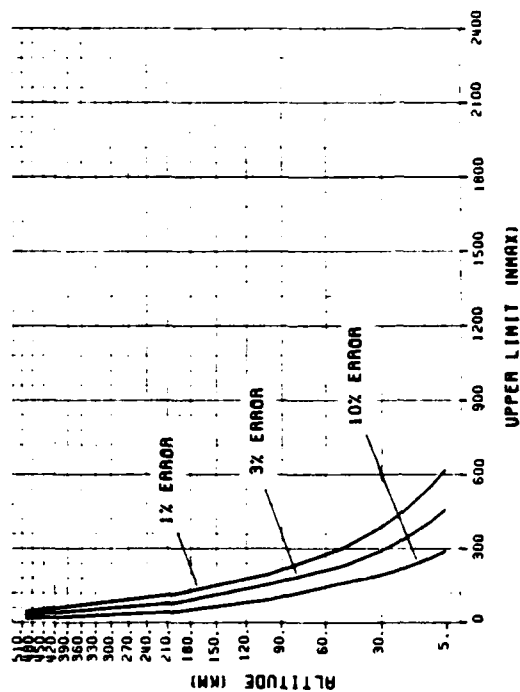


Figure 16. Altitudes for 1%, 3% and 10% Relative Omission Error in Radial or Horizontal Gravity Disturbance, for a Given Maximum Degree N_{\max} of Field Representation, for the Residual-Topography Reduced Field with Airy-Heiskanen Compensation Depth $D = 30$ km.

the vertical location of the boundary surface to which the given anomalies describing the field refer? The vertical location is defined by the heights of boundary surface points above or below the ellipsoid or the geoid. Numerical values for such sensitivities are important because they directly indicate the errors committed in the classical integration procedures in which the topography of the earth is ignored; in such procedures the given anomalies that actually refer to the physical surface of the earth are arbitrarily considered to refer to the geoid (or to the same accuracy, the ellipsoid).

In considering the above sensitivity problem let \bar{C}_n be a general symbol to denote the anomaly degree variances (on a sphere of radius R) of any of the fields in Table 3. For simplicity we will assume a constant error d (e.g., $d=1.5$ km) in the vertical position of the boundary surface to which the given anomalies refer. Specifically, we consider that the correct procedure would be to first analytically downward continue the given surface anomalies to the geoid through the distance d , and then to use the downward continued values in a classical integral representation of the external gravity field. The erroneous procedure would be to directly use the surface anomalies in the integral representation formulas mistakenly considering that these anomalies refer to the geoid. The anomaly error degree variances in this case would be the degree variances of the difference between the downward continued anomalies and the given surface anomalies. We therefore have the following anomaly error degree variances for a field from Table 3:

$$\Delta \bar{C}_n = \left[1 - \left(\frac{R+d}{R} \right)^{n+2} \right]^2 \bar{C}_n, \quad (4.9)$$

in which the second term inside the brackets represents the appropriate factor to downward continue the surface anomalies to the geoid, through the distance d .

We should note that there are upper limits to the values of harmonic degree n and downward continuation depth d that we can use in order for (4.9) to keep giving numerically meaningful results. Too large values of either or both n and d would cause the divergent character of harmonic analytical downward continuation to play a significant role, yielding meaningless numerical results. Numerical investigations on the divergence of downward continuation of the earth's gravity field can be found, for example, in Jekeli (1981). Our numerical experience with downward continuation (details next chapter) is in the context of the Bjerhammar (1964, 1975) approach of analytically downward continuing a finite set of surface gravity anomalies down to an internal sphere. Based on getting useful results while downward continuing a resolution of $5' \times 5'$ values, corresponding to $n_{max} \approx 2500$, down to depths d on the order of 5 km, we conclude that for the purposes of the present

discussions we can use (4.9) with $n_{\max}=2500$ and $d=1.5$ km, as we will do below.

The global RMS (root mean square) effect of $\Delta\bar{C}_n$ on computed radial disturbances at altitude can be obtained by using ΔC_n in place of C_n in (3.29):

$$\Delta\sigma^2(\delta_r) = \sum_{n=2}^{\infty} \left(\frac{n+1}{n-1}\right)^2 \left(\frac{R}{r_1}\right)^{2n+4} \Delta\bar{C}_n. \quad (4.10)$$

The percent error in computed radial disturbance due to the error degree variances $\Delta\bar{C}_n$ can be expressed as:

$$\% \text{ Error} = \frac{\Delta\sigma(\delta_r)}{\sigma(\delta_r)} \times 100\%, \quad (4.11)$$

where $\Delta\sigma(\delta_r)$ is the RMS error in radial disturbance, obtained as the square root of $\Delta\sigma^2(\delta_r)$ in (4.10); and $\sigma(\delta_r)$ is the RMS value of the total radial disturbance signal itself, obtained as the square root of $\sigma^2(\delta_r)$ in (3.29). As before, there is no need to discuss the case of the horizontal disturbance, as practically the same numerical results are obtained for both the radial and horizontal cases.

In Table 4 we show the RMS errors $\Delta\sigma(\delta_r)$ from (4.10) for various types of fields from Table 3, and various altitudes of disturbance computation. For each altitude Table 4 also shows the total RMS disturbance signal $\sigma(\delta_r)$ from (3.29). The following numerical values were used to construct Table 4: $R = 6371$ km; $r_1 = R + \text{altitude}$; vertical position error $d=1.5$ km; compensation depth $D=30$ km; $N=180$; two-component C_n model from (3.36); and all summations to infinity were truncated to $n=2500$. For perhaps easier visualization we also plotted the % error from (4.11) as Figure 17.

It is seen that up to altitude 30 km the errors caused on the residual isostatic field and the 180-field may still be considered significant, but are considerably smaller than the errors caused on both the total field and the residual topographic field. This result could have been expected since the residual isostatic and 180-fields are "smooth" fields, the smoothness being directly caused by the isolation of the residual topographic field (Figures 15 and 16). For smooth fields the downward continued anomalies and the given surface anomalies are relatively close in magnitude, leading to anomaly degree variances $\Delta\bar{C}_n$ from (4.9) having low energy, and low propagated energy through (4.10), at all frequencies. Aside from confirming a general expectation, Table 4 and Figure 17 are useful in providing a feeling for actual errors incurred due to an error in defining the vertical position of the boundary surface to which the anomaly data refer. The error

Table 4. RMS Error in Various Types of Disturbance Fields Due to a 1.5 km Error in the Vertical Position of the Boundary Surface for the Anomaly Data.

Altitude	5 km	10 km	30 km	100 km	500 km
RMS Disturbance of Total Field (mgal)	36.92	32.63	26.04	20.60	13.11
Field Designation	RMS Error (mgal)				
Residual Topographic Field	2.84	1.75	0.53	0.04	0.00
Total Field	2.63	1.57	0.49	0.11	0.02
Residual Isostatic Field	0.44	0.35	0.16	0.02	0.00
180-field	0.49	0.44	0.30	0.10	0.02

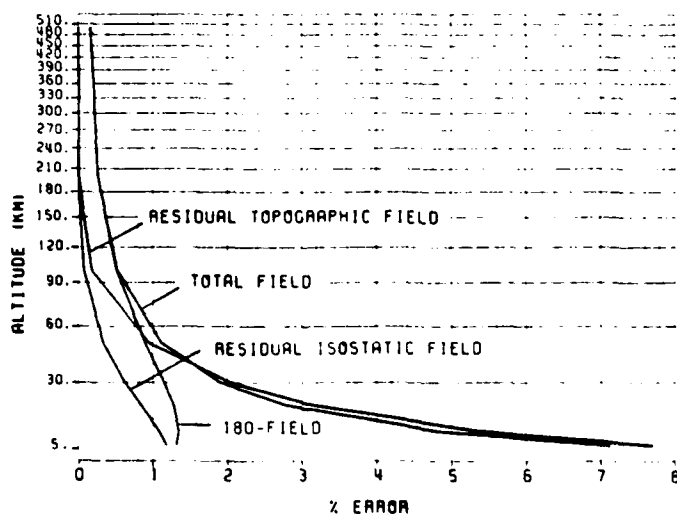


Figure 17. Percentage Error of Various Disturbance Fields at a Given Altitude, Due to a 1.5 km Error in the Vertical Position of the Boundary Surface for the Anomaly Data.

magnitudes shown are in close agreement with real data computations, to be presented later this chapter, over a mountainous area in New Mexico.

The considerations of this section provide the rationale for a practical set of procedures to be detailed in the next sections, for improving the classical integral representation where the topography of the earth is neglected in modeling the external gravity field. Essentially, detailed (1 km x 1 km) topographic height information and a reference topography to spherical harmonic degree 180 will be used, along with an assumed standard crustal density (2.67 g/cm³), to isolate the field roughness caused by the residual topographic field beyond degree 180. A spherical harmonic model of the gravity field to degree 180 will also be removed to minimize remote zone effects. The remaining smooth field, which is primarily the residual isostatic field, will then be represented by classical integral formulas. The smoothness of the latter field will allow the minimization of the errors associated with the assumption of the classical integral representation, namely, that the boundary surface (which in reality is the earth's topography) is a level surface. The spherical harmonic gravity model will be separately evaluated using available operational programs (Rapp, 1982b; Rizos, 1979). The residual topographic field will be evaluated by direct integration of the gravitational effects of the residual topographic masses, using the operational program of Forsberg (1984).

4.2 Complementary Models

Here we summarize the spherical harmonic, residual integral, and residual topographic models that we will combine for the computation of the gravity disturbance vector in space. Pre-requisite for the combination of the different models is the ability to compute their implied gravity anomaly values on the earth's surface where the original anomaly data refer, and to compute their implied disturbance components at the computation points in space. We now summarize the equations and operational programs for the required computations using the three models.

4.2.1 The Spherical Harmonic Model

On the earth's surface, the implied gravity anomaly is conveniently written in the truncated Taylor series form:

$$\Delta g^s(h, \phi, \lambda) = \Delta g^s(r_E, \varphi, \lambda) + \left[\frac{\partial \Delta g^s}{\partial r} (r_E, \varphi, \lambda) \right] h, \quad (4.12)$$

where (See Figure 18):

s superscript to denote the spherical harmonic model

- h, ϕ, λ geodetic coordinates of the surface point
 $r_E, \bar{\varphi}, \lambda$ geocentric coordinates of the point on the ellipsoid, along the same normal as the surface point (h, ϕ, λ).
 $\frac{\partial \Delta g^s}{\partial r}$ radial derivative of the spherical harmonic model.

For the maximum degree of spherical harmonic model that we will use in this report ($n_{\max}=180$) the higher order terms omitted in (4.12) can often be neglected. This was found from numerical tests related to the "Test 3" to be discussed in Section 4.3.4. Higher order terms can be used if this becomes necessary. Note also that the valid approximation is made that the radial derivative $\partial \Delta g^s / \partial r$ can be used instead of the strictly required derivative $\partial \Delta g^s / \partial h$ along the ellipsoidal normal. We have:

$$\Delta g^s(r_E, \bar{\varphi}, \lambda) = \frac{kM}{a^2} \sum_{n=2}^{\infty} \sum_{m=-n}^n (n-1) \left(\frac{a}{r_E} \right)^{n+2} \bar{C}_{nm}^* \bar{Y}_{nm}(\bar{\varphi}, \lambda) \quad (4.13)$$

$$\frac{\partial \Delta g^s}{\partial r}(r_E, \bar{\varphi}, \lambda) = \frac{-kM}{a^3} \sum_{n=2}^{\infty} \sum_{m=-n}^n (n+2)(n-1) \left(\frac{a}{r_E} \right)^{n+3} \bar{C}_{nm}^* \bar{Y}_{nm}(\bar{\varphi}, \lambda) \quad (4.14)$$

where:

- kM geocentric gravitational constant
 a equatorial radius
 \bar{C}_{nm}^* fully normalized potential coefficients referred to those of the reference ellipsoid.

The advantage of the form (4.12) is that the quantities (4.13) and (4.14) that refer to the point ($r_E, \bar{\varphi}, \lambda$) can be evaluated in a very fast way on a grid of constant latitudes and longitudes. For these evaluations we will use the program by Rizos (1979). A fast evaluation is needed since for typical applications we need dense values of $\Delta g^s(h, \phi, \lambda)$ that are on a regular (ϕ, λ)-grid although at varying heights h . For example, for the tests to be presented later this chapter, we needed a $5^\circ \times 5^\circ$ grid of values covering a $7^\circ \times 9^\circ$ area leading to $84 \times 108 = 9072$ values; such a large number of values would be prohibitive to compute if we were to evaluate the spherical harmonic series directly at the individual (h, ϕ, λ) - positions.

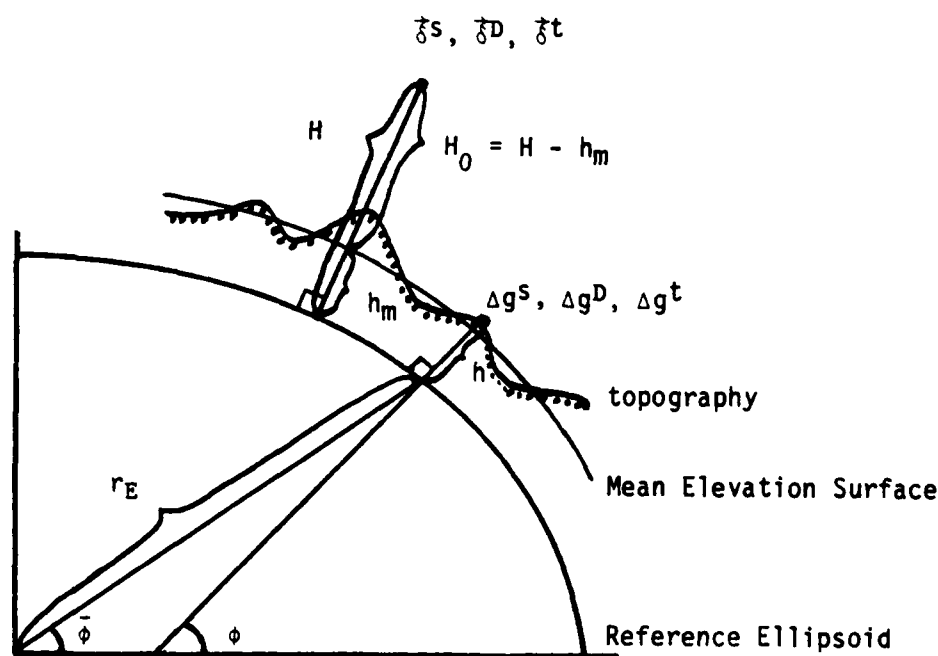


Figure 18. Notations for Gravity Disturbance Vector Modeling.

At altitude, we need the spherical harmonic expressions for the disturbance vector components. These expressions are:

$$\delta r^s = \frac{kM}{a^2} \sum_{n=2}^{\infty} \sum_{m=-n}^n (n+1) \left(\frac{a}{r}\right)^{n+2} \bar{C}_{nm}^* \bar{Y}_{nm}(\bar{\varphi}, \lambda) \quad (4.15)$$

$$\delta \bar{\varphi}^s = \frac{kM}{a^2} \sum_{n=2}^{\infty} \sum_{m=-n}^n \left(\frac{a}{r}\right)^{n+2} \bar{C}_{nm}^* \frac{\partial \bar{Y}_{nm}(\bar{\varphi}, \lambda)}{\partial \bar{\varphi}} \quad (4.16)$$

$$\delta \lambda^s = \frac{kM}{a^2 \cos \bar{\varphi}} \sum_{n=2}^{\infty} \sum_{m=-n}^n \left(\frac{a}{r}\right)^{n+2} \bar{C}_{nm}^* \frac{\partial \bar{Y}_{nm}(\bar{\varphi}, \lambda)}{\partial \lambda}, \quad (4.17)$$

where (r, φ, λ) are the geocentric coordinates of the computation point. Since for our applications we needed evaluations only at isolated points in space (not on a regular grid), we used the operational program described in Rapp (1982b) to evaluate (4.15)-(4.17) on a point by point basis. For fast evaluations of (4.15)-(4.17) on a regular grid the program by Rizos (ibid.) can be modified (which we have done, and the program is available).

4.2.2 The Residual Integral Model

On the earth's surface, the implied gravity anomaly of this model is found by subtracting from the originally given surface anomaly $\Delta g(h, \phi, \lambda)$ the anomalies implied by other complementary models. With $\Delta g^s(h, \phi, \lambda)$ being the spherical harmonic gravity anomaly from (4.12), and denoting by $\Delta g^t(h, \phi, \lambda)$ the topographic gravity anomaly to be discussed later, then we have the surface gravity anomaly of the residual integral model as:

$$\Delta g^D = \Delta g - \Delta g^s - \Delta g^t, \quad (4.18)$$

where the superscript D denotes the classical direct integration method (Heiskanen and Moritz, 1967, Sec. 6-4) where Δg^D will be used.

At altitude, the disturbance components of the residual integral model are expressed as integrals of the Δg^D of (4.18), under the assumption that the Δg^D refer to a level surface, particularly the geoidal surface. For our purposes, we consider the slight modification that the Δg^D might be considered to refer to a level surface at some elevation h_m from the geoid (See Figure 18), where h_m is some mean elevation of the anomaly data. Note that in these discussions there is no need to distinguish between the geoid and the ellipsoid as a reference surface for heights. The effect of introducing h_m is to change the vertical distance between the computation point in space and the reference level for the data, from H (when $h_m=0$) to $H_0=H-h_m$ (when $h_m \neq 0$), where H is the altitude of the computation point above the ellipsoid (or the geoid) - see Figure 18. It is important to distinguish between H_0 and H , as their relative difference can be large, for example, $H=5$ km and $h_m=1.5$ km give $H_0=3.5$ km. On the other hand, there is no need to modify the mean earth radius $R=6371$ km to $R'=R+h_m$, as the relative difference between R and R' is small (e.g., even with $h_m=4$ km, h_m/R is only 6×10^{-4}).

We now summarize the expressions for the disturbance components at altitude, based on the residual integral model. For the implementation of these expressions the operational program fully described in Rapp (1966b) can be used. From Rapp (ibid.) the disturbance components at geodetic coordinates (H, ϕ, λ) become:

$$\delta_r^D = \frac{1}{2\pi} \int \int_{\sigma} \Delta g^D F_1 d\sigma \quad (4.19)$$

$$\delta_{\psi}^D = \frac{1}{2\pi} \int \int_{\sigma} \Delta g^D F_2 \cos \alpha d\sigma \quad (4.20)$$

$$\delta_{\lambda}^D = \frac{1}{2\pi} \int \int_{\sigma} \Delta g^D F_2 \sin \alpha d\sigma \quad (4.21)$$

where:

$$F_1 = \frac{1}{2} t^2 \left[\frac{1-t^2}{D^3} + \frac{4}{D} + 1-6D-t \cos \psi \left(13 + 6 \ln \frac{D+1-t \cos \psi}{2} \right) \right] \quad (4.22)$$

$$F_2 = t^3 \sin \psi \left[\frac{1}{D^3} + \frac{3}{D} - 4 + \frac{3}{2} \left(\frac{D+1-t \cos \psi}{D \sin^2 \psi} - \ln \frac{D+1-t \cos \psi}{2} \right) \right] \quad (4.23)$$

and:

$$t = \frac{R}{R + H_0} \quad , \quad R = 6371 \text{ km} \quad (4.24)$$

$$H_0 = H - h_m \quad (\text{Figure 18}) \quad (4.25)$$

$$D^2 = (1 - 2t \cos \psi + t^2) \quad (4.26)$$

$$d\sigma = \cos \phi d\phi d\lambda \quad (\text{rectangular blocks as integration elements}) \quad (4.27)$$

ψ : angular distance between the projected computation point (R, ϕ_p, λ_p) and the moving integration point (R, ϕ_m, λ_m)

α : azimuth (clockwise from North) from the projected computation point (R, ϕ_p, λ_p) to the moving integration point (R, ϕ_m, λ_m) .

For our tests we used a modified program extracted from the program in Rapp (ibid.), where the modification consists of a simplified input/output and the use of only one anomaly block size (5'x5') instead of all the mean anomaly block sizes 2.5 x 2.5, 5'x5', 30'x30', and 1°x1° used by the original program. The subtraction of Δg^t in (4.18) removed much of the roughness of the Δg -field, and the subtraction of Δg^s drastically

reduced remote zone effects, so that for the purposes of our tests we used only 5'x5' mean blocks covering 7"x9" area around the computation points in New Mexico. To be able to make computations at low altitudes (values of H_0 down to 3.5 km were used) the integrated kernel evaluation implemented in Rapp (ibid.) for 2.5x2.5 blocks was also implemented in the modified program, at least for those 5'x5' blocks whose centers were within a distance of 10' from a computation point.

4.2.3 The Residual Topographic Model

This model is advocated in Forsberg and Tscherning (1981) and Forsberg (1984) for use in general gravity field modeling problems. The model is generated as the gravitational influence of residual topographic masses that lie between the actual topography with elevation h and a reference topography with elevation h^s . The residual masses may be positive ($h > h^s$) or negative ($h^s > h$). The reference topography is conveniently a spherical harmonic expansion of the topography, e.g., to degree 180, but it can also be any averaged version of detailed topographic information.

An alternative model is the topographic/isostatic model used in Sunkel (1983a) and Moritz (1983). This model is generated as the gravitational influence of the topographic masses (masses between the geoid and the topography) and its isostatic compensation. However, for our applications we choose the residual topographic model because of its definite computational advantages (Forsberg, 1984) over the topographic/isostatic model, namely, less remote zone and edge effects, no necessity to compute for the effects of compensating masses, and availability of a simple approximate expression for the model gravity anomalies on the earth's surface (see (4.28) below). The use of the residual topographic model compares favorably with the use of the topographic/isostatic model as complementary model to collocation for the prediction of gravity anomalies and deflections of the vertical in a mountainous test area in New Mexico (Forsberg and Tscherning, ibid.).

Details of the generation of various gravimetric quantities (radial gravity disturbance, deflections of the vertical, height anomaly, and gravity anomaly) implied by the residual topographic model are given along with an operational computer program in Forsberg (1984). The quantities can be computed on the earth's surface and in space by integrating the gravitational effects of the residual masses of assumed constant density (2.67 g/cm³ is a standard crustal density). The prism is the basic integration element used. Close to the computation point exact prism formulas are used, while farther away approximate formulas from spherical harmonics and point mass effects are used for economy and stability of computations.

On the earth's surface, the implied gravity anomaly Δg^t of the residual topographic model can be obtained either by direct prism integration using Forsberg's program, or by using the approximate

relation (Forsberg, *ibid.*, p. 39):

$$\Delta g^t = 2\pi G\rho (h-h^s) - tc, \quad (4.28)$$

where:

- G gravitational constant
- ρ density
- h elevation of surface point
- h^s elevation of reference topography
- tc terrain correction.

Equation (4.28) is useful in the case when the tc is already given from the data records, or as we will see later, in the case when tc can be neglected due to Δg^t being sufficiently far from the spatial points where the disturbance components are being computed. In the latter case the approximate residual topographic anomaly is given by:

$$\overline{\Delta g^t} = 2\pi G\rho (h-h^s). \quad (4.29)$$

At altitude, the disturbance components δ_r^t , δ_φ^t , δ_λ^t implied by the residual topographic model can be obtained by direct prism integration using Forsberg's program. A slight modification is necessary, to compute the meridional δ_φ^t and prime vertical δ_λ^t disturbance components instead of the deflections of the vertical; we have (Rapp, 1982b, p. 6):

$$\delta_\varphi^t = -\gamma \xi, \quad \delta_\lambda^t = -\gamma \eta, \quad (4.30)$$

where ξ is the meridional and η is the prime vertical component of the deflection of the vertical, and γ is normal gravity on the ellipsoid linearly attenuated (0.3086 mgal/m) to account for the height of computation point above the ellipsoid (Rapp, *ibid.*, p. 8).

4.3 Numerical Investigations

4.3.1 The Data

For our numerical tests we used the 5'x5' mean values of surface gravity anomaly and elevation developed over a 7°x9° area in New Mexico in Cruz and Laskowski (1984). For certain inner zone computations required in Forsberg's (1984) prism integration program we also used the detailed 1 km x 1 km grid point elevation data supplied earlier (April, 1983) by the National Geodetic Survey (NGS). The reference topography used in the residual topographic model was generated from a set of spherical harmonic coefficients to degree 180 (tape GS140, file 15). The spherical harmonic gravity model used was that developed in Rapp (1981b) up to degree 180, which here will be referred to as the Rapp-180 field.

For immediate visualization Figure 19 and 20 show, respectively, a contour map of 5'x5' mean elevations (contour interval = 50 meters) and 5'x5' mean gravity anomalies (contour interval = 5 mgals) in a portion of our New Mexico test site. The anomalies shown are actually Faye anomalies, i.e., terrain-corrected anomalies (*ibid.*, Figure 14). The Faye anomaly is expectedly even more correlated with elevation than the terrain-uncorrected free-air anomaly (Moritz, 1968, p. 33). This correlation is clearly observed from Figures 19 and 20, where the contour intervals were chosen to be in a 1 m to 0.1 mgal ratio to approximate the standard correlation factor of 0.1119 mgal/m.

If now we remove the influence of topographic masses by subtracting the Δg^t of (4.28) from the free-air anomaly or, the same thing, by subtracting the first term of (4.28) from the Faye anomalies, then we should see a considerable smoothing of the anomaly field. This is shown in Figures 21 and 22. In Figure 21 the entire topographic masses (i.e., $h^*=0$ in (4.28)) were removed, while in Figure 22 only the residual masses (h^* =reference topography to degree 180) were removed. The field shown in Figure 21, associated with the subtraction of $(2\pi G\rho h - tc)$ from the free-air anomalies, is called refined Bouguer anomalies in Heiskanen and Moritz (1967, Sec. 3-3). Figure 22 additionally reflects the removal of the Rapp-180 field as Δg^* , so that the figure actually shows the residual anomaly Δg^0 of (4.18). In effect, Figure 22 can be obtained by subtracting from Figure 21 the quantity $(\Delta g^* - 2\pi G\rho h^*)$. Since the latter quantity can be interpreted as a reference Bouguer anomaly (see *ibid.*), then we can call the field shown in Figure 22 as a residual refined Bouguer anomaly field.

Figure 21 is indeed much smoother than Figure 20, although one can observe the well-known large negative bias of Bouguer anomalies associated with the removal of the entire topography but not its isostatic compensation. Figure 22 avoids the bias because positive and negative masses were removed or, as an alternative interpretation, because relatively high frequency topographic masses (beyond degree 180) which have only small isostatic compensation were removed.

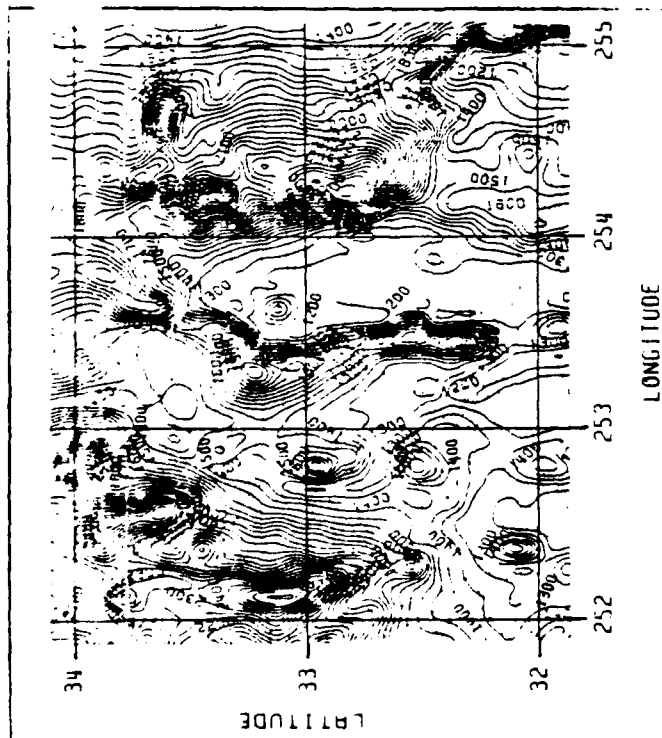


Figure 19. Topography in a Portion of the New Mexico Test Site. Contour Interval = 50 meters.

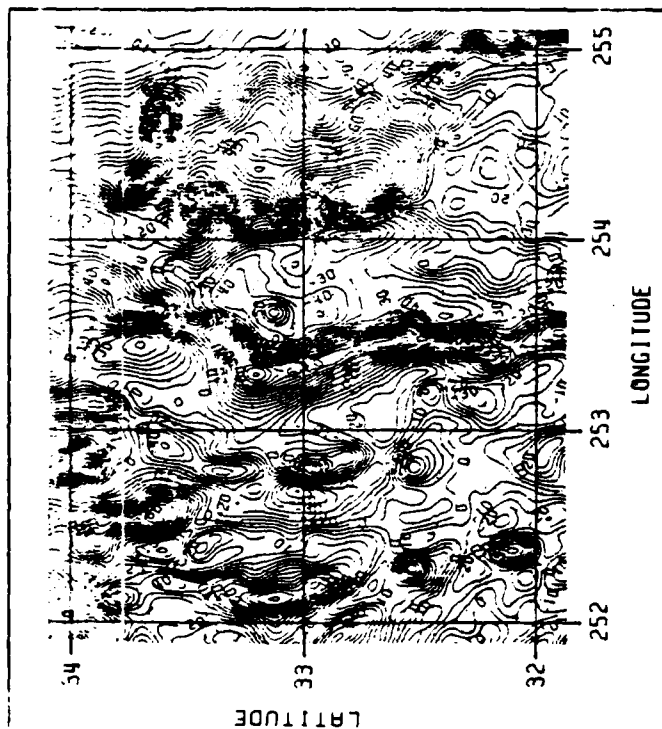


Figure 20. Faye Anomalies in a Portion of the New Mexico Test Site. Contour Interval = 5 mgals.

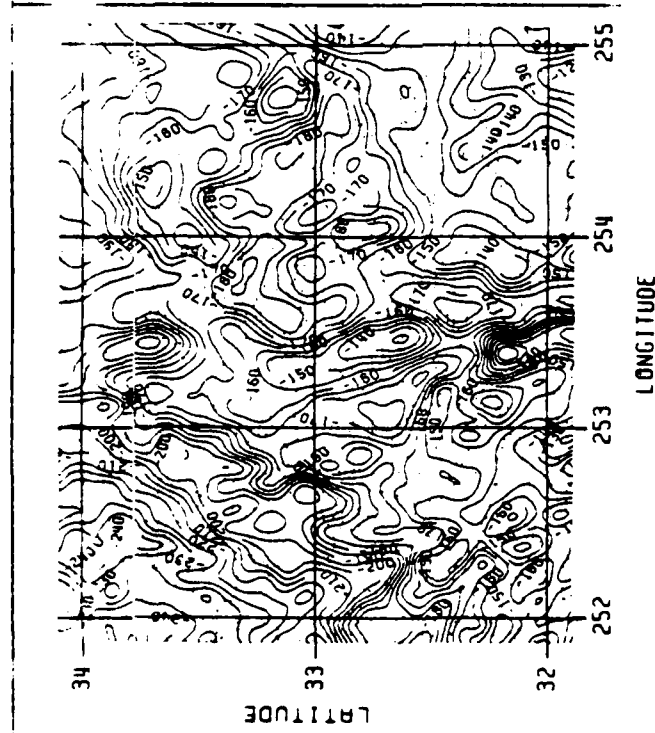


Figure 21. Refined Bouguer Anomalies in a Portion of the New Mexico Test Site. Contour Interval = 5 mgals.

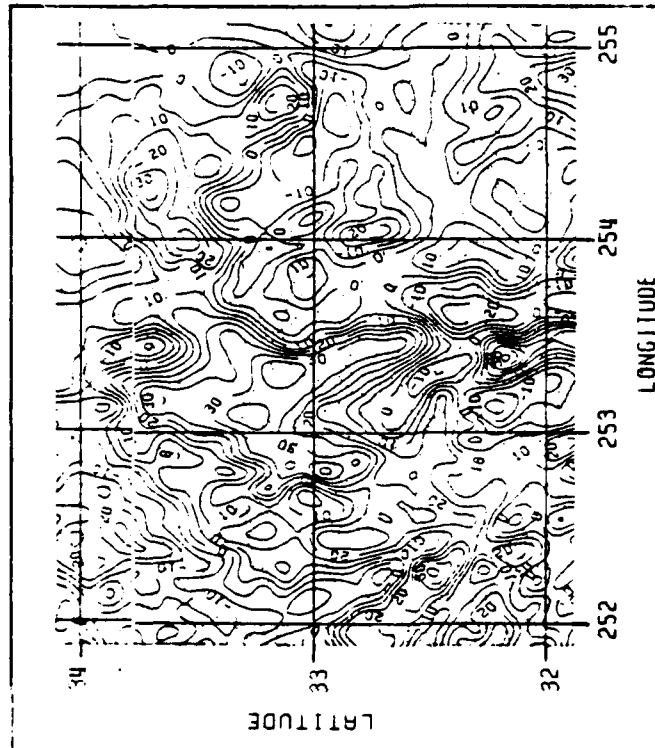


Figure 22. Residual Refined Bouguer Anomalies in a Portion of the New Mexico Test Site. Contour Interval = 5 mgals.

Since Figure 22 reflects the removal of the lower 180 harmonics and the influence of topographic masses beyond degree 180, the field shown can be interpreted as the residual isostatic field discussed in Section 4.1 (See Table 4.1). In reality, Figure 22 also contains the errors of the Δg^* and Δg^t fields (see (4.18)). Nevertheless, one can see the degree of smoothness of Figure 22 compared with Figure 20. In fact the RMS anomaly value reduced by 42%, from 26 mgal for the field shown in Figure 20 to 15 mgal for the field shown in Figure 22, considering all anomaly values in the $7^\circ \times 9^\circ$ test area described in Section 4.3.2. This provides a good real data confirmation of our earlier general study that the topography-unreduced field (Figure 20) might require a representation to degree $n=2500$ ($5' \times 5'$ resolution) for low-altitude disturbance computations, whereas the topography reduced field might need only a representation to $n=620$ ($17' \times 17'$ resolution) - see the discussions related to Figures 15 and 16.

4.3.2 The Test Area

For testing the combination of the various models discussed in Section 4.2, we used gravity and elevation data in the $7^\circ \times 9^\circ$ New Mexico area shown in Figure 23. The figure shows the reference topography to degree 180 with a contour interval of 50 meters. The figure also shows five symmetrically arranged points in a $1^\circ \times 1^\circ$ area, these points being foot points of five vertical trajectories (i.e., lines) along which test computations were performed. Test computations were performed at points along the trajectories, at altitudes 5, 10, 30, 100, and 500 km above the ellipsoid. The locations of the five trajectories were chosen in an area of significant gradient of the disturbance component fields. To show the gradients, the $3^\circ \times 3^\circ$ area marked off in Figure 23 was taken for plotting the disturbance components at altitudes 0 km and 30 km using a contour interval of 5 mgals. The plots are shown in Figure 24. The disturbance components were plotted from $0.25^\circ \times 0.25^\circ$ grid point values generated from the Rapp-180 field using the modified Rizos program mentioned in Section 4.2.

Figure 25 shows the labeling that we will use to identify the test points at a given altitude. Also shown is the area (Area I) which contains the $5' \times 5'$ blocks where the integrated kernel form (Rapp, 1966b) was used in the numerical integration of the integral model. The integrated kernel form avoids the large errors of the center-point kernel evaluation, for integration elements close to the computation point at low altitudes. Figure 25 also shows the area (Area II) where rigorous values of Δg^t from Forsberg's program were used in the residual topographic model. Outside Area II, it will be shown in the tests that it is sufficient to approximate Δg^t by the first term of (4.28).

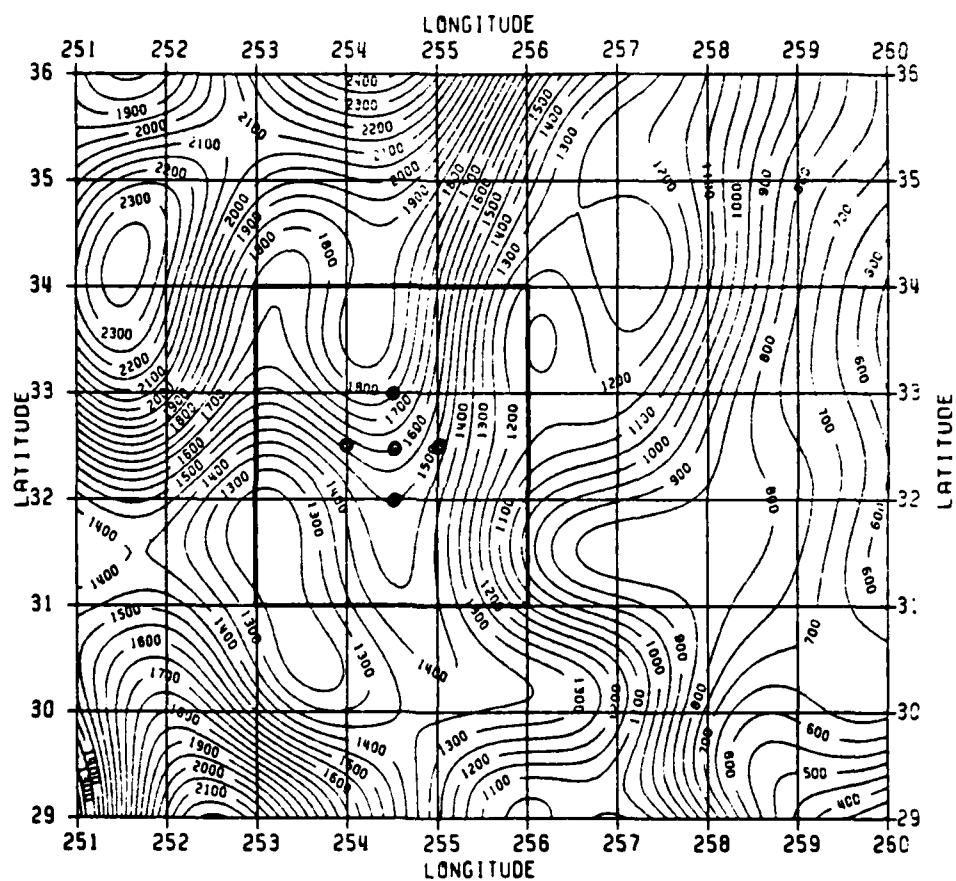


Figure 23. 180 x 180 Spherical Harmonic Expansion of the Topography and Trajectory Foot Points in the New Mexico Test Site. Contour Interval = 50 meters.

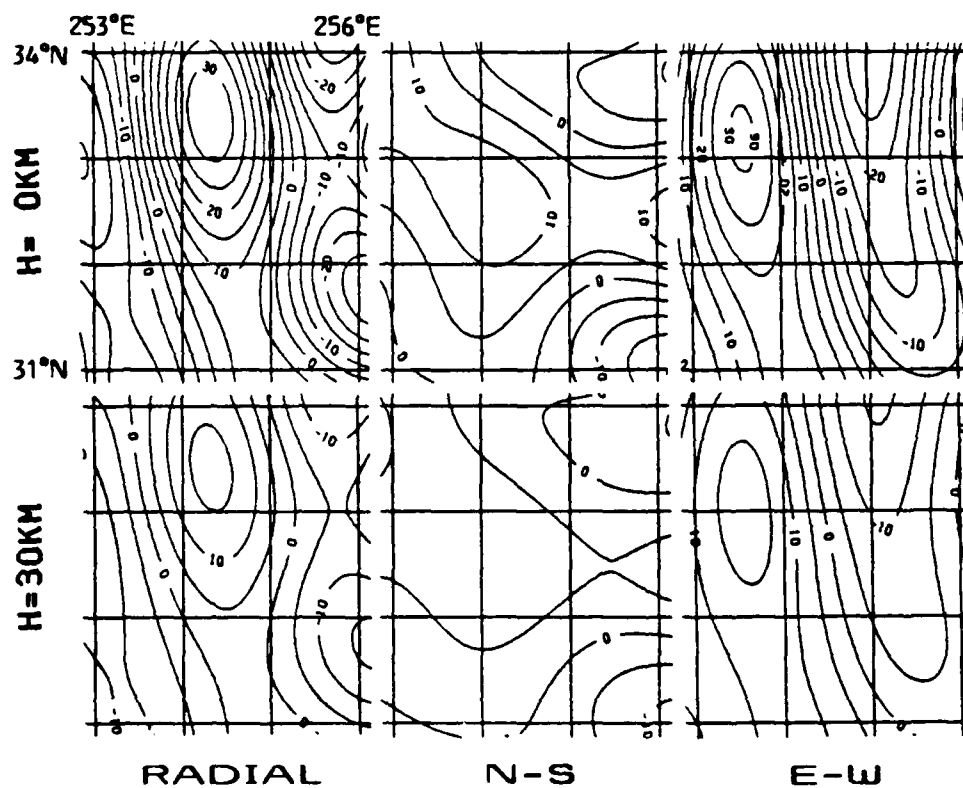


Figure 24. Rapp-180 Spherical Harmonic Expansion of the Radial (δ_r), North-South (δ_ϕ), and East-West (δ_λ) Disturbance Components at Altitudes 0 and 30 km in the Vicinity of the Test Trajectories in New Mexico. Contour Interval = 5 mgal.

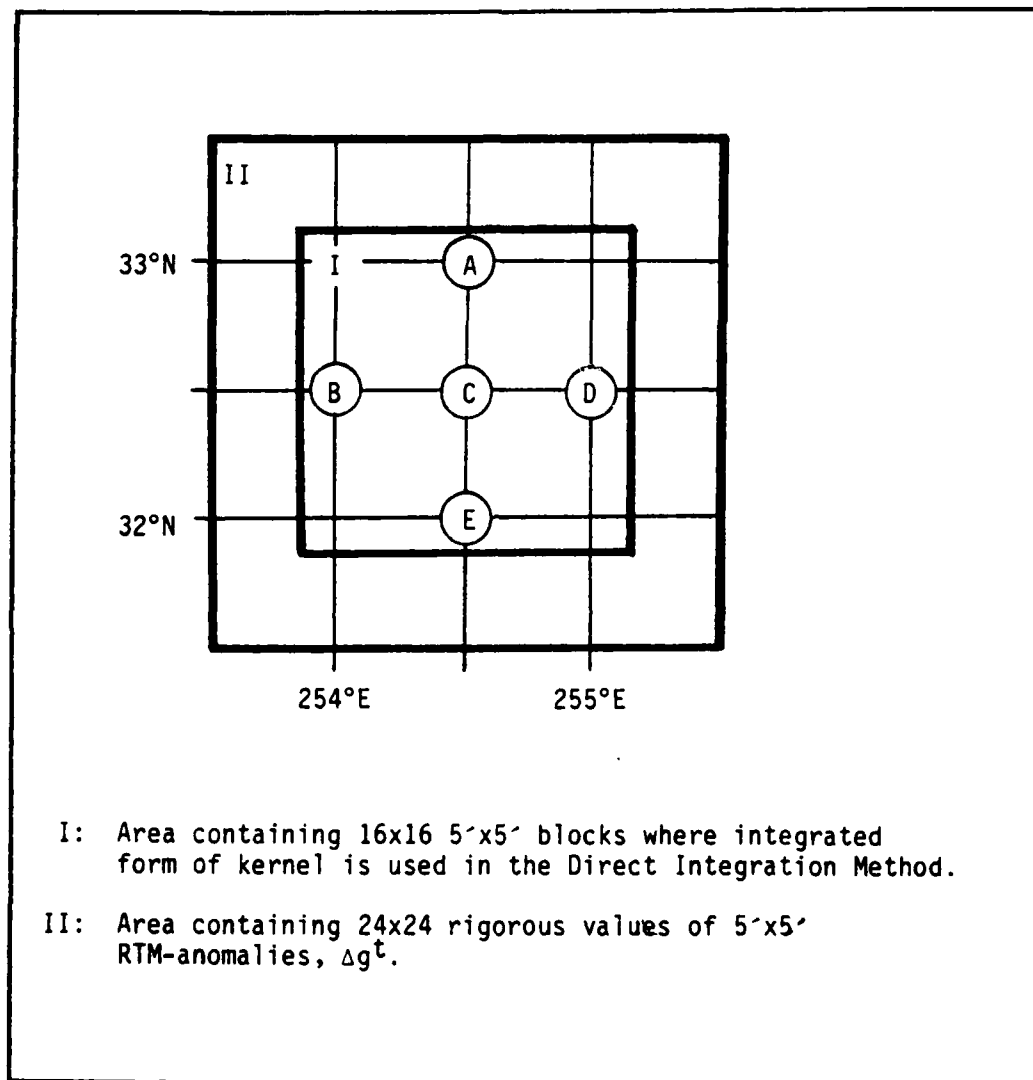


Figure 25. Test Points and Inner Zone Data Configuration.

AD-A166 730

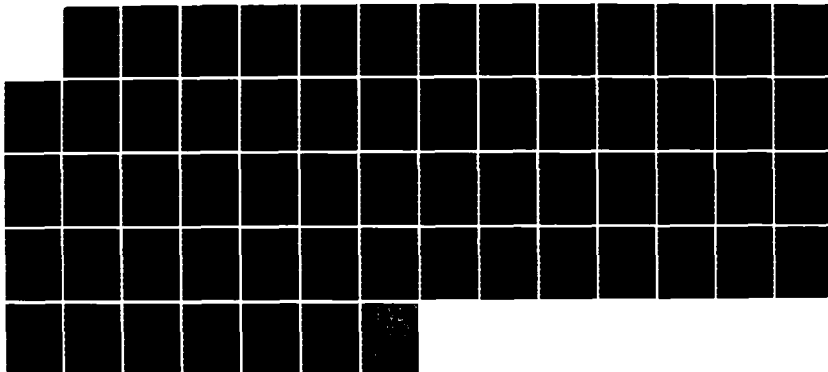
DISTURBANCE VECTOR IN SPACE FROM SURFACE GRAVITY
ANOMALIES USING COMPLENE.. (U) OHIO STATE UNIV COLUMBUS
DEPT OF GEODETIC SCIENCE AND SURVEYI.. J Y CRUZ AUG 85
OSU/DGSS-366 AFGL-TR-85-0209

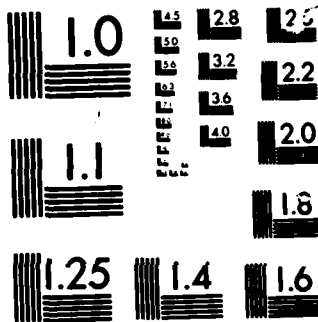
2/2

UNCLASSIFIED

F/G 8/5

NL





CHART

4.3.3 Description of Tests and Numerical Results

Below we describe the various tests conducted using the five vertical trajectories through the points A, B, C, D, E shown in Figure 25. Again, the altitudes tested were 5, 10, 30, 100, and 500 km. To simplify the numerical presentation we give for each particular test and particular disturbance component, the numerical results for only one chosen trajectory omitting the results for the remaining four trajectories. The one trajectory to be presented will be the one showing the greatest sensitivity to the particular test, that is, the one showing the largest absolute values for numerical results. We now describe the various tests, with the results for each presentation trajectory being shown in Table 5 at the end of the test descriptions.

Test 1. Remote Zone Error of Direct Integration Method for $n=2$ to 180

The Rapp-180 field was first evaluated to provide "true" values of disturbance components in space using (4.15)-(4.17), and to provide $5' \times 5'$ "data" values of anomalies on the ellipsoid, in the $7' \times 9'$ test area, using (4.13). The data values were then input into the direct integration method using (4.19)-(4.21) to yield computed values in space. The true values were subtracted from the computed values to yield the errors for this test. The differences are caused by the neglect of the anomaly data outside the data area.

Test 2. Remote Zone Error of Direct Integration Method for $n=21$ to 180

Test 1 was repeated this time using only harmonics from $n=21$ to 180.

Test 3. First Derivative Effect for the 180-Field

$5' \times 5'$ values of the second term in (4.12) were first computed in the $7' \times 9'$ test area using the Rapp-180 field and the $5' \times 5'$ mean values of elevations (not the reference elevations to 180). The resulting values were then input into the direct integration method using (4.19)-(4.21) to yield the first derivative effects for this test.

Test 4. Sensitivity of Field Beyond Degree 180 to Height Error

The spherical harmonic gravity anomaly Δg^s from the Rapp-180 field and (4.12) was first subtracted from the originally given surface anomalies Δg , to form $5' \times 5'$ values of $(\Delta g - \Delta g^s)$ in the $7' \times 9'$ test area. These values were then input into the direct integration method using (4.19)-(4.21), first with $h_m=0$ then with $h_m=1.5$ km in (4.25), where $h_m=1.5$ km was an approximate mean elevation in the test area (see Figure 23). The sensitivities for this test were then formed by subtracting the disturbance results for the case when

$h_m=0$ from those for the case when $h_m=1.5$ km.

Test 5. Residual Topographic Model Outer Zone Effects

5'x5' mean elevations and 30"x30" grid point elevations of the actual topography, along with the reference topography to 180, were input into Forsberg's prism integration program to compute the disturbance components δ_r^t , δ_φ^t , δ_λ^t at altitude. The standard crustal density of 2.67 g/cm³ was used. Two versions were computed, one using data in the entire 7°x9° test area, and the other using only data inside a 2°x2° area centered at the computation points (Area II in Figure 25). The results for the 2°x2° area were subtracted from the results for the 7°x9° area to yield the desired outer zone effects (disturbances) for this test.

Test 6. Error of Using $\Delta\bar{g}^t = 2\pi G\rho(h-h^*)$ as a Simplified Residual Topographic Anomaly in the Outer Zone

5'x5' mean values of $\Delta\bar{g}^t=2\pi G\rho(h-h^*)$ were first generated in the outer zone, outside the Area II of Figure 25 but inside the 7°x9° test area, using 5'x5' values of elevations h and reference elevations h^* to degree 180, and using $2\pi G\rho=0.1119$ mgal/m associated with $\rho=2.67$ g/cm³. These data in the outer zone were then input into the direct integration method (4.19)-(4.21), with $h_m=1.5$ km in (4.25), to yield the spatial disturbances implied by the outer zone $\Delta\bar{g}^t$ -data. From these disturbances, the rigorous outer zone disturbances from Test 5 were subtracted to yield the errors for this test.

Test 7. Sensitivity of the Residual Topographic Field to Height Error

Rigorous values of 5'x5' residual topographic anomalies Δg^t on the earth's surface were first generated inside the 2°x2° inner zone, Area II in Figure 25, by direct prism integration of residual topographic masses using Forsberg's program (see comment above (4.28)). Again, the input data were 5'x5' mean elevations and 30"x30" grid point elevations of the actual topography, reference topography to degree 180, and $\rho=2.67$ g/cm³. These Δg^t values in the inner zone were combined with the $\Delta\bar{g}^t$ values developed for the outer zone in Test 6. The combined 5'x5' data in the 7°x9° area were then input into the direct integration method (4.19)-(4.21), first with $h_m=0$ then with $h_m=1.5$ km in (4.25), where $h_m=1.5$ km was an approximate mean elevation in the test area. The sensitivities for this test were then formed by subtracting the disturbance results for $h_m=0$ from those for $h_m=1.5$ km.

Test 8. Sensitivity of the Residual Integral Field to Height Error

5'x5' values of the residual integral model anomalies Δg^0 from (4.18) were first formed in the 7°x9° test area, by subtracting from the original surface anomalies Δg the spherical harmonic anomalies Δg^s from (4.12) and the residual topographic anomalies Δg^t (inner zone) and Δg^t (outer zone) from Test 7. Again, for computing Δg^s the Rapp-180 field and 5'x5' mean elevations of the actual topography were used. The Δg^0 -data were then input into the direct integration method (4.19)-(4.21), first with $h_m=0$ then with $h_m=1.5$ km in (4.25), where $h_m=1.5$ km was an approximate mean elevation in the test area. The sensitivities for this test were then formed by subtracting the disturbance results for $h_m=0$ from those for $h_m=1.5$ km.

Test 9. Error of the Direct Integration Method in Representing the Residual Topographic Field

5'x5' values of residual topographic anomalies on the earth's surface were first formed in the 7°x9° test area, from the Δg^t (inner zone) and Δg^t (outer zone) values from Test 7. These values were then input into the direct integration method (4.19)-(4.21), with $h_m=1.5$ km in (4.25), to yield the spatial disturbances $(\delta \xi)^0$, $(\delta \phi^t)^0$, $(\delta \lambda^t)^0$ implied by the integral representation method. Corresponding rigorous values $\delta \xi$, $\delta \phi^t$, $\delta \lambda^t$ of the disturbances were generated from Forsberg's prism integration program, using 5'x5' mean elevations and 30"x30" grid point elevations of the actual topography along with reference topography to degree 180 and $\rho=2.67$ g/cm³. The errors for this test were then as the differences $[(\delta \xi)^0 - \delta \xi]$, $[(\delta \phi^t)^0 - \delta \phi^t]$, and $[(\delta \lambda^t)^0 - \delta \lambda^t]$.

4.3.4 Discussion of Numerical Results

Test 1 shows that the remote zone errors caused by the omission of anomaly data outside the 7°x9° test area are significant.

Comparison of Tests 1 and 2 shows that a large part of the remote zone errors are caused by very long wavelength harmonics between degrees 2 to 20, with the errors caused by degrees 21 to 180 being below 1 mgal but can still be considered to be significant biases. The characterization of the errors as biases comes from the fact that the errors attenuate very slowly with altitude. Extrapolating the results of Tests 1 and 2, it can be expected that the remote zone errors caused by harmonics above degree 180 are negligible. This expectation also follows from the analysis of truncation errors as presented in Chapter 3. This means that it will be sufficient to use a spherical harmonic model to degree 180 (as we did in our tests) as a complementary model to account for remote zone data outside the 7°x9° test area.

Table 5. Maximal Values (mgals) of the Different Quantities Being Computed in Tests 1 to 9 of Chapter 4 (see text).

TEST	POINT	5 km	10 km	30 km	100 km	500 km
1	δ_r A	7.16	7.20	7.37	7.15	6.35
	δ_φ A	-3.34	-3.32	-3.27	-3.08	-1.65
	δ_λ A	-3.20	-3.18	-3.09	-2.78	-2.13
2	δ_r A	-0.48	-0.12	-0.20	-0.11	-0.07
	δ_φ A	0.29	0.29	0.30	0.27	0.22
	δ_λ A	-0.80	-0.79	-0.75	-0.55	-0.23
3	δ_r A	-1.35	-1.19	-0.75	-0.20	-0.02
	δ_φ C	-0.50	-0.43	-0.26	-0.07	0.00
	δ_λ D	0.60	0.53	0.34	0.08	0.01
4	δ_r D	-2.84	-1.64	-0.31	-0.03	0.00
	δ_φ C	-3.29	-1.88	-0.51	-0.02	0.00
	δ_λ A	2.54	1.53	0.24	0.00	0.00
5	δ_r D	-0.21	-0.41	-1.05	-1.32	-0.36
	δ_φ B	-1.72	-1.71	-1.62	-1.17	-0.16
	δ_λ D	-2.18	-2.14	-1.75	-0.48	-0.07
6	δ_r D	-0.20	-0.27	-0.43	-0.33	-0.06
	δ_φ B	-0.33	-0.33	-0.31	-0.20	-0.02
	δ_λ D	-0.69	-0.67	-0.51	-0.09	0.00
7	δ_r D	-2.87	-1.74	-0.29	-0.01	0.00
	δ_φ C	-3.71	-2.19	-0.64	-0.02	0.00
	δ_λ A	1.35	1.29	0.27	-0.03	0.00
8	δ_r A	1.69	1.02	0.24	0.01	-0.01
	δ_φ E	-0.76	-0.20	0.02	0.00	0.00
	δ_λ A	1.18	0.24	-0.02	0.02	0.00
9	δ_r D	-3.32	-1.96	-0.30	-0.29	-0.08
	δ_φ B	-3.85	-2.98	-1.58	-0.33	-0.22
	δ_λ A	8.18	4.85	1.83	0.34	0.00

Test 3 shows that for the purpose of subtracting the spherical harmonic model to degree 180 from surface gravity anomaly data, it is not sufficient to simply use the values of the spherical harmonic model on the surface of the ellipsoid. Rather, the first radial derivative of the field has to be used also as in (4.12) to account for the varying heights of the surface points above the ellipsoid. Tests not shown here indicate that the effects of the second radial derivative are one order of magnitude below those of the first radial derivative, and thus such effects can be neglected. Again, we point out that the evaluation of the spherical harmonic model using the truncated Taylor series (4.12) is a means to control the amount of computer time required for evaluations of the model on a dense grid of surface points.

Test 4 shows that after subtracting the spherical harmonic model to degree 180 from the original field, the residual field is still such that it makes a significant difference in the direct integration method whether the boundary values are assumed to refer to the geoid or to some mean elevation in the area. This significant sensitivity to data height error is noted for altitude below 30 km. This significant sensitivity is expected since the field roughness has not been removed through the subtraction of the 180-field. The field roughness directly causes high sensitivity of the modeling procedures to height errors, since high frequency field irregularities are drastically affected by upward or downward continuations. Even the use of a mean elevation surface as assumed reference level for the data is, of course, in error since the anomaly data actually refer to the physical topography which is not an equipotential (level) surface. To reduce the error it is desirable to use the residual topographic model as complementary model to smooth the field.

Test 5 is of interest to show the effects of residual topographic masses outside the $2^\circ \times 2^\circ$ area surrounding the computation points. These outer zone effects were, on the average, 12% of the total residual topographic effects at our computation points.

Test 6 was used to see if the approximate residual topographic anomaly Δg^t of (4.29) can be used in place of the rigorous Δg^t outside the $2^\circ \times 2^\circ$ area surrounding the computation points. The resulting errors from this test can be considered tolerable, since these errors are actually the effect of two types of errors: one is the error of approximating Δg^t by Δg^t , and the other is the error of the direct integration method in representing the residual topographic field (more about this in Test 9). It is important to be able to approximate Δg^t by Δg^t in some outer zone because, for example, the computation of rigorous values of Δg^t for the entire $7^\circ \times 9^\circ$ test area would lead to $84 \times 108 = 9072$ values which would be prohibitive to compute using Forsberg's prism integration program. The computation of a 24×24 array of rigorous Δg^t -values inside the $2^\circ \times 2^\circ$ inner zone area already took about 10 minutes of CPU time on the OSU Amdahl system.

Comparing Test 7 with Test 4 we see very similar errors, supporting the idea that most of the errors caused by varying data level occur in the (high frequency) residual topographic part of the total field.

Comparing Test 8 with Test 4, we see significantly smaller errors for Test 8. This is due to the smoothness of the residual integral field used in Test 8. The low sensitivity of the residual integral field with changing data level means that now the assumption of the integral model, namely, that the surface data refer to a single level, will produce only small errors. It is indicated from Test 8 that at very low altitudes, below 10 km, we still encounter a significant although small model sensitivity to changing data level.

Test 9 shows the magnitudes of errors that can be encountered when using the direct integration method to model a rough field. Part of the errors can be attributed to the inability of the direct integration method to properly account for the changing level of the given anomaly data, (i.e., to properly account for the shape of the topography).

Note that in Test 9 a value of $h_m=1.5$ km was used in (4.25). In a separate testing we also used $h_m=0$, and generated the corresponding errors as in Test 9. This was done to confirm that the use of the mean elevation $h_m=1.5$ km would yield smaller errors than the use of $h_m=0$. The statistics of the errors for $h_m=0$ and $h_m=1.5$ km are shown in Table 6. We see a clear tendency for the mean and standard deviation of the errors associated with $h_m=1.5$ km to be smaller than those for $h_m=0$ km, so that $h_m=1.5$ km is the preferable value to use.

We close this section by giving Table 7, which shows the final model values for the test trajectory through point A (Figure 25). The total disturbance values were obtained by adding together the values from the spherical harmonic, residual topographic, and residual integral models. Also shown in Table 7 (row V) are the errors of the direct integration method in representing the residual topographic field, as explained in the description for Test 9. To get the disturbance values for the case when the residual topographic model is not used as a complementary model, we have to add corresponding numbers given in rows IV and V of Table 7.

Table 6. "Mean \pm Standard Deviation" (mgals) of the Errors of the Direct Integration Method in Representing the Disturbance Components of the Residual Topographic Field. The statistics were computed from the five test points of the given altitude.

Altitude	$h_m = 0 \text{ km}$		$h_m = 1.5 \text{ km}$	
	$\epsilon \delta r$	$\epsilon \delta \phi$	$\epsilon \delta r$	$\epsilon \delta \lambda$
500 km	-0.08 \pm 0.00	-0.02 \pm 0.00	-0.09 \pm 0.01	0.00 \pm 0.01
100 km	-0.49 \pm 0.19	-0.24 \pm 0.12	-0.48 \pm 0.18	0.23 \pm 0.10
30 km	-1.19 \pm 0.87	-0.78 \pm 0.79	-0.97 \pm 0.76	0.98 \pm 0.53
10 km	1.96 \pm 1.61	-1.48 \pm 1.85	-1.25 \pm 0.49	2.13 \pm 1.73
5 km	-2.96 \pm 3.33	-2.07 \pm 2.42	-1.89 \pm 2.02	3.03 \pm 3.05

Table 7. Values of the Disturbance Components in Space as Evaluated from the Models of Chapter 4, for the Test Point A ($\phi = 33^\circ\text{N}$, $\lambda = 254.5\text{E}$). Row V gives the errors of the direct integration method in representing the residual topographic model (see Test 9). Units: mgals.

MODEL		5 km	10 km	30 km	100 km	500 km
I (spherical harmonic model)	δ_r^s	26.31	23.41	14.56	1.60	-5.03
	δ_ϕ^s	8.52	8.00	6.41	3.88	1.48
	δ_λ^s	-3.43	-2.80	-1.00	1.14	1.83
II (residual topographic model)	δ_r^t	47.18	39.62	17.48	-0.64	-0.49
	δ_ϕ^t	-5.00	-3.92	-1.77	-0.64	-0.11
	δ_λ^t	-22.50	-14.59	-1.73	0.48	-0.07
III (residual integral model)	δ_r^D	-12.50	-7.72	-0.71	2.60	0.67
	δ_ϕ^D	4.97	3.46	2.01	1.31	0.20
	δ_λ^D	-4.97	-2.52	-2.09	-1.64	-0.08
IV (total)	δ_r	60.99	55.31	31.33	3.56	-4.85
	δ_ϕ	8.49	7.54	6.65	4.55	1.57
	δ_λ	-30.90	-19.91	-4.82	-0.02	1.68
V	$(\delta_r^t)^D - \delta_r^t$	0.35	-0.68	-1.25	-0.62	-0.09
	$(\delta_\phi^t)^D - \delta_\phi^t$	-1.28	0.01	0.19	-0.05	-0.02
	$(\delta_\lambda^t)^D - \delta_\lambda^t$	8.18	4.85	1.83	0.34	0.00

5. DISCRETE APPROACHES TO MODELING THE SPATIAL DISTURBANCE VECTOR

Discrete approaches to modeling the external gravity field are based on solving the so-called Bjerhammar problem. Bjerhammar (1964) formulated the modeling problem in this way: given a finite number of gravity anomalies at points of a non-spherical surface, find an analytical approximation to the disturbing potential T in space such that the given anomaly values are satisfied. Solutions that have been developed for the Bjerhammar problem now include possibilities to:

1. satisfy heterogeneous data types (e.g., gravity anomalies, deflections of the vertical, gravity gradients) at the given observation points;
2. filter the data to minimize the influence of measurement errors;
3. remove systematic influences that make T non-harmonic, such as time dependent variations, reference system errors in orientation and geocentricity, and station position errors (Tscherning, 1981).

Well-known solutions presented for the Bjerhammar problem are based on collocation, which is a numerical method for fitting an analytical approximation of a function to a finite number of given functionals of the function (see Moritz, 1978b; see also Moritz, 1978a, p. 32, for a simple example of collocation). In fact, the Bjerhammar problem as stated above reads as a collocation problem. Details of the application of collocation in solving the Bjerhammar problem have been presented under different analytical structures. Original presentations are given by Krarup (1969) using Hilbert spaces, Moritz (1970a) using Wiener prediction and filtering, and Bjerhammar (1975) using Dirac functions. Extensive treatment of various aspects, both for practical application and for deeper analytical understanding of collocation, are given by Moritz (1980). Review papers dealing with the theory of collocation are given by Moritz (1978a, 1978b) and Bjerhammar (1978). Tscherning (1981) gives a review paper comparing the theory and computational properties of different gravity field representations, including collocation and its combination with other methods, and summarizing also the results of previous numerical investigations by various authors.

Of special interest are the numerical investigations of Sjöberg (1975, 1978), who used both model computations and limited real data computations to predict gravity anomalies and deflections of the vertical

on the surface of the topography, starting from given surface gravity anomalies. He concludes that similar prediction results are obtained from the use of different base functions in the collocation procedure (details of the procedure are given below), provided that the radius of the internal sphere is properly chosen for each base function. In this chapter we will investigate the validity of this conclusion for gravity disturbance vector computations in space.

Of interest to us also are the numerical investigations of Katsambalos (1981) who performed simulation studies, precisely on the computation of the gravity disturbance vector in space from surface gravity anomaly data. He used model values using the "Molodensky mountain model" (Molodensky et al., 1962). Key conclusions of Katsambalos were questioned by Tscherning (1983a) with regards to the least squares collocation approach, and by Bjerhammar and Sjöberg (1982, private communications) with regards to the so-called Dirac approach. Both the least squares collocation and Dirac approaches are collocation techniques, as we will detail below. The results of our own numerical experiments, to be presented in this chapter, support the validity of the questions raised. Specifically, our results show the following:

1. the least squares collocation and Dirac approaches can give about the same quality of results if the free parameters of the base function used (degree variances, radius of the Bjerhammar sphere) are properly selected.
2. the conclusions of Katsambalos based on his Tables 9.3 and 9.4 (ibid., p. 116), namely, that the "Dirac approach should not be used for the interpolation of gravity anomalies on the surface of the earth, unless the data is sufficiently dense to ensure an accurate prediction", should be modified. His Table 9.3 was incorrectly computed, with the correct table being given in Sjöberg (1978, p. 68, Table 8.3). His Table 9.4 represents only a very specific example, and cannot be generalized to form the conclusion that the Dirac approach tends to predict zero values in between the data points. The conclusion should rather be, that the Dirac approach can be used for interpolation provided the radius of the internal sphere is properly selected. The large prediction errors noted by Katsambalos (ibid., p. 113) when doing real data computations over Canada was due to the relatively large spacing between the given data points (see Figure 28 of this chapter), and not due to a deficiency in the least squares collocation or Dirac prediction methods as Katsambalos suggested. We will present additional computations using the mentioned real data in Canada.

5.1 The Collocation Procedure

We already mentioned that the word collocation denotes the construction of an approximation to a function by fitting an analytical

approximation of the function to a finite number of given functionals of the function (see Moritz, 1978a, 1978b, for example). In gravimetric geodesy the fundamental function to be approximated is usually the disturbing potential T , and the given functionals are (for example) gravity anomalies Δg , deflections of the vertical ξ and η , and height anomalies ζ , which are all related to T through well-known linearized relations in spherical approximation:

$$\Delta g = -\frac{\partial T}{\partial r} - \frac{2}{r} T \quad (5.1)$$

$$\xi = -\frac{1}{r\gamma} \frac{\partial T}{\partial \phi} \quad (5.2)$$

$$\eta = -\frac{1}{r\gamma \cos \varphi} \frac{\partial T}{\partial \lambda} \quad (5.3)$$

To briefly explain the use of collocation in constructing an approximation to the disturbing potential T in space, we use the presentation of Moritz (1978b). It is first postulated that T can be approximated by a function f in the form:

$$T(P) \approx f(P) = \sum_{j=1}^k b_j \phi_j(P), \quad (5.4)$$

where

- P computation point in space
- b_j constant collocation coefficients to be determined
- ϕ_j a priori selected base functions

It is considered that T is harmonic outside the earth's masses, and to enforce harmonicity on the approximating function f , the selected base functions are harmonic:

$$\Delta \phi_j = 0, \quad (5.5)$$

where Δ denotes here the Laplace operator. For the determination of the collocation coefficients b_j it is assumed that errorless values of ℓ_i are given at k spatial points on or above the earth's surface, where the ℓ_i are linear functionals (Moritz, 1980, p. 36) of T or f :

$$\epsilon_i = L_i T = L_i f, \quad (5.6)$$

where L_i denotes the linear operation to transform T (or f) to ϵ_i . For example, (5.1) is in the form (5.6) with

$$\epsilon_i = \Delta g_i \quad (5.7)$$

$$L_i = - \left[\frac{\partial}{\partial r_i} + \frac{2}{r_i} \right]. \quad (5.8)$$

The collocation condition is now the exact reproduction of the given ϵ_i by the function f , i.e., substituting (5.4) into (5.6):

$$\sum_{j=1}^k b_j L_i \phi_j (P_i) = \epsilon_i. \quad (5.9)$$

In matrix notation, condition (5.9) becomes:

$$B b = \epsilon, \quad (5.10)$$

where the elements of the B -matrix are:

$$B_{ij} = L_i \phi_j (P_i), \quad (5.11)$$

i.e., the operator L_i is applied to the base function ϕ_j and the result evaluated at the point P_i where ϵ_i is given. From (5.10) we formally get the collocation coefficients:

$$b = B^{-1} \epsilon. \quad (5.12)$$

In actual implementation, (5.10) may be solved for b by iteration or by a linear equation solution, instead of the direct matrix inversion in (5.12).

Knowing the collocation coefficients b_j , (5.4) gives the required approximation to T . Any other functional L_i of T can be found in space by applying the operator L to (5.4):

$$LT(P) \approx Lf(P) = \sum_{j=1}^k b_j L\phi_j(P) . \quad (5.13)$$

For example, in computing the components of the gravity disturbance vector in space we have the linear relations:

$$\delta_r = -\frac{\partial T}{\partial r} \quad (5.14)$$

$$\delta_{\varphi} = \frac{1}{r} \frac{\partial T}{\partial \varphi} \quad (5.15)$$

$$\delta_{\lambda} = \frac{1}{r \cos \varphi} \frac{\partial T}{\partial \lambda} . \quad (5.16)$$

Note that (5.13) is also of the form (5.4), with the fundamental function T replaced by the derived function LT , and the fundamental base function $\phi_j(P)$ replaced by the "propagated" base function $L\phi_j(P)$. This completes our brief account of the use of collocation in approximating T and quantities derived from T (see (5.4) and (5.13)).

An important issue in the above collocation procedure is the choice of base function. In this report we will examine two major approaches in selecting the base function, namely, the Dirac approach (Bjerhammar, 1975; Sjöberg, 1978) and the least squares collocation approach (see, e.g., Moritz, 1978b). We realize from the geodetic literature on collocation that a set of equations purportedly defining one method can in certain cases be interpreted as defining another method. Examples of this are found in Sjöberg (1978, pp. 9, 12), Tscherning (1983a), Lelgemann (1981), Brennecke and Lelgemann (1984), Bjerhammar (1975, 1978). For our purposes we will distinguish between the Dirac approach and least squares collocation approach in a simple way, by specifying the equations we are using under each method. Then we will conduct numerical experiments using the equations and compare the results. The reader interested in a theoretically refined distinction between the Dirac and least squares collocation approaches, and in their relationship to each other and to other models, should consult the references cited and Moritz (1980, starting from Sections 12, 30, 38).

5.2 The Dirac Approach to Collocation

The Dirac approach to collocation has been interpreted as a generalized point mass modeling (Sjöberg, 1978, p. 13; see also Forsberg, 1984, pp. 24-27; and Brennecke and Lelgemann, 1984). In this

interpretation the collocation coefficients b_j of (5.4) are generalized point mass values, and the base functions $\phi_j(P)$ are the harmonic potentials of the generalized point masses. This generalization is a discrete analogue of that applied by Bravar (1964) who, in solving the continuous (i.e., non-discrete) geodetic boundary value problem, used a generalized surface density layer on the telluroid in place of the usual density layer used by Molodenskii et al., 1962, sec. V-15; see Moritz (1980, p. 365). The generalized point masses in the Dirac approach are distributed on a geocentric sphere of chosen radius entirely embedded within the earth, specifically at the points of intersection between the internal sphere and the verticals passing through the points at which the functionals f_j (see (5.6)) are given. The internal sphere is also called Bjerhammar sphere, or geosphere. Since all the information of the approximation f to T become concentrated at the "point masses," these points have also been called "carrier points," "impulses," or "Dirac impulses" (Bjerhammar, 1975).

We have the following equation for the Dirac approach:

$$T(P) \approx f(P) = \sum_{j=1}^k u_j^* \text{base}(T(P), u_j^*), \quad (5.17)$$

where

u_j^* impulses on the Bjerhammar sphere.
 $\text{base}(T(P), u_j^*)$ base function, harmonic as a function of P , relating $T(P)$ and u_j^* .

We write the base function in the general form:

$$\text{base}(T(P), u_j^*) = R_g \sum_{n=2}^{\infty} k_n \frac{r_p^{n-1}}{R_g^{n+1}} \left(\frac{r_p}{R_g} \right)^{n+1} P_n(\cos \psi_{pj}), \quad (5.18)$$

where

R_g chosen radius of the Bjerhammar sphere
 r_p geocentric radius to the computation point P (under the spherical approximation, $r_p = R + h_p$ with $R = 6371$ km and $h_p = \text{height of } P \text{ above the geoid}$)
 k_n factor to be chosen, function of n
 ψ_{pj} angular distance between P and the impulse point j

with

$$\cos \psi_{pj} = \sin \phi_p \sin \phi_j + \cos \phi_p \cos \phi_j \cos (\lambda_j - \lambda_p), \quad (5.19)$$

$\phi, \lambda \dots$ geodetic latitude and longitude.

The base function (5.18) is in the form of the kernel function E used in the Brovar solution mentioned earlier (see Moritz, 1980, p. 366).

Various choices of the k_n in (5.18) result in various further interpretations of the quantities u_j^* appearing in (5.17). To see this we first create from the impulses u_j^* a function u^* on the Bjerhammar sphere (Bjerhammar, 1975, (3)):

$$u^*(Q) = 4\pi R_B^2 \sum_{j=1}^k u_j^* \delta(Q-j), \quad (5.20)$$

where

Q arbitrary point on the Bjerhammar sphere
 $\delta(Q-j)$ Dirac delta function (see, e.g., Moritz, 1980, pp. 27-30). This function has the characteristics that $\delta(Q-j)=0$ if $Q \neq j$, and that the integral of $\delta(Q-j)$ is equal to one for every neighborhood of point j however small this neighborhood is chosen to be.

Then, (5.17) can be rigorously written in the integral form (compare Bjerhammar, 1975, (1)-(5a) or Katsambalos, 1981, (5.33)-(5.35):

$$T(P) \approx f(P) = \frac{1}{4\pi} \int_{\sigma} u^*(Q) \text{base}(T(P), u^*(Q)) d\sigma(Q), \quad (5.21)$$

where the integration is carried over the unit sphere σ and the integral kernel is, from (5.18):

$$\text{base}(T(P), u^*(Q)) = R_B \sum_{n=2}^{\infty} k_n \frac{2n+1}{n-1} \left(\frac{R_B}{r_p} \right)^{n+1} P_n(\cos \psi_{pq}). \quad (5.22)$$

From the theory of eigenvalues and eigenfunctions of isotropic integral operators (see, e.g., Jekeli, 1980) we can write from (5.21) and (5.22) the

following relation between the n^{th} surface harmonics of T^* and u^* on the Bjerhammar sphere:

$$T_n^* = \frac{R_a}{n-1} k_n u_n^* . \quad (5.23)$$

(The "*" denotes reference to the Bjerhammar sphere). The last equation reveals directly what type of quantity the u^* is, in relation to the disturbing potential T . For example, if $k_n=1$ is chosen then the spectral relation (5.23) reveals that the u^* being solved on the Bjerhammar sphere is the gravity anomaly (see (5.24) below); from (5.20) the u_j^* in this case can be termed "gravity anomaly impulses." We have from (5.23):

$$\Delta g_n^* = k_n u_n^* . \quad (5.23a)$$

In this report we will numerically experiment on three types of choices for the k_n in (5.22). These choices will be those that imply the solution on the Bjerhammar sphere of the gravity anomaly Δg^* , the single-layer density μ^* , and the double-layer density $\bar{\mu}^*$. More details on these quantities follow:

1. the gravity anomaly Δg^* . Here, the Δg_j^* are gravity anomaly impulses. This is the original system used by Bjerhammar (1964), and for which numerical experiments were performed by Sjöberg (1975, pp. 86-89; 1978, pp. 64-69) and Katsambalos (1981) under the label of "Dirac approach." From Heiskanen and Moritz (1967, p. 89) we have the spectral relation between T^* and Δg^* :

$$T_n^* = \frac{R_a}{n-1} \Delta g_n^* . \quad (5.24)$$

Comparing (5.23) and (5.24) the choice of k_n in this case is:

$$k_n(\Delta g^*) = 1 . \quad (5.25)$$

The base function (5.18) then becomes the extended Stokes function, with closed form (see *ibid.*, (6-30), (6-45):

$$\text{base}(T(P), \Delta g_j^*) = R_a t \left[\frac{2}{D} + 1 - 3D - t \cos \psi \left(5 + 3j_n \frac{1 - t \cos \psi + D}{2} \right) \right] \quad (5.26)$$

where

$$t = \frac{R_a}{r_p} \quad (5.27)$$

$$r_p = R + h_p \quad (R = 6371 \text{ km; } h_p = \text{height of P above the geoid}) \quad (5.28)$$

$$\cos \psi = \cos \psi_{pj} \quad (\text{see (5.19)}) \quad (5.29)$$

$$D^2 = 1 - 2t \cos \psi + t^2. \quad (5.30)$$

2. the single-layer density μ^* . Here, the μ_j^* are point masses. This system (of Dirac approach to collocation) is discussed in Sunkel (1981b, 1983b). From Sunkel (1981b, (2.5)) we get the following spectral relation between T^* and μ^* :

$$T_n^* = \frac{1}{R_g(2n+1)} \mu_n^*. \quad (5.31)$$

Comparing (5.23) and (5.31) the choice of k_n in this case is:

$$k_n(\mu^*) = \frac{(n-1)}{R_g^2(2n+1)}. \quad (5.32)$$

The base function (5.18) becomes simply the reciprocal distance function, with closed expression (Heiskanen and Moritz, 1967, p. 35):

$$\text{base}(T(P), \mu_j^*) = \frac{1}{R_g} \sum_{n=0}^{\infty} \left(\frac{R_g}{r_p} \right)^{n+1} P_n(\cos \psi_{pj}) = \frac{1}{\ell}, \quad (5.33)$$

where

$$\ell^2 = r_p^2 + R_g^2 - 2 R_g r_p \cos \psi_{pj}. \quad (5.34)$$

Note that for exact agreement of (5.18) and (5.33) we should start the summation in (5.18) from $n=0$.

3. the double-layer density $\bar{\mu}^*$. Here, the $\bar{\mu}_j^*$ are point dipoles. The concept of point dipoles, and in general multipoles, is discussed in Meissl (1981, pp. 184-190). The base function corresponding to the use of multipoles on the Bjerhammar sphere can be expressed as a derivative of (5.33) with respect to R_g (ibid., 7.7)):

$$\frac{\partial N}{\partial R_g^N} \left[\frac{1}{R_g} \sum_{n=0}^{\infty} \left(\frac{R_g}{r_p} \right)^{n+1} P_n(\cos \psi_{pj}) \right]; \text{ or } \frac{\partial N}{\partial R_g^N} \left[\left(\frac{1}{\ell} \right) \right], \quad (5.35)$$

where the order N of differentiation is the order of the multipole, e.g., $N=1$ for a dipole and $N=0$ for a monopole (i.e., a point mass). Using (5.35) with $N=1$, we get the following base function for our dipole system, in series form:

$$\text{base}(T(P), \bar{\mu}_j^*) = \frac{1}{R_g^2} \sum_{n=1}^{\infty} n \left(\frac{R_g}{r_p} \right)^{n+1} P_n(\cos \psi_{pj}) , \quad (5.36)$$

and in closed form (differentiating (5.34)):

$$\text{base}(T(P), \bar{\mu}_j^*) = \frac{r_p \cos \psi_{pj} - R_g}{r_p^3} . \quad (5.37)$$

Comparing (5.18) and (5.36) gives the implied k_n :

$$k_n(\bar{\mu}^*) = \frac{n(n-1)}{R_g^3(2n+1)} . \quad (5.38)$$

Using (5.38) into (5.23) we get the spectral relation between the disturbing potential T^* and the double-density layer $\bar{\mu}^*$ on the Bjerhammar sphere:

$$T_n^* = \frac{n}{R_g^2(2n+1)} \bar{\mu}_n^* . \quad (5.39)$$

We have now completed the description of the various Dirac systems that we will use in our numerical experiments. These systems have been defined through particular choices of k_n in the base function (5.18). In principle, the choice of k_n in (5.18) is arbitrary, provided only that (5.18) converges and that we can solve for the collocation coefficients b_j in the collocation formula (5.4) (details of the computation of the b_j are given later). We have chosen the k_n -expressions (5.25), (5.32), and (5.38), leading respectively to the gravity anomaly impulses, point masses and point dipole systems, because the said systems are relatively well-known in the geodetic literature. More numerical experiments are needed on these systems, especially using real data and computations in space.

Note that both the $k_n(\Delta g^*)$ of (5.25) and $k_n(\mu^*)$ of (5.32) are proportional to a constant for $n \rightarrow \infty$, whereas the $k_n(\bar{\mu}^*)$ of (5.38) is proportional to n for $n \rightarrow \infty$. Adopting the terminology of Leigemann (1981), the order of $k_n(\Delta g^*)$ and $k_n(\mu^*)$ are equal to zero, whereas the order of $k_n(\bar{\mu}^*)$ is equal to 1. The order of k_n in n , denoted by $O(k_n)$,

is defined as "the highest power of n within the explicit expression for k_n , e.g., for $k_n = (2n+1)/(n+1)$ we obtain $O(k_n) = 0$ " (ibid.). Analogous to the empirical findings of Lelgemann in his interpolation problems, we also found that the $O(k_n)$ strongly influences the optimal radius R_g that should be chosen for good collocation results, and that systems with the same $O(k_n)$ have about the same optimal R_g . The Δg^* - and μ^* -systems required about the same depth to the Bjerhammar sphere, these two systems having the same $O(k_n)$. The $\bar{\mu}^*$ -system required a deeper Bjerhammar sphere, because this system had a larger $O(k_n)$ than the other two systems. From (5.23a) one can see that the larger the $O(k_n)$ the smoother (less high frequency energies) the u^* relative to Δg^* , with $O(k_n)=0$ implying the same smoothness for u^* and Δg^* . One should remember that spectral multiplication by n implies amplification of high frequency energies of a function.

Let us now turn to the computation of functionals of T , from the general representation (5.17) of the Dirac approach. In accordance with (5.13), a functional LT of T can be found by applying the operator L to (5.17):

$$LT(P) \approx Lf(P) = \sum_{j=1}^k u_j^* L \text{ base}(T(P), u_j^*) . \quad (5.40)$$

From (5.40) we can write:

$$\text{base}(LT(P), u_j^*) = L \text{ base}(T(P), u_j^*) . \quad (5.41)$$

The last equation expresses a "propagation of base function," analogous to the propagation of covariance functions well-known in least squares collocation (see Moritz, 1980, p. 86). As an example of (5.40) and (5.41) let $LT(P) = \Delta g(P)$ and $u_j^* = \Delta g_j^*$; using (5.40), (5.41), and the operator (5.8) for Δg we have:

$$\Delta g(P) = \sum_{j=1}^k \Delta g_j^* \text{ base}(\Delta g(P), \Delta g_j^*) , \quad (5.42)$$

where the propagated base function is:

$$\text{base}(\Delta g(P), \Delta g_j^*) = \left[\frac{-\partial}{\partial r_p} - \frac{2}{r_p} \right] \text{ base}(T(P), \Delta g_j^*) , \quad (5.43)$$

and the fundamental base function $\text{base}(T(P), \Delta g_j^*)$ is given by (5.26). In the following we show the propagated base functions (5.41) for our gravimetric quantities of interest (i.e., for $LT = \Delta g$, δ_r , δ_φ , and δ_λ), and under our various u_j^* -systems (i.e., $u_j^* = \Delta g_j^*$, μ_j^* , $\bar{\mu}_j^*$).

1. Δg_j^* -system. Formally we can apply (5.41) to get the propagated base functions for this system. However, we already know these functions to be the Poisson kernel for the upward continuation of gravity anomalies (Heiskanen and Moritz, 1967, sec. 2-15), and the kernels for the "direct method" of horizontal and radial disturbance computations (ibid., sec. 6-4). We have:

$$\text{base}(\Delta g(P), \Delta g_j^*) = \frac{t^2(1-t^2)}{D^3}; \quad (5.44)$$

$$\begin{aligned} \text{base}(\delta_r(P), \Delta g_j^*) = t^2 \left[\frac{1-t^2}{D^3} + \frac{4}{D} + 1 - 6D - \right. \\ \left. - t \cos \psi \left[13 + 6 \ln \frac{1 - t \cos \psi + D}{2} \right] \right]; \end{aligned} \quad (5.45)$$

$$\begin{aligned} \begin{pmatrix} \text{base}(\delta_\varphi(P), \Delta g_j^*) \\ \text{base}(\delta_\lambda(P), \Delta g_j^*) \end{pmatrix} = \begin{pmatrix} \cos \alpha \\ \sin \alpha \end{pmatrix} t^3 \sin \psi \left[\frac{2}{D^3} + \right. \\ \left. + \frac{6}{D} - 8 - 3 \frac{1 - t \cos \psi - D}{D \sin^2 \psi} - 3 \ln \frac{1 - t \cos \psi + D}{2} \right]. \end{aligned} \quad (5.46)$$

In (5.46) α is the clockwise azimuth from North, from the projection of P on the Bjerhammar sphere to the point of Δg_j^* . We have (Rapp, 1966b, p. 17):

$$\cos \alpha = \cos \alpha_{pj} = \frac{\cos \phi_p \sin \phi_j - \sin \phi_p \cos \phi_j \cos(\lambda_j - \lambda_p)}{\sin \psi}. \quad (5.47)$$

$$\sin \alpha = \sin \alpha_{pj} = \frac{\cos \phi_j \sin(\lambda_j - \lambda_p)}{\sin \psi}. \quad (5.48)$$

2. μ_j^* -system (Point Masses). For this system we need to apply the operators in (5.1), (5.14), (5.15), (5.16) to the fundamental base

function (5.33) to obtain the propagated base functions. The results are:

$$\text{base}(\Delta g(P), \mu_j^*) = \frac{1}{r_p^2} \left(\frac{1 - t \cos \psi}{D^3} - \frac{2}{D} \right); \quad (4.49)$$

$$\text{base}(\delta_r(P), \mu_j^*) = \frac{1}{r_p^2} \left(\frac{1 - t \cos \psi}{D^3} \right); \quad (5.50)$$

$$\begin{pmatrix} \text{base}(\delta_\varphi(P), \mu_j^*) \\ \text{base}(\delta_\lambda(P), \mu_j^*) \end{pmatrix} = \begin{pmatrix} \cos \alpha \\ \sin \alpha \end{pmatrix} \frac{t \sin \psi}{r_p^2 D^3}. \quad (5.51)$$

In deriving (5.51) we have used (Heiskanen and Moritz, 1967, p. 234):

$$\frac{\partial \psi}{\partial \varphi} = -\cos \alpha; \quad \frac{\partial \psi}{\partial \lambda} = -\cos \varphi \sin \alpha. \quad (5.52)$$

3. μ_j^* -system (Point Dipoles). Again we apply the operators in (5.1), (5.14), (5.15), (5.16), this time to the fundamental base function (5.37) to obtain the propagated base functions for this system. The results can be written as follows:

$$\text{base}(\Delta g(P), \bar{\mu}_j^*) = \frac{1}{r_p^3} \left(\frac{3 \cos \theta \cos \beta - \cos \psi}{D^3} - \frac{2 \cos \theta}{D^2} \right); \quad (5.53)$$

$$\text{base}(\delta_r(P), \bar{\mu}_j^*) = \frac{1}{r_p^3} \left(\frac{3 \cos \theta \cos \beta - \cos \psi}{D^3} \right); \quad (5.54)$$

$$\begin{pmatrix} \text{base}(\delta_\varphi(P), \bar{\mu}_j^*) \\ \text{base}(\delta_\lambda(P), \bar{\mu}_j^*) \end{pmatrix} = \begin{pmatrix} \cos \alpha \\ \sin \alpha \end{pmatrix} \frac{\sin \psi}{r_p^3 D^3} \left(\frac{3 t \cos \theta}{D} + 1 \right); \quad (5.55)$$

where

$$\cos \theta = \frac{\cos \psi - t}{D} \quad (5.56)$$

$$\cos \beta = \frac{1 - t \cos \psi}{D}. \quad (5.57)$$

Since the fundamental base function (5.37) for the point dipole system has been found by differentiating the base function (5.33) for the point mass system with respect to the radius R_0 , then it follows from the idea of base function propagation that (5.53) - (5.55) can also be obtained by differentiating (5.49) - (5.51) with respect to R_0 .

Finally, to complete our description of the Dirac approach to the collocation problem, we need to discuss the computation of the coefficients u_j^* (the generalized point masses) appearing in (5.17). We will determine the u_j^* ($j = 1, 2, \dots, k$) using k given functionals LT of T on the earth's surface, and an inversion of the $k \times k$ system of linear equations arising from (5.40). In the principle the Dirac system can handle heterogeneous data types, i.e., different types of functionals of T such as gravity anomalies, deflections of the vertical, and height anomalies. In principle also, a filtering of observational errors can be built into the method by using more than k given functionals and performing a least squares fit to the data based on (5.40).

However, our study will be limited to the use of a homogeneous data type, the gravity anomaly, and a unique solution of $k \times k$ system of linear equations to solve for the u_j^* . The gravity anomaly is still the most common gravimetric data type, being the observable arising from the Molodensky formulation (Molodenskii, et al., 1962) of the geodetic boundary value problem (g.b.v.p.). Bjerhammar and Svenson (1983) discuss the straightforward application of the Dirac approach to the so-called "fixed boundary" formulation of the g.b.v.p., where the observables are gravity disturbances. Regarding the use of a unique solution for the u_j^* instead of a least squares solution, we believe that it would be best to separate the problem of modeling the external field from surface data on the one hand, and the problem of the establishment of an optimal set of surface data on the other hand. The latter problem can be handled in an a priori step involving editing, prediction, filtering, and adjustment of observational data.

To solve for the collocation coefficients u_j^* ($j = 1, 2, \dots, k$) from k given gravity anomaly values on the surface of the earth, we first form the $k \times k$ system of linear equations (see (5.40), (5.41)):

$$\Delta g_i = \sum_{j=1}^k u_j^* \text{ base}(\Delta g_i, u_j^*), \quad i = 1, 2, \dots, k, \quad (5.58)$$

where in our case, $\text{base}(\Delta g_i, u_j^*)$ can be any of (5.44), (5.49), or (5.53). Since the system (5.58) tends to be large, we employ an iterative solution. The number of iterations required for a convergent solution indicates the degree of stability of the equation system. We will use the Gauss-Seidel iteration method employed also by Katsambalos (1981, p. 64). Letting (m) denote the current iteration step, we have:

$$u_i^{*(m)} = \frac{1}{A_{ii}} \left[\Delta g_i - \sum_{j=1}^{i-1} A_{ij} u_j^{*(m)} - \sum_{j=i+1}^k A_{ij} u_j^{*(m-1)} \right], \quad (5.59)$$

where

$$A_{ij} = \text{base}(\Delta g_i, u_j^*). \quad (5.60)$$

Note from (5.59) that the most recently computed value of u_j^* is used at each iteration step. The gravity anomalies implied by a current iteration step are:

$$\Delta g_i^{(m)} = \sum_{j=1}^k u_j^{*(m)} A_{ij} \quad (i = 1, 2, \dots, k), \quad (5.61)$$

and the current residuals are:

$$\varepsilon_i^{(m)} = \Delta g_i - \Delta g_i^{(m)}, \quad (i = 1, 2, \dots, k). \quad (5.62)$$

It is reasonable to terminate the iterations when at least one of these conditions is met (Sjoberg, 1978, p. 68):

$$\left. \begin{array}{l} \text{RMS} \{ \varepsilon_i^{(m)}, i = 1, 2, \dots, k \} < \varepsilon_{\text{RMS}} ; \\ \text{Max} \{ \varepsilon_i^{(m)}, i = 1, 2, \dots, k \} < \varepsilon_{\text{max}} ; \\ m > m_{\text{max}} \end{array} \right\} \quad (5.63)$$

where the tolerances ε_{RMS} (RMS residual), ε_{max} (maximum residual), and m_{max} (maximum number of iterations) are to be prescribed, for example (ibid.):

$$\left. \begin{array}{l} \varepsilon_{\text{RMS}} = 0.25 \text{ mgal} \\ \varepsilon_{\text{max}} = 0.5 \text{ mgal} \\ m_{\text{max}} = 30 \end{array} \right\} . \quad (5.64)$$

This completes our description of the Dirac approach to collocation. To summarize, the formal procedure in the Dirac approach is to model $T(P)$ as the sum of potentials of k generalized point masses (see (5.17)) that are distributed on an internal sphere of chosen depth (a Bjerhammar sphere of radius R_B). The values of the "point masses" can be solved from k given functionals $L_j T(P_j)$ of T on the earth's surface by an inversion of a $k \times k$ linear equation system arising from (5.40) in general, or (5.58) in our particular case. Various choices of the free factor k_n in the base function (5.18) lead to different types of "point masses" on the Bjerhammar sphere. We decided to use gravity anomaly impulses, the usual point masses, and point dipoles as generalized point masses for our later numerical experiments.

In the above Dirac approach, and in the least squares collocation approach to be discussed in the next section, it is important that we also use the spherical harmonic and residual topographic models of Chapter 4 as complementary models. The reason is the limitation in the size k of the linear system (5.58) that can be feasibly solved. Since k is equal to the number of data points, then it is important to (a) use the spherical harmonic model to account for remote zone effects, thereby reducing the required data coverage for the collocation solution; and (b) use the residual topographic model to account for very detailed gravity field information, thereby reducing the required density of data for the collocation solution.

5.3 The Least Squares Collocation Approach

In the Dirac approach to the collocation problem, the base functions used are the k harmonic functions $\text{base}(T(P), u_j^*)$ relating the disturbing potential $T(P)$ to each of the k Dirac impulses u_j^* on the Bjerhammar sphere (see (5.17)). In the least squares collocation approach, the base functions to use are the k empirical covariance functions between $T(P)$ and each of the k given functionals $L_j T(J)$ on the earth's surface. This choice of base functions arises from adding to the collocation condition (5.9) the condition that the RMS difference between the approximation function f and the true function T be statistically minimized (see, e.g., Moritz, 1978a, 1978b). Apart from this statistical interpretation, the least squares collocation approach can also be justified as a purely analytical approximation technique, in the context of the more general "minimum norm collocation" in a Hilbert space of harmonic functions (see, e.g., Tscherning, 1977) or in the context of the minimum norm Bjerhammar solution discussed by Sjöberg (1975, 1978). Our interest in this study is to first give the equations defining our use of the least squares collocation approach, then later perform numerical experiments using these equations.

We have the following representation in the least squares collocation approach:

$$T(P) \approx f(P) = \sum_{j=1}^k b_j \text{cov}(T(P), L_j T(J)) , \quad (5.65)$$

where

b_j collocation coefficients

$\text{cov}(T(P), L_j T(J))$ empirical covariance between $T(P)$ and the given functional $L_j T$ at point J . This is derived from an analytical expression of suitable form (see (5.71)) fitted to the covariance behavior of real data in the area of computation.

As already mentioned, the given functionals in our case are homogeneously the gravity anomalies Δg_j on the earth's surface so that we will use (5.65) in the form:

$$T(P) \approx f(P) = \sum_{j=1}^k b_j \text{cov}(T(P), \Delta g_j) . \quad (5.66)$$

Any functional LT of T can be expressed by applying the operator L to (5.66) and employing covariance propagation (Moritz, 1980, p. 86):

$$LT(P) \approx Lf(P) = \sum_{j=1}^k b_j \text{cov}(LT(P), \Delta g_j) . \quad (5.66a)$$

For the sake of our discussions the covariance function in (5.66) is now written in the general form:

$$\text{cov}(T(P), \Delta g_j) = \frac{r_0^2}{r_j} \sum_{n=2}^{\infty} d_n^2 \frac{2n+1}{n-1} \left(\frac{r_0^2}{r_p r_j} \right)^{n+1} P_n(\cos \psi_{pj}) , \quad (5.67)$$

where

r_0 chosen radius of the internal sphere (Bjerhammar sphere)

d_n non-negative factors to be chosen, function of n .

The covariance function (5.67) is in the same form as the base function (5.18) of the Dirac approach, except for the replacement:

$$R_B \rightarrow \frac{r_0^2}{r_j} . \quad (5.68)$$

The implied auto-covariance function of Δg follows from (5.67) using covariance propagation (ibid.) and the spectral relation between T and Δg (see (5.24):

$$\text{cov}(\Delta g(P), \Delta g_j) = \sum_{n=2}^{\infty} d_n^2 (2n+1) \left(\frac{r_0^2}{r_P r_j} \right)^{n+2} P_n(\cos \psi_{Pj}) . \quad (5.69)$$

Similarly, we obtain the implied auto-covariance function of T :

$$\text{cov}(T(P), T_j) = r_0^2 \sum_{n=2}^{\infty} d_n^2 \frac{2n+1}{(n-1)^2} \left(\frac{r_0^2}{r_P r_j} \right)^{n+1} P_n(\cos \psi_{Pj}) . \quad (5.70)$$

The last equation is in the proper general form of the homogeneous and isotropic auto-covariance function of the disturbing potential (see, e.g., Tscherning and Rapp, 1974):

$$\text{cov}(T(P), T_j) = \sum_{n=2}^{\infty} \sigma_n \left(\frac{r_0^2}{r_P r_j} \right)^{n+1} P_n(\cos \psi_{Pj}) , \quad (5.71)$$

where the σ_n are the degree variances of T on the sphere of radius r_0 . From (5.70) and (5.71):

$$\sigma_n = r_0^2 d_n^2 \frac{2n+1}{(n-1)^2} . \quad (5.71a)$$

For local applications of least squares collocation, the analytical expression being used for the covariance function should be fitted to the local covariance behavior of the data in the area of computation. Usually, a fit is made to Δg -data, these being the most readily available

data. In this case the free parameters d_n and r_0 should be adjusted together so that (5.69) will have the desired fit to the data. Moritz (1980, pp. 174-177) has discussed "three essential parameters" that define a locally fitted covariance function, namely, the variance, the correlation length, and the curvature parameter of the covariance function, after the function is restricted to the sphere where the given data refer. A good fit to the variance of the data is important for yielding realistic error estimates from the collocation procedure. The correlation length carries information on the "smoothness" of the field, i.e., on the spectral distribution of the total variance. The curvature parameter, measuring the curvature of the covariance function at $\psi=0^\circ$, carries information about the very local behavior of the field.

A discussion on the determination of the three essential parameters of a covariance function from real data is given in a paper by Schwarz and Lachapelle (1980). In our present study, where the data were assumed errorless in order to concentrate on modeling errors, a properly fitted variance was unimportant. Also in our study, a fit to the curvature parameter and correlation length was not explicitly performed unlike in the above paper. Rather, the analytical expression for the covariance was "tailored" to real data by the criteria of yielding the least RMS error of actual predicted values at withheld test points in the local area (see Table 8).

For the purpose of covariance function modeling it is useful to treat the anomalous gravity field as being generated by a white noise u^* -layer on the internal sphere of radius r_0 . Actual generations of covariance functions from white noise distributions at depth is discussed in Heller and Jordan (1979). The covariance function of a white noise u^* -layer is (Cruz and Laskowski, 1984, sec. 6.2):

$$\text{cov}(u^*(P), u^*(J)) = \sigma_0^2 \sum_{n=2}^{\infty} (2n+1) P_n(\cos \psi_{PJ}), \quad (5.72)$$

where σ_0^2 is the variance of a single harmonic u_n^* . On the other hand, the covariance function of the disturbing potential T^* on the r_0 -sphere is, from (5.70):

$$\text{cov}(T^*(P), T^*(J)) = r_0^2 \sum_{n=2}^{\infty} d_n^2 \frac{2n+1}{(n-1)^2} P_n(\cos \psi_{PJ}). \quad (5.73)$$

Comparing (5.72) and (5.73) and using the covariance propagation concept, then we can conclude that T^* and u^* are spectrally related as follows:

$$T_n^* = \frac{r_0}{n-1} \frac{d_n}{\sigma_0} u_n^* . \quad (5.74)$$

Equation (5.74) defines the u^* in relation to the disturbing potential, and is analogous to equation (5.23) of the Dirac approach. For example, if $d_n = \sigma_0$ is chosen then the u^* is seen from (5.74) to be the gravity anomaly Δg^* ; in this case the anomalous gravity field can be interpreted as being generated from a white noise gravity anomaly distribution on the internal sphere. From the discussions of Sjöberg (1975, 1978), one can also conclude an alternative interpretation of the u^* of (5.74), namely, that the (least squares collocation) solution essentially minimizes the variance (sum of degree variances) of the quantity u^* on the Bjerhammar sphere of radius r_0 . A similar interpretation in terms of norm minimization, presented in a different way, may be found in Tscherning (1972, 1983a).

In this report we will numerically experiment on two types of choices for the d_n in (5.74). These choices will be those that imply the presence on the Bjerhammar sphere of a white noise distribution of (1) gravity anomaly Δg^* , and (2) disturbing potential T^* . More details on these two systems will now be given.

1. the white noise Δg^* -system. As already mentioned the choice of d_n in this case is:

$$d_n(\Delta g^*) = \sigma_0 . \quad (5.75)$$

The covariance function (5.67) then becomes exactly in the form of the base function (5.18) of the Dirac approach, except for the replacement (5.68). The closed covariance expression therefore follows easily using (5.26) and the replacement (5.68):

$$\text{cov}(T(P), \Delta g_j) = r_p s^2 \sigma_0^2 \left[\frac{2}{E} + 1 - 3E - s \cos \psi \left(5 + 3en \frac{1-s \cos \psi + E}{2} \right) \right] , \quad (5.76)$$

where

$$s = \frac{r_0^2}{r_p r_j} \quad (5.77)$$

$$E^2 = 1 - 2 s \cos \psi + s^2 . \quad (5.78)$$

Equation (5.76) checks with the result of Sjöberg (1975, p. 106). Similarly, we can use the replacement (5.68) into (5.44) - (5.46) to obtain the propagated covariance functions:

$$\text{cov}(\Delta g(P), \Delta g_j) = \sigma_0^2 \frac{s^2(1-s^2)}{E^3} ; \quad (5.79)$$

$$\begin{aligned} \text{cov}(\delta_r(P), \Delta g_j) = \sigma_0^2 s^2 \left[\frac{1-s^2}{E^3} + \frac{4}{E} + 1 - 6E - \right. \\ \left. - s \cos \psi \left(13 + 6 \ln \frac{1-s \cos \psi + E}{2} \right) \right] ; \end{aligned} \quad (5.80)$$

$$\begin{aligned} \begin{bmatrix} \text{cov}(\delta_\varphi(P), \Delta g_j) \\ \text{cov}(\delta_\lambda(P), \Delta g_j) \end{bmatrix} = \sigma_0^2 \begin{bmatrix} \cos \alpha \\ \sin \alpha \end{bmatrix} s^3 \sin \psi \left[\frac{2}{E^3} + \right. \\ \left. + \frac{6}{E} - 8 - 3 \frac{1-s \cos \psi - E}{E \sin^2 \psi} - 3 \ln \frac{1-s \cos \psi + E}{2} \right] . \end{aligned} \quad (5.81)$$

The above equations all agree with *ibid.*, p. 106. The propagated covariance functions are to be used in (5.66a) for computing our functionals of interest.

2. the white noise T*-system. In this system where we have $u^*=T^*$, (5.74) says that the choice of d_n must be:

$$d_n(T^*) = \frac{n-1}{r_0} \sigma_0 . \quad (5.82)$$

The closed covariance expressions of interest to us can be obtained from Sjöberg (*ibid.*, p. 107):

$$\text{cov}(T(P), \Delta g_j) = \sigma_0^2 \frac{s}{2r_j E^3} \left[\frac{3(1-s^2)^2}{E^2} - 5 + s^2 \right] ; \quad (5.83)$$

$$\text{cov}(T(P), T_j) = \sigma_0^2 \frac{s(1-s^2)}{E^3} ; \quad (5.84)$$

$$\text{cov}(\Delta g(P), \Delta g_j) = \sigma_0^2 \frac{s^2}{4r_0^2} \left[\frac{15(1-s^2)^3}{E^7} - \frac{36(1-s^2)}{E^5} + \frac{25-s^2}{E^3} \right]; \quad (5.85)$$

$$\text{cov}(\delta_r(P), \Delta g_j) = \sigma_0^2 \frac{s^2}{4r_0^2} \left[\frac{15(1-s^2)^3}{E^7} - \frac{12(2+s^2)(1-s^2)}{E^5} + \frac{5+3s^2}{E^3} \right]; \quad (5.86)$$

$$\begin{pmatrix} \text{cov}(\delta_\varphi(P), \Delta g_j) \\ \text{cov}(\delta_\lambda(P), \Delta g_j) \end{pmatrix} = \sigma_0^2 \begin{pmatrix} \cos \alpha \\ \sin \alpha \end{pmatrix} \frac{3}{2} \frac{s^3 \sin \psi_P}{r_0^2 E^5} \left[\frac{5(1-s^2)^2}{E^2} - (5-s^2) \right]. \quad (5.87)$$

The white noise T*-system is the same as the "attenuated white noise" covariance model of Heller and Jordan (1979) up to a scale factor. The said covariance model was recently applied by Sunkel (1983a) in his least squares collocation modeling of the geoid in Austria.

This completes our description of the two covariance systems, the Δg^* - and the T*-systems, that we will use in our numerical experiments on the least squares collocation approach. A variety of other covariance systems may be defined, by simply choosing different sets of d_n -values provided the resulting summations converge (see, e.g., (5.69)). It turns out that covariance systems which have d_n -values of the same "order in n " (see second paragraph after (5.39) for the definition of "order in n ") have the same numerical characteristics. This is the reason why, for example, models of degree variances (degree variances are directly related to d_n ; see (5.69) - (5.71a)) have been distinguished in terms of the models' variation with n as n goes to infinity (Tscherning, 1976, p. 2; Moritz, 1980, pp. 181-186). Therefore, the two covariance systems that we have chosen for experimentation actually typify the numerical behavior of two groups of covariance systems. The Δg^* -system typifies systems with order of d_n equal to zero (see (5.75)), and the T*-system typifies systems with order of d_n equal to unity (see (5.82)).

We should mention that the well-known Tscherning/Rapp (1974) anomaly degree variance model, namely:

$$c_n = \frac{A(n-1)}{(n-2)(n+24)}, \quad (5.88)$$

when compared with (5.69) yields a d_n with order equal to -1. For this model the only effective way to produce the very short correlation lengths needed for local computations is to subtract lower harmonics

$3 < n < N$ from the covariance functions (ibid., p. 62). This removal of lower harmonics, say for $N=180$, is expensive in terms of computer time. For this reason we have avoided the use of this model. This is the same problem that caused Sunkel (1983a) to switch to the use of Heller and Jordan's (1979) "attenuated white noise model", which is essentially the T^* -system we have discussed above. For the Δg^* - and T^* -covariance systems that we will use, the correlation length is adjusted simply by changing the radius r_0 of the Bjerhammar sphere in the closed covariance expressions.

Finally, we should discuss the computation of the collocation coefficients b_j ($j=1, 2, \dots, k$) appearing in (5.65). As in the Dirac approach we will solve the coefficients from k given gravity anomaly values on the surface of the earth. We first form the $k \times k$ system of linear equations from (5.66a):

$$\Delta g_i = \sum_{j=1}^k b_j \text{cov}(\Delta g_i, \Delta g_j), \quad i = 1, 2, \dots, k, \quad (5.89)$$

where in our case $\text{cov}(\Delta g_i, \Delta g_j)$ will be either (5.79) or (5.85). Equation (5.89) is analogous to (5.58) of the Dirac approach. For a direct comparison between the Dirac and least squares collocation approaches we will also employ the Gauss-Seidel iteration to solve (5.89). (Note that Katsambalos (1981) used the direct matrix inversion to solve (5.89), but employed the Gauss-Seidel iteration to solve (5.58)). The employed Gauss-Seidel algorithm has already been given in (5.59) - (5.64), the only change being the replacement of (5.60) by:

$$A_{ij} = \text{cov}(\Delta g_i, \Delta g_j). \quad (5.90)$$

This completes our description of the least squares collocation approaches to the collocation problem.

5.4 Numerical Investigations

5.4.1 Tailoring of Covariance Functions

The theory of least squares collocation requires that the covariance function being used approximates the local empirical covariance function in the area of computations. This "tailoring" or fitting of an analytical covariance expression to an empirical one is normally performed with respect to the gravity anomaly auto-covariance function. Also, it is usually sufficient to fit just the variance and correlation length, ignoring the very irregular curvature parameter. A fit to the variance of local data does not present any problems, as this can be done by

simply scaling the entire analytical covariance function to reflect the desired variance (value at $\psi=0^\circ$). A fit to the correlation length, on the other hand, will be simple if it can be done by just changing the radius of the Bjerhammar sphere occurring in the covariance expression. This is indeed the case for the Δg^* and T^* covariance systems that we have chosen for our numerical experiments.

Figure 26 shows the covariance functions on the mean earth sphere R for the Δg^* and T^* systems, as the depth D to the Bjerhammar sphere takes on values $D=10, 20, 30, 50, 100, 500$ km. The functions were scaled to a variance of 1 mgal^2 . Figure 26 resulted from (5.79) for the Δg^* -system and (5.85) for the T^* -system. For the quantity s in (5.77) we set $r_p=r_j=R=6371$ km, and $r_o=R-D$. The graphs reveal that to a good approximation the correlation length ξ of the Δg^* -system is related to D by:

$$\xi(\Delta g^*) \approx 1.5 D . \quad (5.91)$$

Similarly, we find for the T^* -system:

$$\xi(T^*) \approx 0.75 D . \quad (5.92)$$

Equation (5.91) is still true if Δg^* is replaced by other white noise systems with $O(d_n)=0$ (see discussion above (5.88)). In fact, we found practically the same covariance graphs when using systems generated by white noise distribution on the internal sphere of single density layer, potential gradient, radial disturbance, and total deflection of the vertical, all these systems having $O(d_n)=0$. The covariance expressions for these systems are given in Sjöberg (1975). On the other hand, (5.92) remains valid also for the covariance system generated from white noise double layer distribution on the Bjerhammar sphere, this system having $O(d_n)=1$ like the T^* -system. Again, covariance expressions based on a white noise double layer distribution may be found in Sjöberg (1975). The point is that for the described systems of $O(d_n)=0$ and $O(d_n)=1$ a desired correlation length ξ may be easily implemented by specifying the proper value for D . Specifically, very short ξ -values on the order of 15 km, needed in detailed local applications, can be easily set.

In contrast, the Tscherning and Rapp (1974) model entails a more difficult tailoring procedure to reach very short correlation lengths, as Figure 27 shows. The only effective way to reach ξ values on the order of 15 km is to remove lower harmonics $3 \leq n \leq 180$, which is an expensive procedure. Changing the radius of the Bjerhammar sphere helps the tailoring procedure, but only in a very limited way since the use of small D (e.g., $D=1$ km) is still not enough to reach ξ values on the order of 15 km.

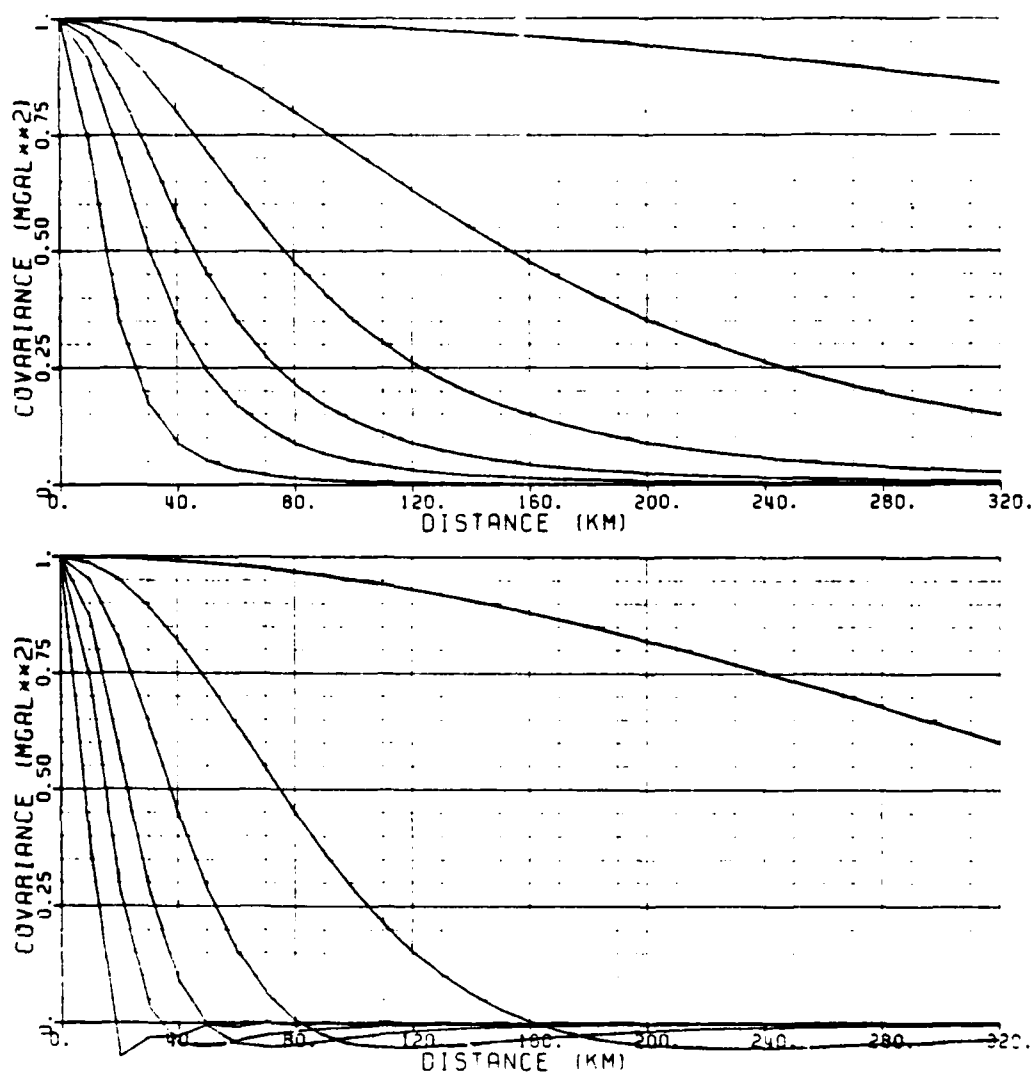


Figure 26. Gravity Anomaly Auto-Covariance Functions on the Mean Earth Sphere ($R=6371$ km), Generated from White Noise Distribution of Gravity Anomaly (top diagram) and Disturbing Potential (bottom diagram) on an Internal Sphere at Depth $D=10, 20, 30, 50, 100, 500$ km. Diagrams reveal that for the white noise gravity anomaly system there is correlation length $\xi \approx 1.5 D$, and for the white noise disturbing potential system $\xi \approx 0.75 D$.

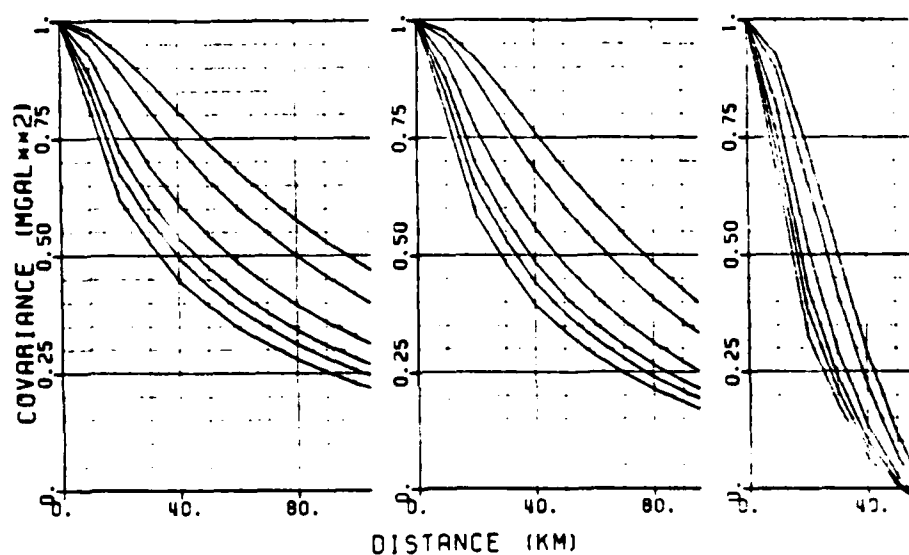


Figure 27. Gravity Anomaly Auto-Covariance Functions on the Mean Earth Sphere ($R=6371$ km), Tailored from the Tscherning and Rapp (1974) Covariance Model by Using Different Depths D to the Internal Sphere ($D=1, 2, 3, 5, 10, 15$ km) and Subtracting Lower Harmonics $3 \leq n \leq N$ (left to right: $N=20, 36, 180$). Very short correlation lengths on the order of 15 km can only be obtained by subtracting the lower 180 harmonics.

5.4.2 Real Data Predictions of Gravity Anomalies in Canada

Sjoberg (1978, Tables 8.1 and 8.2) gives surface gravity anomaly data with station elevations, that can be used for intercomparison of gravity anomaly prediction techniques. The points, located in Manitoba, Canada, are shown in Figure 28. Eighty-seven points (shown as circles) are considered as "observation points" and 50 points (shown as crosses) are considered as "prediction points" but are also known. An important characteristic of the point distribution is that the observation points are spaced almost regularly in a 0.5×0.5 grid, while the prediction points are generally near the centers of the data gaps. Since the actual gravity anomaly function can easily have features beyond the maximum 0.5×0.5 resolution implied by the data points, one should not expect a highly accurate prediction of the withheld test points.

The non-uniqueness of the collocation solution in between the data points is illustrated in Figure 29. The two collocation solutions shown are for the $2^\circ \times 3^\circ$ area marked off in Figure 28. The solutions were generated using the Dirac approach with gravity anomaly impulses on the Bjerhammar sphere of radius = (6371 km-D). The depth $D=30$ km was used for the solution shown on the left, while $D=75$ km was used for the solution on the right. In accordance with the collocation condition (5.9) the two solutions agree closely with the data values and with each other at the approximately 0.5×0.5 grid locations where the data are given. The agreement at the data points is not exact in this case, because of the use of an iterative linear equation solver (see (5.59) which was terminated after 5 iterations. Although the solutions approximately agree at the data locations, they may have very different behavior in between the data points. As expected the $D=75$ km solution appears smoother (larger correlation length) than the $D=30$ km solution. It is important to state that both solutions were contoured from predicted point values in a 0.25×0.25 grid, not just a 0.5×0.5 grid. This was to make sure that the surface shown in between the original 0.5×0.5 data points was the actual predicted surface, and not the surface which would have been artificially produced by the contouring algorithm if contours were generated from 0.5×0.5 point values.

Which then is the optimal Bjerhammar sphere radius to use under a given base function system in collocation? Different techniques have been devised in the literature to answer this question. The reader interested in details should consult Needham (1970), Blaha (1983), and Sunkel (1981b, 1983b) for the case of the point mass system, which is also applicable to any Dirac system. For an optimal internal sphere radius in the least squares collocation approach and for the more general minimum norm collocation approach, see Sjoberg (1975) and Lelgemann (1981). For the least squares collocation approach, there is a built-in theory to determine an optimal radius, namely, to use a radius that will cause the covariance function to fit the correlation length of local data in the area of computation. However, the most direct method to determine an optimal radius from the data themselves is to examine the prediction errors at withheld test points in the area, for various

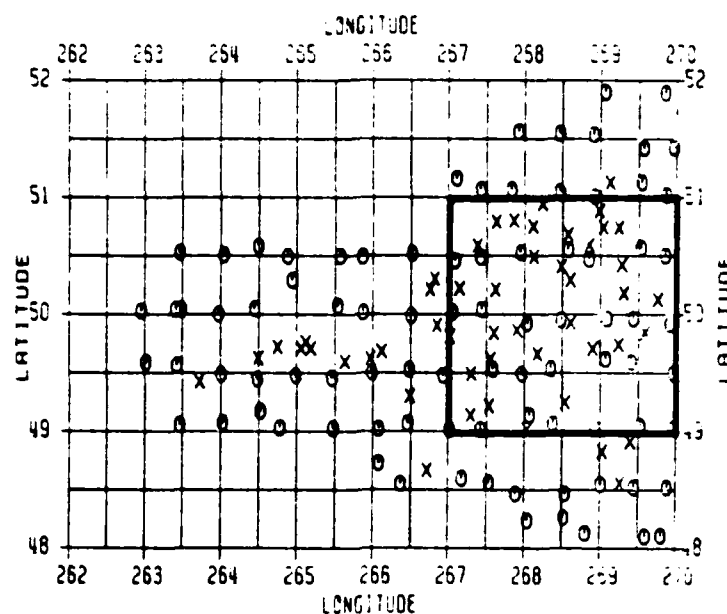


Figure 28. Point Location of Surface Gravity Anomalies in Manitoba, Canada (plotted from Sjöberg, 1978, Tables 8.1 and 8.2). (Circles: observation points; crosses: withheld prediction points).

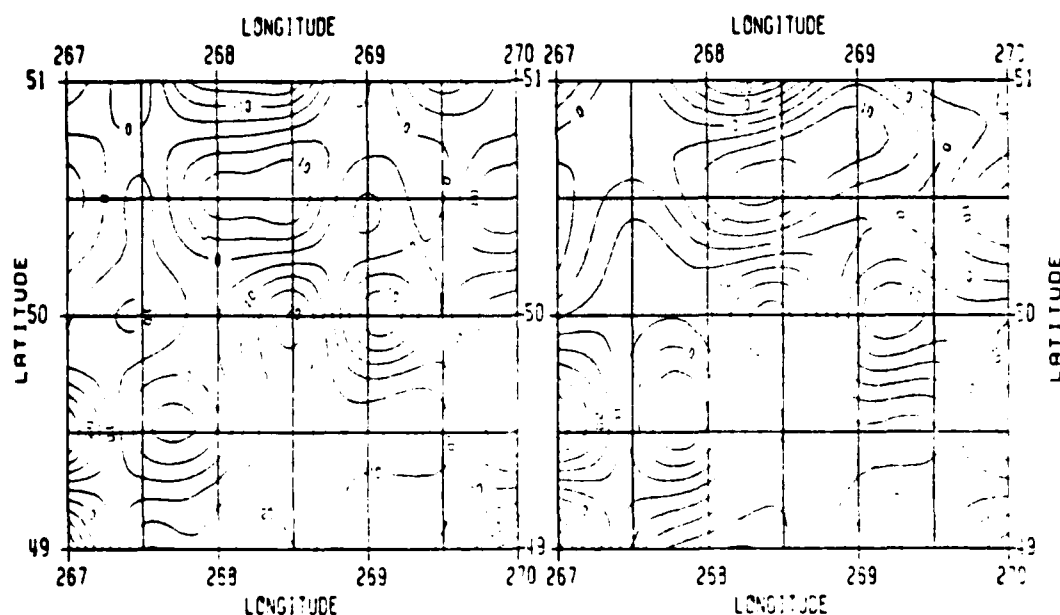


Figure 29. Two Gravity Anomaly Solutions (C.I.=5 mgals) for the Area marked off in Figure 28. Predicted Using the Dirac Approach with Gravity Anomaly Impulses on the Internal Sphere of Radius = (6371 km-D). Left: D=30 km; Right: D=75 km; No. of iterations=5.

choices of internal sphere radius. This last approach was specifically applied by Sjöberg (1975, 1978) in order to determine an optimal radius for a given base function. It is here that Sjöberg concluded that as long as an optimal radius is used, various base function systems yield the same quality of results.

We decided to repeat the gravity anomaly predictions of Sjöberg (1978, Table 8.3) since conflicting results were presented by Katsambalos (1981, Table 9.3). The data used were the observation points and withheld test points shown in Figure 28. The methods compared were the least squares collocation approach with white noise gravity anomalies on the internal sphere, which we denote by l.s.c. (Δg^*), versus the Dirac approach with gravity anomaly impulses on the internal sphere, which we denote by Dirac (Δg^*). We additionally used the other two Dirac systems that we discussed earlier, namely, the point mass and point dipole Dirac systems, which we denote by Dirac (μ^*) and Dirac ($\bar{\mu}^*$), respectively. The number of iterations to satisfy the criteria (5.64), and RMS prediction error at the 50 test points, are shown in Table 8 for various depths D to the internal sphere.

Our results are in complete agreement with Sjöberg's Table 8.3, for the l.s.c. (Δg^*) and Dirac (Δg^*) solutions. At the optimal depths of 15 km for the l.s.c. (Δg^*), 30 km for the Dirac (Δg^*), 30 km for the Dirac (μ^*), and 50 km for the Dirac ($\bar{\mu}^*$), the various systems yielded about the same RMS error of 10.2 mgal, and required about the same number of iterations of 5 for convergence under criteria (5.64). Since the RMS anomaly for the 50 prediction points is 13.53 mgals, we have the following normalized measure of "unrecovered" information (see Tscherning, 1981, sec. 4):

$$\begin{aligned} \rho &= \frac{\text{RMS Variation (Observed - Computed)}}{\text{RMS Variation of Observations}} & (5.93) \\ &= \frac{10.2}{13.5} = 76\% , \end{aligned}$$

which is within expectation, considering the large data spacing of 0.5×0.5 (see *ibid.*, Figure 1).

Table 8 shows that the Dirac (Δg^*) and Dirac (μ^*) systems produced practically identical results, a consequence of the fact that both systems have $0(k_n)=0$ (see discussion above (5.40)). The Dirac ($\bar{\mu}^*$) system which has $0(k_n)=1$ behaved differently, requiring a deeper Bjerhammar sphere than the other two Dirac systems. As observed by Sjöberg (1978) and proven by him theoretically, the system of equations arising from the Dirac formulation is inherently more stable than that arising from the least squares collocation approach, for a given radius of the internal sphere. This difference in stability is reflected in Table 8 as differences in required number of iterations. Also, the l.s.c. solution is

Table 8. "Number of Iterations/RMS Error (mgal)" Under Various Discrete Approaches, When Predicting 50 Withheld Gravity Anomalies from 87 Known Gravity Anomalies in Manitoba, Canada.

Depth to Internal Sphere(km)	l.s.c. (Δg^*)	Dirac (Δg^*)	Dirac (μ^*)	Dirac ($\bar{\mu}^*$)
0	1/13.5	1/13.5	1/13.5	1/13.5
5	2/11.9	1/13.2	1/13.2	1/13.6
10	4/10.4	2/12.0	2/12.1	2/13.6
15†	5/10.2†	2/11.0	2/11.0	2/13.1
20	11/10.4	3/10.4	3/10.4	2/12.5
25	25/10.6	3/10.2	3/10.2	2/11.9
30†	30/10.9	4/10.2†	4/10.2†	2/11.4
35	30/11.1	5/10.2	5/10.2	3/10.9
40	30/11.3	7/10.3	7/10.3	3/10.6
45	30/11.5	9/10.5	9/10.5	4/10.5
50†	30/11.7	12/10.6	12/10.6	5/10.5†
55	30/11.8	16/10.7	16/10.7	6/10.5
60				8/10.6
65				10/10.7
70				14/10.8
75				18/10.9
80				24/11.0
85				30/11.2
90				30/11.3

† optimal results. Iterations were terminated when RMS Residual < 0.25 mgal, or Maximum Residual < 0.5 mgal, or No. of Iterations > 30.

much more sensitive than the Dirac solution, to changes in the radius of the internal sphere. This is evidenced by the narrow range of useful depths (e.g., 10 km to 25 km) that can be used for the l.s.c. method, as compared with the broad range of useful depths for the Dirac systems (20 km to 55 km for the Dirac (Δg^*) and Dirac (μ^*); 30 km to 65 km for the Dirac ($\bar{\mu}^*$)).

5.4.3 Comparison of Discrete and Continuous Models in the New Mexico Test Area

In this section we compare the various models discussed earlier, in terms of their ability to model the high frequency portion of the radial,

North-South, and East-West components of the disturbance vector in space. The problem is again the computation of the external field from gravity anomaly data on the earth's (non-spherical) topography. We concentrate on the high frequency part of the total field, because this is the part affected most by the topography problem. We will intercompare the discrete solutions (solutions to the Bjerhammar problem) discussed in this chapter, as well as the classical integral solution used in Chapter 4. Computation points will be along the five vertical test lines in a $1^\circ \times 1^\circ$ area in New Mexico, already described in Chapter 4 (Figure 25). Altitudes of computation will again be at 5, 10, 30, 100, and 500 km, giving 25 test points in all (5 points per line, times 5 test lines).

To serve as the "true" field we took the residual topographic model (RTM), generated from the gravitational influence of the positive and negative topographic masses lying between the actual topography and a reference topography to spherical harmonic degree 180. Specifically, we used the field generated in Test 7 of Chapter 4. The field was generated from topographic data in a $2^\circ \times 2^\circ$ area centered at the computation foot points. The integration of gravitational influences was performed using Forsberg's (1984) prism integration program along with $30'' \times 30''$ point elevations, $5' \times 5'$ mean elevations, reference topographic elevations to degree 180, and an assumed density of 2.67 g/cm^3 . Values were generated for $5' \times 5'$ surface gravity anomalies in the $2^\circ \times 2^\circ$ area and for the disturbance components at the 25 test points in space. These values were then considered as the self-consistent or "true" set of values for testing different techniques for modeling the spatial disturbance vector field from surface gravity anomaly data. The three disturbance components at each of the 25 test points in space are shown in Table 9. The overall RMS of the values in Table 9 is 12.36 mgals.

As a first step we performed computations analogous to Table 8 to determine for each base function system an optimal internal sphere radius to use with the given surface gravity anomaly data. This time, optimal radii were determined not by minimizing the RMS anomaly prediction error at withheld surface points, but by minimizing the RMS difference between computed and "true" (Table 9) disturbance components in space. The results are shown in Table 10, giving the number of iterations performed (see (5.59)) and the RMS disturbance error (computed - "true" value) for various depths to the Bjerhammar sphere and various base function systems. To repeat, for visualization one can use the interpretations that: the Dirac (Δg^*) solves for gravity anomaly impulses on the internal sphere; the Dirac ($\bar{\mu}^*$) solves for point dipoles on the internal sphere; the l.s.c. (Δg^*) uses the attenuated white noise gravity anomaly covariance function; and the l.s.c. (T^*) system uses the attenuated white noise potential covariance function. The number of iterations allowed was reduced from the 30 used in Table 8 to just 10, as the results did not significantly improve with more iterations. The point mass system Dirac (μ^*) was confirmed to yield practically identical results as the Dirac (Δg^*) system, and is now omitted from our numerical presentations. Based on the results of

Table 9. Disturbance Components (mgals) Along the Vertical Test Lines A, B, C, D, E, Generated by Prism Integration of the Gravitational Influence of Residual Topographic Masses in the 2°x2° New Mexico Test Area.

H =	δr					$\delta \lambda$				
	A	B	C	D	E	A	B	C	D	E
500 km	-0.11	0.11	0.11	0.11	-0.11	0.01	0.00	0.00	0.00	0.02
100 km	0.65	0.34	0.17	0.17	1.18	0.31	0.34	0.74	0.36	0.74
30 km	18.09	1.39	5.82	10.19	-5.19	-0.64	1.39	2.64	1.52	-1.27
10 km	39.85	-0.76	13.58	28.15	5.65	-2.81	-0.76	2.98	-0.04	-14.09
5 km	47.32	-2.65	19.29	37.69	-1.90	-3.89	-2.65	4.49	-3.50	-22.00
		0.11	0.01	0.02	-0.11		0.01	0.02	0.10	0.02
	-1.42	1.12	-0.17	0.90	1.18		1.12	0.90	-0.03	0.22
	8.00	9.56	5.82	2.64	-5.19		9.56	2.64	3.45	-1.97
	-22.25	18.02	13.58	2.98	5.65		18.02	2.98	15.26	-5.11
	-30.23	19.41	19.29	4.49	-1.90		19.41	4.49	24.59	-9.11

Table 10 we selected the optimal depth of 10 km for the Dirac (Δg^*), 15 km for the Dirac ($\bar{\mu}^*$), 3.5 km for the l.s.c. (Δg^*), and 15 km for the l.s.c. (T^*). Note that for the Dirac (Δg^*) the result for depth 20 km is even slightly better than that for depth 10 km, but a shallower depth is preferable because in principle the system will be more stable. The results corresponding to these optimal depths were then used in any further comparisons of the different methods. Note from Table 10 that the Dirac systems have faster convergence (fewer number of iterations) than the least squares collocation systems. Also, it is indicated that the Dirac systems have better agreement with the residual topographic model (RTM) than do the l.s.c. systems.

Table 10. "Number of Iterations/RMS Error (mgals)" Under Various Discrete Approaches, When Modeling the Disturbance Components of the Residual Topographic Field, from 5'x5' Surface Gravity Anomalies in the 2°x2° New Mexico Test Area.

Depth to Internal Sphere (km)	Dirac (Δg^*)	Dirac ($\bar{\mu}^*$)	l.s.c. (Δg^*)	l.s.c. (T^*)
1	3/6.01	2/11.88	10/2.39	10/12.17
3.5	5/1.79	3/8.50	10/1.55+	10/6.28
5	7/1.23	3/5.21	10/1.96	10/4.12
10	10/1.14+	5/1.08	10/2.57	10/2.26
15	10/1.23	10/1.05+	10/3.17	10/1.82+
20	10/0.98	10/1.11	10/2.96	10/2.67

+ optimal results. Iterations were terminated when RMS Residual < 0.25 mgal, or Maximum Residual < 0.5 mgal, or No. of Iterations > 10.

Next, we now attempt to provide a specific feeling for the numerical differences among the various discrete models, and the classical integral model used in Chapter 4. As presented in Chapter 4, the integral model can account for the mean topography through the quantity h_m in the formulas, where h_m is a mean topographic elevation in the area of computation. Obviously, the neglect of topographic variations around the mean is a modeling error being committed in this approach. Our present comparisons will give a feeling for the magnitude of this error (in fact, this error was also examined in Chapter 4). The interest in using the integral model lies in its relative economy, not requiring any solution of a linear equation system in contrast to the discrete models.

We compared the various models by pairs, resulting in a total of nine pairings. In every pairing, each of the two models involved had its own set of 75 disturbance values analogous to Table 9. We differenced the two tables of disturbances involved in each pairing, producing nine tables containing 75 disturbance differences each. Based on looking at the nine tables of differences we decided that for the analysis and presentation of results it would be sufficient to represent each table by:

- the RMS value of the 75 differences contained in the table; and
- the test line or lines (out of A, B, C, D, E; see Chapter 4) which show maximal differences for the δ_r , δ_ϕ , δ_λ disturbance components.

The results for the nine pairings are shown in Table 11.

For the integral model involved in pairings (1) and (9), a mean topographic elevation of $h_m=1.5$ km was used as in Chapter 4. When the value of $h_m=0$ km was tested, thereby assuming the given gravity anomalies to refer to the geoid, the RMS difference with the RTM (pairing (1)) increased significantly from 1.75 mgal to 2.26 mgal, and the RMS difference with the Dirac (Δg^*) (pairing (9)) increased from 0.98 mgal to 1.65 mgal. Therefore, we specifically conclude that there is a significant gain in accuracy when the mean topography is accounted for through h_m in the classical integral formulas.

Pairings (1) - (5) show the comparison of the integral model plus the four "discrete approach" models against the residual topographic model (RTM). Again, we assume the RTM to be the "true" field and call the differences shown as "errors".

Comparing (1) with either (2) or (3), one can see a significant although not drastic increase in accuracy with the use of the Dirac model over the integral model. Improvement is especially evident at altitudes 10 km and 30 km. Above 30 km the choice of model is not critical, as high frequency effects are greatly attenuated at such altitudes. The residual errors of the Dirac models especially at low altitudes can be attributed to the use of $5' \times 5'$ gravity anomalies and elevations, which automatically limits the resolution of field representation. The RTM inherently has more detailed resolution, with its use of up to 1 km x 1 km topographic height data (which directly converts to 1 km x 1 km resolution of gravity data because of correlation between elevation and gravity anomalies). Therefore, we conclude a significant gain in accuracy with the use of a Dirac model over the integral model. But at the same time, the Dirac model (or any of the other collocation models) cannot represent the very high resolution attainable with the RTM at very low altitudes. The RTM should always be used as one of the complementary models at low altitudes, whenever

detailed height information is available.

Examining pairings (4) and (5), no evidence can be found of any improvement with the use of the least squares collocation (l.s.c.) models over the Dirac or the integral models. The problem encountered during computations with the l.s.c. systems was the instability of linear equation systems. The use of more widely spaced gravity anomaly data (say, $10' \times 10'$) would have made the systems more stable, but this would also have automatically reduced the achievable resolution of the field. We conclude that for very detailed field representations, the stability of the arising linear equation system plays a significant role in the discrete approaches, and in such cases the Dirac systems are preferable to the least squares collocation systems.

Examining pairing (6), one can see that with the use of their respective optimal radii to the internal sphere, the Dirac systems agree with each other in the submilligal level even at the low altitude of 5 km. Therefore, from this test we do not see any preference to the point gravity anomaly, or the point mass, or the point dipole systems with respect to each other.

On the other hand, pairing (7) shows that the l.s.c. system is much more sensitive to the choice of either the T^* - or the Δg^* -system (This is equivalent to the choice of norm to be minimized; see remarks after (5.74)). Also, the great sensitivity of the l.s.c. systems to the depth of the Bjerhammar sphere (See Tables 10 and 8) contributes to the differences found in pairing (7). Also, the results for the l.s.c. systems refer to linear equation solutions that have not satisfactorily converged (see (5.64) for convergence criteria) in the course of the iterations. Therefore, convergence problems also play a role in the differences found in pairing (7). We should note that direct matrix inversions were not tried in these types of tests, but they should have been.

Pairing (8) compares the Dirac (Δg^*) with the l.s.c. (Δg^*). Again, the significant differences can be attributed to the stability problems mentioned above for the l.s.c. system.

Finally, pairing (9) shows how the integral model performs in comparison with the Dirac model. As one can see, the differences between the two models are not very large, although they are significant. The differences indicate how much additional information about the disturbance field is gained by accounting for the full variations of the topography (as in the Dirac system), not just the mean topography (as in the integral system). Above 30 km the integral model is sufficient, but at very low altitudes the Dirac system should be used for accurate determinations.

Table 11. RMS and Maximal Differences Between Various Models of Disturbance Vector Components (mgals).

RMS Difference	Test Lines with Maximal Differences					
	LINE	5 km	10 km	30 km	100 km	500 km
(1) 1.75 [Integral - RTM]	C δ_r	-3.13	-1.30	-0.67	-0.28	-0.02
	B δ_φ	-3.52	-2.65	-1.28	-0.13	0.00
	A δ_λ	8.48	5.14	2.10	0.44	0.00
(2) 1.14 [Dirac (Δg^*) - RTM]	A δ_r	2.36	0.97	0.24	-0.07	-0.04
	A δ_φ	-2.43	-0.75	-0.16	-0.06	0.00
	A δ_λ	6.41	2.84	0.88	0.30	0.01
(3) 1.05 [Dirac ($\bar{\mu}^*$) - RTM]	A δ_r	3.12	1.53	0.71	0.52	0.09
	A δ_φ	-2.07	-0.59	-0.26	-0.13	-0.01
	A δ_λ	5.37	1.89	0.16	-0.09	-0.01
(4) 1.55 [l.s.c. (Δg^*) - RTM]	C δ_r	-3.23	-1.09	-0.20	0.08	-0.01
	C δ_φ	-4.56	-3.41	-1.11	-0.07	0.00
	D δ_λ	4.28	2.38	0.83	0.17	0.01
(5) 1.82 [l.s.c. (T*) - RTM]	C δ_r	-3.28	-1.01	-0.33	0.40	0.10
	C δ_φ	-3.32	-2.23	-0.62	-0.02	0.00
	D δ_λ	8.24	4.64	1.33	-0.02	-0.02
(6) 0.49 [Dirac (Δg^*) - Dirac ($\bar{\mu}^*$)]	A δ_r	-0.76	-0.56	-0.46	-0.59	-0.13
	A δ_φ	-0.36	-0.16	0.09	0.07	0.01
	A δ_λ	1.04	0.95	0.71	0.39	0.02
(7) 1.38 [l.s.c. (Δg^*) - l.s.c. (T*)]	D δ_r	-4.07	-3.38	-1.79	-0.46	-0.11
	A δ_φ	3.10	2.67	0.56	0.05	0.01
	D δ_λ	-3.96	-2.26	-0.50	0.19	0.03
(8) 1.30 [Dirac (Δg^*) - l.s.c. (Δg^*)]	A δ_r	4.44	3.02	1.22	-0.09	-0.03
	C δ_φ	4.92	3.43	0.98	0.00	0.00
	D δ_λ	-3.24	-1.31	-0.28	0.02	0.01
(9) 0.98 [Integral - Dirac (Δg^*)]	A δ_r	-1.85	-1.48	-1.27	-0.26	0.01
	B δ_φ	-2.20	-1.61	-0.72	-0.02	0.00
	B δ_λ	2.77	2.23	0.42	0.09	0.00

6. SUMMARY, CONCLUSIONS, RECOMMENDATIONS

In this report we have discussed the modeling of the external gravity disturbance vector of the earth, from surface gravity anomaly data. This work is a continuation of the work of Katsambalos (1981) with important differences and expansion of treatment as noted in Section 1.1. In principle the disturbance vector is modeled as $\vec{g} = \text{grad } T$, with the disturbing potential T being in turn related to the gravity anomaly Δg through (1.9) or its spherical approximation (1.12). Under the assumption that T is harmonic outside the earth's attracting masses, the knowledge for Δg at every point on the earth's surface is sufficient to define T in all of space. More details on preliminary concepts are given in Section 1.2, discussing the precise definition of Δg , the relation between Δg and T at a point, and the realization of Δg from observational data on the earth's surface. In Section 1.3 a discussion is given outlining the scope of the entire study.

Chapter 2 discusses the re-parameterization of the long-wavelength components of the anomalous gravity field, from the given surface gravity anomalies to a set of spherical harmonic coefficients of the earth's disturbing potential. The focus is on the analytical continuation of the surface gravity anomaly data to values that refer to a spherical boundary surface. The Δg -values on a sphere are the values directly useable in the determination of spherical harmonic coefficients. It is recommended that the analytical continuation be carried out in two steps: (a) analytical continuation of surface values to the ellipsoid; followed by (b) analytical continuation of values from the ellipsoid to a sphere, most appropriately the equatorial sphere.

Step (a) above can be implemented by Taylor series expansion using the vertical gradients of the field. Operationally, such gradients can be obtained from an existing spherical harmonic expansion, in application of the ideas of Rapp (1984). Step (b) can also be implemented by Taylor series, but because the deviation between ellipsoid and sphere is a simple function of latitude it is possible in this case to analytically expand the terms of the Taylor series into spherical harmonics. Specifically, Taylor terms involving up to second order gradients have been expanded in Chapter 2. Our main contribution via Chapter 2 is in showing that such spherical harmonic expansions of Taylor series terms lead to the ellipsoidal correction terms of Pellinen (1982). As a result, it is shown that the application of Pellinen's ellipsoidal corrections is an analytical implementation of step (b) above. This is in contrast to the numerical implementation of step (a). It is also shown that the use of the ellipsoidal corrections as given in Pellinen (ibid.) implies the use of a relation between Δg and T that neglects only terms of $O(e^4)$, i.e., the relation (1.13).

Tables 1 and 2 of Chapter 2 indicate the number of Taylor series terms that need to be considered in the analytical continuation of values from ellipsoid to sphere. The higher the maximum degree N_{\max} of spherical harmonic series development the more Taylor terms need to be used. For example, with $N_{\max} = 300$ it is indicated that terms up to the second-order gradient need to be considered, leaving (gravity anomaly, height anomaly) errors of about (0.8 mgal, 2 cm) in the polar areas. The corresponding effects of the analytical continuation of surface values to values on the ellipsoid are an order of magnitude smaller, because of the shorter vertical distances involved in the analytical continuation.

For the complete modeling of the disturbance vector signal in its entire frequency range, locally valid models must be used to complement the globally valid spherical harmonic model. Before studying such local models in Chapters 4 and 5, however, Chapter 3 first gives a familiarization study of the signal characteristics to aid the design of models and numerical experiments. Information is presented on the spectral energy distribution (Section 3.2) and data response characteristics (Section 3.3) of the disturbance vector signal as a function of altitude in space. For example, according to Figures 4 and 5 a representation to $n = 360$ ($0.5^\circ \times 0.5^\circ$ resolution) will resolve at least 90% of the RMS signal value for altitudes above 30 km; for an altitude of (5, 10, 20) km such representation to $n = 360$ leaves about (16, 10, 5) mgals unresolved.

At the low altitude of 5 km, for example, a representation to $n = 2500$ ($5' \times 5'$ resolution) is needed to resolve 99% of the RMS radial or horizontal disturbance signal. On a point by point computation of signal from gravity anomaly data, however, it is not necessary to have data of such uniform resolution all over the earth. Rather, data of less and less resolution (and accuracy) can be used farther and farther away from the computation point. Such data response characteristics of the signal are studied in Section 3.3 using the tools of truncation theory. Under the formulation of truncation theory we obtain the so-called truncation error, i.e., the amount of error propagated into the computed signal due to the use of a particular set of data in the "remote zone". There are four factors affecting the truncation error: the data accuracy, the data resolution, the truncation method used (i.e., the kernel modification used), and the distance of the data from the computation point (i.e., the cap size). The influences of these factors are shown in Figures 7 to 14, for the radial and horizontal disturbance components at a high altitude of 100 km and a low altitude of 5 km.

As an example of the use of Figures 7 to 14, consider first Figure 7 showing the case of radial disturbance computations at altitude 100 km. For the assumed data error model (see (3.64)), the data resolution to $N_{ref} = 20$ ($\approx 9^\circ \times 9^\circ$ resolution), the unmodified truncation method, and the cap size $\psi_0 = 13^\circ$, we find from Figure 7 that the propagated error to the signal is about 0.2 mgal. If we change to the use of errorless data (circled plot in Figure 7) the required cap size to maintain a 0.2

mgal error reduces from $\psi_0 = 13^\circ$ to $\psi_0 = 9^\circ$. If, moreover, we increase the data resolution to $N_{ref} = 36$ ($\approx 5^\circ \times 5^\circ$ resolution), then the required cap size for a 0.2 mgal error reduces further from $\psi_0 = 9^\circ$ to $\psi_0 = 5^\circ$. Now looking at Figure 8, we see that the originally required cap size of $\psi_0 = 13^\circ$ can also be drastically reduced (to $\psi_0 = 6^\circ$) if we change from the use of the unmodified truncation to the use of the improved Molodensky truncation.

General conclusions can be stated based on Figures 7 to 14 as follows. The horizontal disturbance is much more sensitive to remote zone data than the radial disturbance, as evidenced by the larger data caps (more than 2 times larger than the radial case) needed to keep truncation error below, e.g., a 0.2 mgal level. The improved Molodensky truncation method gives better results than the unmodified truncation for relatively large cap sizes only; anticipating the use of remote zone data to resolution $n_{ref} \geq 180$, then we can say that for cap sizes and accuracy levels of interest the improved Molodensky method offers no significant gain over the unmodified method for radial or horizontal disturbance computations in space.

Chapter 4 starts the study of local models that can be used to complement the globally valid spherical harmonic model studied in Chapter 2. In the global discussions of Chapter 2, the problem of the shape of the boundary surface lies in the deviations of the earth's surface from the equatorial sphere; these deviations can amount to 20 km at the poles. In contrast, for the local models such as those of Chapter 4, the problem with the shape of the boundary surface consists only in the deviations of the earth's surface from an equipotential surface. The equipotential surface is then considered as a sphere, after a formal neglect of the earth's flattening under the spherical approximation (see Figure 2). Therefore, whereas in the spherical harmonic model both the topography and ellipticity are important issues in the modeling, in the case of the local models of Chapters 4 and 5 only the topography needs to be of special concern.

In Section 4.1 a degree variance analysis is first performed to quantify the role of the topography in the modeling problem. The observed degree variances of the earth's anomalous gravity field are expressed as the combined effect of the gravitational influence of condensed topographic masses and their Airy-Heiskanen isostatic compensation at depth D . It is then numerically shown the considerable smoothing of the field that results from the removal of shallow topographic masses associated with topographic heights beyond harmonic degree N (see Figures 15 and 16 for $N = 180$). The smoothing of the field reduces the errors associated with the assumption that the topography is a level surface (see Table 4 and Figure 17 for a numerical example). The considerations of Section 4.1 lead to a feasible hybrid model: the spherical harmonic model accounts for remote zone effects; the residual topographic model accounts for high frequency variations of the field; and the classical integral model accounts for whatever is the residual field not already modeled by the first two models. The

smoothness of the residual field allows the minimization of the errors associated with assumption of the classical integral model, namely that the earth's surface is a level surface.

Section 4.2 summarizes the equations and operational programs associated with the above three complementary models. Then, numerical tests are conducted in Section 4.3, over a mountainous test area in New Mexico. Radial and horizontal disturbance values are computed along five vertical test lines, at altitudes 5, 10, 30, 100, and 500 km. The tests are designed to (a) confirm earlier discussions and conclusions (see Tests 1, 2, 4, 7, 8); (b) establish operational details of implementation (see Tests 3, 5, 6); and (c) assess the quality of the results (see Test 9). An auxiliary test to Test 9 is conducted (Section 4.3.4), concluding a significant improvement caused by accounting for the mean topography in the classical integral models (see Table 6).

Test 9 shows errors (maximal value = 8 mgals) that can be encountered if the classical integral model is used to represent the residual topographic field. Part of the errors is caused by the neglect of the variations of the topography with respect to the mean topography. However, as to be indicated in the tests of Chapter 5, most of the errors can be attributed to the inherently less resolution of the data used in the integral model (i.e., $5' \times 5'$ anomalies) as compared with the data used to generate the residual topographic model (i.e., $30'' \times 30''$ topographic heights).

To eliminate the theoretical modeling error caused by the neglect of topographic variations around the mean elevation, we can resort to the use of the so-called discrete approaches. These approaches arise from solving the Bjerhammar problem. Two major discrete approaches are studied in Chapter 5, namely, the Dirac approach and the least squares collocation approach. Three versions of the Dirac approach are experimented on, those based on solving on the internal sphere the (a) gravity anomaly impulses Δg^* ; (b) point masses μ^* ; and (c) point dipoles $\bar{\mu}^*$. For the least squares collocation (l.s.c.) approach two versions are experimented on, those based on generating the empirical covariance function from (a) white noise gravity anomaly Δg^* ; and (b) white noise disturbing potential T^* . All these discrete approaches rigorously take as input data a finite number of gravity anomalies given on the earth's surface. The techniques then produce artificial continuity from the finite data by postulating the form of the harmonic approximating function to T (see (5.17) for the Dirac case, and (5.65) for the l.s.c. case) and fitting this form to the given data.

The Dirac (Δg^*) and Dirac (μ^*) produced practically the same results in the numerical tests, because their base functions behave similarly in the limit as $n \rightarrow \infty$. Such high degree harmonics are the ones important for local modeling problems. The Dirac ($\bar{\mu}^*$) required a deeper Bjerhammar sphere compared with the Dirac (Δg^* or μ^*) because of the faster decay of the base function in the Dirac (Δg^* or μ^*) (see (5.26), (5.33), (5.37)). Exactly the same situation exists for the l.s.c. systems.

The l.s.c. (T^*) system, which as noted under (5.92) behaves similarly as a l.s.c. ($\bar{\mu}^*$) system, required twice as deep Bjerhammar sphere as the l.s.c. (Δg^*) system (see (5.91), (5.92), Figure 26) in order to generate the same correlation lengths on the earth's surface.

Comparing the Dirac and l.s.c. systems, we numerically found the former to result in more stable linear equation systems (see also Sjöberg, 1978). For the relatively large 0.5×0.5 spacing of surface data used in our tests in Canada, no matrix stability problems were encountered and all the Dirac and l.s.c. systems tested produced the same quality of results at their optimal depths to the Bjerhammar sphere. For the dense $5' \times 5'$ data used in our New Mexico tests, however, the Dirac results were superior to those of the l.s.c. because of the ill-conditioned matrices in the latter system.

Considering the rest of the tests in Section 5.4.3 and summing up the report: we recommend the hybrid model of Chapter 4 for operational modeling of the spatial disturbance vector, with possible replacement of the classical integral model by a collocation procedure for accurate determinations over mountainous areas. The residual topographic model should always be used whenever a detailed DTM is available, since both the integral and collocation models are necessarily limited in resolution through the use of gravity anomaly data with practical spacing that can only be expected to be around $5' \times 5'$. The limitation of resolution can be a more significant concern than the non-rigorous accounting of the topography in the integral model (see pairings (1), (2), and (9) of Table 11). The integral model with mean topography accounted for is in reasonably good agreement with a collocation procedure (the Dirac model, see pairing (9) of Table 11). Matrix conditioning problems with the l.s.c. approach support preference to the Dirac systems for rigorous treatment of the topography at detailed ($5' \times 5'$) resolutions.

A collected summary of the suggested computational procedures discussed in this report, with references to pertinent equations found in the body of the report, is given as an Appendix.

APPENDIX

Summary of Suggested Computational Procedures for the Computation of the Gravity Disturbance Components in Space from Surface Gravity Anomaly Data.

A. The Spherical Harmonic Model (SHM)

1. To compute spherical harmonic potential coefficients \bar{C}_{nm}^* from surface gravity anomalies Δg , apply these steps:
 - (a) reduce Δg to gravity anomalies Δg_E on the ellipsoid, using (2.3);
 - (b) compute conventional potential coefficients C_{nm} from Δg_E employing ellipsoidal corrections, using (2.9) and (2.54)-(2.56), with the R_{nm} 's denoting the quantity in braces in (2.32) and the S_{nm} 's being given by (2.51). This solution implies the use of up to second radial derivative of the Δg -field to analytically continue Δg_E to gravity anomalies Δg_s on the equatorial sphere, and should be sufficient for n up to the envisioned $n = 360$;
 - (c) fully normalize the C_{nm} using (2.19) to finally obtain \bar{C}_{nm}^* .
2. See Figures 4 and 5 to know approximately how much information is left unresolved by the available degree N_{ref} of SHM at the altitude H of interest. For example, given $N_{ref} = 180$ and $H = 30$ km we find a 6-mgal RMS signal left to be resolved by local models. Since the total RMS signal at $H = 30$ km is seen to be 26 mgals, we then have $6/26 = 23\%$ of the signal energy left unresolved using $N_{ref} = 180$.
3. Decide on how large cap of local gravity anomaly data should be used to complement the SHM. This can be judged from the magnitude of truncation error that can be tolerated. The truncation error in this case consists of the commission and omission errors due to the use of the SHM to represent the remote zone. The truncation error is expressed by (3.52) for the radial disturbance and (3.62) for the total horizontal disturbance. Anticipating the use of a high degree SHM ($N_{ref} \approx 180$) then we have shown that it will be sufficient to use unmodified truncation coefficients for the values k_n^* and v_n^* needed in (3.52) and (3.62). These unmodified coefficients can be computed using the subroutines of Shepperd (1979). A general idea of reasonable cap sizes for given altitudes and accuracies may be obtained from the discussions and figures of Chapter 3 or from earlier experience, e.g., in Rapp (1966b) and Sunkel (1981a).

4. To generate a dense regular grid of surface gravity anomalies Δg^s implied by the SHM, use (4.12)-(4.14) and the fast program by Rizos (1979). The Δg^s are to be subtracted from the originally given surface gravity anomaly data which should also have been established on a regular grid using procedures described in Cruz and Laskowski (1984, sec. 8).
5. To generate the spatial disturbance components implied by the SHM, use (4.15)-(4.17). Point by point evaluations can be done using the program by Rapp (1982b). Evaluations on a regular grid in a limited area can be done efficiently, using a program that we modified from Rizos (1979) to compute all three disturbance components in a single run.

B. The Residual Topographic Model (RTM)

1. To generate rigorous values of surface gravity anomalies Δg^t implied by the RTM, use the program of Forsberg (1984). To limit the expense in computer time, an option exists to use the approximate Δg^t given by (4.28) or even (4.29) in an outer zone, e.g., outside a 1° -radius from the spatial points at which the disturbances are to be computed. Tests directly related to the use of an approximate Δg^t are given as Tests 5 and 6 in Chapter 4. The Δg^t , like the Δg^s of the SHM, are to be subtracted from the surface gravity anomalies to form residual gravity anomalies that continue to refer to the earth's surface (see (4.18)).
2. To generate the spatial disturbance components implied by the RTM, again use the program of Forsberg (ibid.). Introduce the transformation (4.30) into Forsberg's program to compute the North-South and East-West disturbance components instead of the deflections of the vertical.

C. The Integral Model

1. The residual gravity anomaly Δg^0 of (4.18) can be input into the integral model to complete the modeling of the disturbance vector in its entire frequency range. The Δg^0 are assumed to refer to an equipotential surface, one passing through the mean topographic elevation h_m in the local area of computations. The h_m is specifically used in (4.25).
2. The actual generation of the spatial disturbance components is performed in the integral model using (4.19)-(4.21). A program modified from Rapp (1966b) can be used for this purpose. Our modified program accepts $5' \times 5'$ mean anomalies, and the so-called integrated kernel evaluation was implemented for those $5' \times 5'$ blocks whose centers were within a distance of $10'$ from a computation point. The last procedure was implemented to avoid large kernel

discretization errors associated with the use of the center point kernel evaluation at low altitudes.

3. The disturbance components computed from the integral model can be added to those from the spherical harmonic and residual topographic models, to form the final disturbance values in space (see Table 7).

Note: If the RTM had not been used as one of the complementary models, then the part of the field that would have been represented by the RTM would in this case be included in the field represented by the integral model. Errors would be introduced in this way, the magnitudes of which were studied over mountainous area in Test 9 of Chapter 4 (see also row V of Table 7 and pairing (1) of Table 11). It has been concluded that a large part of the observed errors is due to the unavoidable loss of resolution caused by the use of 5'x5' anomalies in the integral model as opposed to the use of 30"x30" height information in the RTM. A smaller (but still significant) part of the error is caused by the non-rigorous treatment of the topography in the integral model, and this error source could in theory be avoided through the use of collocation techniques in space (for a numerical study of this point compare, e.g., pairings (1) and (2) of Table 11).

D. The Collocation Model

1. Motivation for Use. For high accuracies in mountainous areas it is recommended to employ collocation techniques to rigorously account for the shape of the topography. For economy and improved convergence of the solution it would again be advisable to use the RTM to remove most of the roughness of the original field, leaving a relatively smooth residual field. The data would then be surface residual anomalies Δg^c , which can in fact be the Δg^D of (4.18).
2. Summary of our Results. We have seen no preference of one over the other, among the use of gravity anomaly impulses, point masses, and point dipoles under the Dirac approach to collocation. We have concluded a preference of the Dirac over the least squares collocation systems, for reason of stability of linear equation system at such high resolution as 5'x5'. The base functions and covariance functions needed for disturbance computations under the studied collocation systems are given in Chapter 5.
3. Operational Procedures. Either use collocation to replace the integral model entirely, or, for reasons of computer economy, one may choose to simply complement the integral model by collocation in an inner zone close to the computation points. For the latter option, numerical implementation may be patterned after Lachapelle (1977) but using the base function or covariance function desired.

Note that in our studies we were specifically concerned with the verification and comparison of various collocation solutions, not with the development of fully operational procedures for implementing such solutions. Therefore, we worked under controlled conditions: regularly gridded data and a high frequency field with negligible remote zone effects outside the small $2^\circ \times 2^\circ$ test area (see Chapter 5). In operational cases we would like to efficiently apply collocation using data in larger areas (see, e.g., Blaha (1983)), and/or be able to establish and use variable data density depending on the roughness of particular sections of the computation area (see, e.g., Sunkel (1983a)). Other important issues are the operational establishment of optimal depth to the Bjerhammar sphere, and the formation and numerical solution of the relevant linear equation systems. For developing operational collocation procedures we refer the reader to recent works, of which we mention Blaha (1983), Brennecke and Leigemann (1984), Sunkel (1983a, 1983b), Tscherning and Forsberg (1983).

LIST OF REFERENCES

- Bjerhammar, A., "A New Theory of Geodetic Gravity," Division of Geodesy, The Royal Institute of Technology, Stockholm, No. 243, 1964.
- Bjerhammar, A., "Reflexive Prediction," Sixth Symposium on Mathematical Geodesy (3rd Hotine Symposium), Siena, Italy, April 1975.
- Bjerhammar, A., "A Review of Discrete Methods in Physical Geodesy," in Approximation Methods in Physical Geodesy, H. Moritz and H. Sunkel (eds.), Herbert Wichmann Verlag, Karlsruhe, 1978.
- Bjerhammar, A. and L. Svenson, "On the Geodetic Boundary Value Problem for a Fixed Boundary Surface - A Satellite Approach," Bulletin Geodesique, vol. 57, No. 4, pp. 382-393, 1983.
- Blaha, G., "Point-Mass Modeling of the Gravity Field with Emphasis on the Oceanic Geoid," AFGL Technical Report No. 83-0007, Air Force Geophysics Laboratory, Hanscom AFB, Massachusetts, February 1983, ADA130535.
- Brennecke, J. and D. Leigemann, "Geoid and Gravity Anomalies in the North Sea Area Derived from SEASAT Altimeter Data," Manuscripta Geodaetica, vol. 8, No. 4, pp. 301-320, March 1984.
- Brovar, V.V., "On the Solution of Molodensky's Boundary Value Problem," Bulletin Geodesique, vol. 72, pp. 167-173, 1964.
- Chen, J.Y., "Methods for Computing Deflections of the Vertical by Modifying Vening-Meinesz' Function," Bulletin Geodesique, vol. 56, No. 1, pp. 9-26, 1982.
- Colombo, O., "Convergence of the External Expansion of the Gravity Field Inside the Bounding Sphere," Manuscripta Geodaetica, Vol. 7, No. 3, pp. 209-246, October 1982.
- Cruz, J.Y. and P. Laskowski, "Upward Continuation of Surface Gravity Anomalies," Report No. 360, Dept. of Geodetic Science and Surveying, The Ohio State University, December 1984, AFGL-TR-84-0331, ADA154973.
- Forsberg, R. and C.C. Tscherning, "The Use of Height Data in Gravity Field Approximation by Collocation," J. Geophys. Res., Vol. 86, No. B9, pp. 7843-7854, September 1981.

- Forsberg, R., "A Study of Terrain Reductions, Density Anomalies, and Geophysical Inversion Methods in Gravity Field Modelling," Report No. 355, Dept. of Geodetic Science and Surveying, The Ohio State University, April 1984, AFGL-TR-84-0174, ADA150788.
- Gerstl, M. and R. Rummel, "Stability Investigations of Various Representations of the Gravity Field," Reviews of Geophysics and Space Physics, vol. 19, No. 3, pp. 415-420, 1981.
- Heiskanen, W.A. and H. Moritz, Physical Geodesy, W.H. Freeman and Co., San Francisco, 1967.
- IAG, "Geodetic Reference System 1967," Special Publication, Bulletin Geodesique, 1970.
- Heller, W.G. and S.K. Jordan, "Attenuated White Noise Statistical Gravity Model," J. Geophys. Res., Vol. 84, No. B9, pp. 4680-4688, August 1979.
- Jekeli, C., "Reducing the Error of Geoid Undulation Computations by Modifying Stokes' Function," Report No. 301, Dept. of Geodetic Science and Surveying, The Ohio State University, May 1980, NGR-36-008-161, N80-27872/4.
- Jekeli, C. and R.H. Rapp, "Accuracy of the Determination of Mean Anomalies and Mean Geoid Undulations from a Satellite Gravity Field Mapping Mission," Report No. 307, Dept. of Geodetic Science, The Ohio State University, August 1980, NGR-36-008-161, N81-12669/0.
- Jekeli, C., "The Downward Continuation to the Earth's Surface of Truncated Spherical and Ellipsoidal Harmonic Series of the Gravity and Height Anomalies," Report No. 323, Dept. of Geodetic Science and Surveying, The Ohio State University, December 1981, AFGL-TR-81-0361, AD-A112 237/3.
- Jekeli, C., "Optimizing Kernels of Truncated Integral Formulas in Physical Geodesy," presented at IAG, General Meeting, Tokyo, Japan, May 7-15, 1982.
- Katsambalos, K.E., "Simulation Studies on the Computation of the Gravity Vector in Space from Surface Data Considering the Topography of the Earth," Report No. 314, Dept. of Geodetic Science and Surveying, The Ohio State University, June 1981, AFGL-TR-81-0187, AD-A109 856/5.
- Krarup, T., "A Contribution to the Mathematical Foundation of Physical Geodesy," Meddelelse No. 44, Geodetisk Institut, Copenhagen, 1969.
- Krarup, T., Letters on Molodensky's Problem I-IV, Communication to the members of IAG Special Study Group 4.31, unpublished, 1973.

- Lachapelle, G., "Estimation of Disturbing Potential Components Using a Combined Integral Formulae and Collocation Approach," Manuscripta Geodaetica, vol. 2, No. 4, pp. 233-262, 1977.
- Lambeck, K., "Methods and Geophysical Applications of Satellite Geodesy," Rep. Prog. Phys., vol. 42, pp. 547-628, 1979.
- Lelgemann, D., "Untersuchungen zue einer genaueren Lösung des Problems von Stokes," Deutsche Geodätische Kommission, Series C, No. 155, 1970.
- Lelgemann, D., "Spherical Approximation and the Combination of Gravimetric and Satellite Data," Bolletino di Geodesia e Scienze Affini, vol. 32, No. 4, pp. 241-250, 1973.
- Lelgemann, D., "On Numerical Properties of Interpolation with Harmonic Kernel Functions," Manuscripta Geodaetica, vol. 6, No. 2, pp. 157-191, October 1981.
- Meissl, P., "A Study of Covariance Functions Related to the Earth's Disturbing Potential," Report No. 151, Dept of Geodetic Science, The Ohio State University, April 1971, AFCRL-71-0240, AD 728688.
- Meissl, P., "The Use of Finite Elements in Physical Geodesy," Report No. 313, Dept. of Geodetic Science and Surveying, The Ohio State University, April 1981, AFGL-TR-81-0114, AD-A104 164/9.
- Molodenskii, M.S., V.F. Eremeev and M.I. Yurkina, Methods for Study of the External Gravitational Field and Figure of the Earth, Translated from Russian, Israel Program for Scientific Translations, Jerusalem, 1962.
- Moritz, H., "On the Use of the Terrain Correction in Solving Molodensky's Problem," Report No. 108, Dept. of Geodetic Science, The Ohio State University, May 1968, AFCRL-68-0298, AD 676302.
- Moritz, H., "Least Squares Estimation in Physical Geodesy," Report No. 130, Dept. of Geodetic Science, The Ohio State University, March 1970a, AFCRL-70-0202, AD707508.
- Moritz, H., "Molodensky's Series and Analytical Continuation," Report No. 145, Dept. of Geodetic Science, The Ohio State University, September 1970b, AFCRL-70-0698, AD724133.
- Moritz, H., "Advanced Least Squares Methods," Report No. 175, Dept. of Geodetic Science, The Ohio State University, June 1972a, AFCRL-72-0363, AD749873.
- Moritz, H., "Convergence of Molodensky's Series," Report No. 183, Dept. of Geodetic Science, The Ohio State University, September 1972b, AFCRL-72-0663, AD754251.

- Moritz, H., "Integral Formulas and Collocation," Report No. 234, Dept. of Geodetic Science, The Ohio State University, December 1975, AFCRL-TR-75-0628, AD-A022 976/5GA.
- Moritz, H., "Introduction to Interpolation and Approximation," in Approximation Methods in Physical Geodesy, H. Moritz and H. Sunkel (eds.), Herbert Wichmann Verlag, Karlsruhe, 1978a.
- Moritz, H., "Least Squares Collocation," Reviews of Geophysics and Space Physics, vol. 16, No. 3, pp. 421-430, 1978b.
- Moritz, H., Advanced Physical Geodesy, Herbert Wichmann Verlag, Karlsruhe, 1980.
- Moritz, H., "Local Geoid Determination in Mountain Regions," Report No. 352, Dept. of Geodetic Science and Surveying, The Ohio State University, December 1983, AFGL-TR-0042, ADA145799.
- Needham, P.E., "The Formation and Evaluation of Detailed Geopotential Models Based on Point Masses," Report No. 149, Dept. of Geodetic Science, The Ohio State University, December 1970, AFCRL-70-0718, AD725060.
- Noe, H., "Numerical Investigations on the Problem of Molodensky," der geodatischen Institute der Technischen Universität, Graz, Folge 36, 1980.
- Paul, M.K., "Recurrence Relations for the Truncation Error Coefficients for the Extended Stokes Function," Bulletin Geodesique, vol. 57, No. 2, pp. 152-166, 1983.
- Pellinen, L.P., "Effects of the Earth Ellipticity on Solving Geodetic Boundary Value Problem," Bolletino di Geodesia e Scienze Affini, vol. 41, No. 1, pp. 89-103, 1982.
- Rapp, R.H., "A FORTRAN Program for the Computation of the Normal Gravity and Gravitational Field of the Earth," Report No. 52, Dept. of Geodetic Science, The Ohio State University, January 1966a, AFCRL-66-288, AD486264L.
- Rapp, R.H., "A FORTRAN Program for the Computation of the Disturbance Components of Gravity," Report No. 76, Dept. of Geodetic Science, The Ohio State University, August 1966b, AFCRL-66-670, AD805292L.
- Rapp, R.H., "Potential Coefficient and Anomaly Degree Variance Modeling Revisited," Report No. 293, Dept. of Geodetic Science, The Ohio State University, September 1979, AFGL-TR-79-0245, AD-A082 322/9.
- Rapp, R.H., "Geometric Geodesy," vol. 1 (class notes), Department of Geodetic Science and Surveying, The Ohio State University, 1980.

- Rapp, R.H., "Ellipsoidal Corrections for Geoid Undulation Computations," Report No. 308, Dept. of Geodetic Science and Surveying, The Ohio State University, March 1981a, NGR 36-008-161, N81-25603/4.
- Rapp, R.H., "The Earth's Gravity Field to Degree and Order 180 Using Seasat Altimeter Data, Terrestrial Data, and other Data," Report No. 322, Dept. of Geodetic Science and Surveying, The Ohio State University, December 1981b, AFGL-TR-82-0019, AD-A113 098/8.
- Rapp, R.H., "Degree Variances of the Earth's Potential, Topography and its Isostatic Compensation," Bulletin Geodesique, vol. 56, No. 2, pp. 84-94, 1982a.
- Rapp, R.H., "A FORTRAN Program for the Computation of Gravimetric Quantities from High Degree Spherical Harmonic Expansions," Report No. 334, Dept. of Geodetic Science, The Ohio State University, September 1982b, AFGL-TR-82-0272, ADA123406.
- Rapp, R.H., "The Determination of High Degree Potential Coefficient Expansions from the Combination of Satellite and Terrestrial Gravity Information," Report No. 361, Dept. of Geodetic Science and Surveying, The Ohio State University, December 1984, NGR-36-008-161.
- Rizos, C., "An Efficient Computer Technique for the Evaluation of Geopotential from Spherical Harmonic Models," Aust. J. Geodesy, Photogrammetry and Surveying, No. 31, pp. 161-169, December 1979.
- Rummel, R., "Downward Continuation of Gravity Information From Satellite Tracking or Satellite Gradiometry in Local Areas," Report No. 221, Dept. of Geodetic Science, The Ohio State University, April 1975, NGR-36-008-161, N75-28594.
- Sanso, F., "Recent Advances in the Theory of the Geodetic Boundary Value Problem," Reviews of Geophysics and Space Physics, vol. 19, No. 3, pp. 437-449, August 1981.
- Schwarz, K.-P. and G. Lachapelle, "Local Characteristics of the Gravity Anomaly Covariance function," Bulletin Geodesique, vol. 54, pp. 21-35, 1980.
- Shepperd, S.W., "Molodenskii-type Coefficients with Application to Gravity Disturbance Vector Truncation Errors at Altitude," Report No. R-139, The Charles Stark Draper Laboratory, Inc., Cambridge, MA, October 1979.
- Shepperd, S.W., "A Recursive Algorithm for Evaluating Molodenskii-Type Truncation Error Coefficients at Altitude," Bulletin Geodesique, vol. 56, No. 2, pp. 95-105, 1982.

- Sjoberg, L., "On the Discrete Boundary Value Problem of Physical Geodesy with Harmonic Reductions to an Internal Sphere," Division of Geodesy, The Royal Institute of Technology, Stockholm, 1975.
- Sjoberg, L., "A Comparison of Bjerhammar's Methods and Collocation in Physical Geodesy," Report No. 273, Dept. of Geodetic Science, The Ohio State University, July 1978, AFGL-TR-78-0203, AD-A063 194/5GA.
- Sjoberg, L., "Least Squares Combination of Satellite and Terrestrial Data in Physical Geodesy," presented at the International Symposium on Space Geodesy and its Applications, November 1980. Cannes. Ann. Geophys., vol. 37, No. 1, pp. 25-30, 1981.
- Sunkel, H., "Feasibility Studies for the Prediction of the Gravity Disturbance Vector in High Altitudes," Report No. 311, Dept. of Geodetic Science and Surveying, The Ohio State University, March 1981a, AFGL-TR-81-0084, AD-A102 943/8.
- Sunkel, H., "Point Mass Models and the Anomalous Gravitational Field of the Earth," Report No. 328, Dept. of Geodetic Science and Surveying, The Ohio State University, December 1981b, AFGL-TR-82-0084, AD-A115 216/4.
- Sunkel, H., "The Geoid in Austria," in Proceedings of the International Association of Geodesy (IAG) Symposia, Hamburg, FRG, pp. 348-364, August 1983a.
- Sunkel, H., "The Generation of a Mass Point Model from Surface Gravity Data," Report No. 353, Dept. of Geodetic Science and Surveying, The Ohio State University, December 1983b, AFGL-TR-83-0318, ADA142327.
- Tscherning, C.C., "Representation of Covariance Functions Related to the Anomalous Potential of the Earth Using Reproducing Kernels," Internal Report No. 3, Danish Geodetic Institute, Copenhagen, 1972.
- Tscherning, C.C. and R.H. Rapp, "Closed Covariance Expressions for Gravity Anomalies, Geoid Undulations, and Deflections of the Vertical Implied by Anomaly Degree Variance Models," Report No. 208, Dept. of Geodetic Science, The Ohio State University, May 1974, AFCRL-TR-74-0231, AD 786 417.
- Tscherning, C.C., "Covariance Expressions for Second and Lower Order Derivatives of the Anomalous Potential," Report No. 225, Dept. of Geodetic Science and Surveying, The Ohio State University, January 1976, AFGL-TR-76-0052, AD-A024-720.
- Tscherning, C.C., "A Note on the Choice of Norm when Using Collocation for the Computation of Approximations to the Anomalous Potential," Bulletin Geodesique, vol. 51, No. 2, 1977.

- Tscherning, C.C., "Gravity Prediction Using Collocation and Taking Known Mass Density Anomalies into Account," Geophys. J.R. astr. Soc., vol. 59, pp. 147-153, 1979.
- Tscherning, C.C., "Comparison of Some Methods for the Detailed Representation of the Earth's Gravity Field," Reviews of Geophysics and Space Physics, vol. 19, No. 1, pp. 213-221, 1981.
- Tscherning, C.C. and R. Forsberg, "Prediction Test Using Least Squares Collocation and Residual Terrain Reduction," in Techniques to Predict Gravity Anomalies and Deflections of the Vertical in Mountainous Areas, K.-P. Schwarz (ed.), Report No. 30004, Dept. of Surveying Engineering, The University of Calgary, Alberta, 1983.
- Tscherning, C.C., "On the Use and Abuse of Molodensky's Mountain," in Geodesy in Transition, K.-P. Schwarz and G. Lachapelle (eds.), Report No. 60002, Dept. of Surveying Engineering, The University of Calgary, Alberta, July 1983a.
- Tscherning, C.C., "The Role of High Degree Spherical Harmonic Expansions in Solving Geodetic Problems," presented at symposium: Improved Gravity Field Estimation on a Global Basis, General Assembly of the International Association of Geodesy, Hamburg, August 1983b.
- Tscherning, C.C., R.H. Rapp and C.C. Goad, "A Comparison of Methods for Computing Gravimetric Quantities from High Degree Spherical Harmonic Expansions," Manuscripta Geodaetica, vol. 8, No. 3, pp. 249-272, December 1983.
- Wenzel, H.-G., "Geoid Computation by Least Squares Spectral Combination Using Integral Kernels," presented at the General Meeting of the International Association of Geodesy, Tokyo, May 1982.
- Wong, L. and R. Gore, "Accuracy of Geoid Heights from Modified Stokes Kernels," Geophys. J.R. astr. Soc., vol. 18, pp. 81-91, 1969.

END
FILMED

5-86

DTIC